

Movement of accessible plasma membrane cholesterol by GRAMD1 lipid transfer protein complex

Tomoki Naito¹, Bilge Ercan¹, Logesvaran Krshnan^{1,5}, Alexander Triebel², Dylan Hong Zheng Koh¹, Fan-Yan Wei³, Kazuhito Tomizawa³, Federico Tesio Torta², Markus R. Wenk², Yasunori Saheki^{1,4*}.

¹Lee Kong Chian School of Medicine, Nanyang Technological University, 308232, Singapore

²Department of Biochemistry, Yong Loo Lin School of Medicine, National University of Singapore, 117596, Singapore

³Department of Molecular Physiology, Faculty of Life Sciences, Kumamoto University, Kumamoto 860-8556, Japan

⁴Institute of Resource Development and Analysis, Kumamoto University, Kumamoto 860-0811, Japan

⁵Present address: Sir William Dunn School of Pathology, University of Oxford, South Parks Road, OX1 3RE Oxford, UK

*Address correspondence to:

yasunori.saheki@ntu.edu.sg (Y.S.); Telephone: +65 6592-3996; Fax: +65 6515-0417.

ABSTRACT

Cholesterol is a major structural component of the plasma membrane (PM). The majority of PM cholesterol forms complexes with other PM lipids, making it inaccessible for intracellular transport. Transition of PM cholesterol between accessible and inaccessible pools maintains cellular homeostasis, but how cells monitor PM cholesterol accessibility remains unclear. We show that endoplasmic reticulum (ER)-anchored lipid transfer proteins, the GRAMD1s, sense and transport accessible PM cholesterol to the ER. GRAMD1s bind one another and populate at ER-PM contacts by sensing a transient expansion of the accessible pool of PM cholesterol via GRAM domains and facilitate its transport via StART-like domains. Cells lacking all three GRAMD1s exhibit striking expansion of the accessible pool of PM cholesterol due to less efficient PM to ER transport of accessible cholesterol. Thus, GRAMD1s facilitate movement of accessible PM cholesterol to the ER in order to counteract acute increase of PM cholesterol, activating non-vesicular cholesterol transport.

INTRODUCTION

Sterol is one of the major membrane lipids in eukaryotes. In metazoans, cholesterol represents ~20% of total cellular lipids and is therefore essential for the structural integrity of cellular membranes and for cell physiology (van Meer et al., 2008; Vance, 2015). Sterol is distributed among cellular membranes primarily via non-vesicular transport, a process that is independent of membrane traffic (Baumann et al., 2005; Hao et al., 2002; Heino et al., 2000; Ikonen, 2008; Urbani and Simoni, 1990). Levels of sterol vary considerably between different cellular membranes. Between 60-80% of total cellular cholesterol is concentrated in the plasma membrane (PM), where it represents up to ~45% of total lipids in this bilayer (de Duve, 1971; Lange et al., 1989; Ray et al., 1969). Cellular cholesterol levels are maintained by regulated delivery and production, primarily through receptor-mediated endocytosis of low-density lipoproteins (LDLs) (Goldstein and Brown, 2015) and *de novo* synthesis in the endoplasmic reticulum (ER) that is controlled by activation of SREBP transcription factors (Brown et al., 2018; Goldstein and Brown, 1990). Cholesterol is also supplied to cells via high-density lipoproteins (HDL) through the reverse cholesterol flux pathway (Acton et al., 1996; Phillips, 2014).

Cholesterol within the bilayer membranes exhibits two distinct chemical states, one being free and “accessible” (also known as “unsequestered” or “chemically active”), and the other being “inaccessible” (also known as “sequestered” or “chemically inactive”) due in part to the formation of complexes with other membrane lipids, including sphingomyelin and phospholipids (Chakrabarti et al., 2017; Das et al., 2014; Gay et al., 2015; Lange et al., 2013; Lange et al., 2004; McConnell and Radhakrishnan, 2003; Ohvo-Rekila et al., 2002; Radhakrishnan and McConnell, 2000; Sokolov and Radhakrishnan, 2010). Most cholesterol in the PM is sequestered. However, a small fraction of PM cholesterol (~15% of PM lipids) remains accessible for extraction and transport (Das et al., 2014). Although the majority of cellular cholesterol resides in the PM, the biosynthesis of cholesterol occurs exclusively in the ER. Thus, the ER must communicate with the PM to monitor levels of PM cholesterol and to adjust cholesterol biosynthesis to maintain lipid homeostasis. To achieve this, cells sense transient increases in the accessible pool of PM cholesterol and rapidly transport the newly expanded pool of accessible PM cholesterol to the ER to suppress cholesterol biosynthesis by inhibiting SREBP-2, a master regulator of *de novo* cholesterol synthesis, thereby avoiding cholesterol overaccumulation while maintaining PM cholesterol levels (Das et al., 2014; Infante and Radhakrishnan, 2017; Lange and Steck, 1997; Lange et al., 2014; Scheek et al., 1997; Slotte and Bierman, 1988). Artificially trapping the accessible pool of cholesterol in the PM results in dysregulated activation of SREBP-2 (Infante and Radhakrishnan, 2017; Johnson et al., 2019). Despite its critical importance, the intracellular transport machinery that senses the accessibility of PM cholesterol is unknown. This machinery would likely respond to a sharp change in the accessibility of cholesterol on the cytoplasmic leaflet of the PM and facilitate transport of accessible cholesterol from the PM to the ER, thereby helping the ER communicate with the PM. Such homeostatic system would also allow cells to monitor PM cholesterol accessibility in order to help maintain cellular cholesterol homeostasis.

The ER extends throughout the cytoplasm, forming physical contacts with virtually all other cellular organelles and the PM (Phillips and Voeltz, 2016; Wu et al., 2018). Growing evidence indicates that these membrane contact sites play critical roles in cellular physiology, including lipid exchange and delivery via non-vesicular lipid transport facilitated by lipid transfer proteins (LTPs) (Antonny et al., 2018; Drin, 2014; Elbaz and Schuldiner, 2011; Holthuis and Menon, 2014; Jeyasimman and Saheki, 2019; Kumar et al., 2018; Lahiri et al., 2015; Lev, 2012; Luo

et al., 2018; Nishimura and Stefan, 2019; Petrunaro and Kornmann, 2019; Saheki et al., 2016; Saheki and De Camilli, 2017a; Saheki and De Camilli, 2017b; Wong et al., 2018). Thus, LTPs may participate in intracellular cholesterol transport and help maintain PM cholesterol homeostasis by regulating non-vesicular cholesterol transport between the PM and the ER at ER-PM contact sites.

Decades of biochemical and genetic research into cholesterol metabolism has identified several key LTPs that bind to cholesterol and mediate its non-vesicular transport (Luo et al., 2018; Wong et al., 2018). These proteins include a family of 15 proteins that contain a StAR-related lipid transfer (StART) domain, which binds and transports a wide variety of lipids, including cholesterol, glycerolipids, and sphingolipids (Alpy and Tomasetto, 2014). Five members of this family, namely STARD1, STARD3, STARD4, STARD5, and STARD6, bind and transport cholesterol (Alpy et al., 2013; laea et al., 2017; Lin et al., 1995; Mesmin et al., 2011; Soccio et al., 2002; Stocco, 2001; Wilhelm et al., 2017), but they are not conserved in yeast. This lack of conservation suggests that there may be a more ancient family of sterol transfer proteins that control cholesterol homeostasis in all eukaryotes.

A bioinformatics search for proteins that possess StART-like domains identified a new family of evolutionarily conserved proteins that includes six Lam/Ltc proteins in budding yeast (Gatta et al., 2015; Murley et al., 2015), and five GRAM domain-containing proteins (GRAMDs) in metazoans. These GRAMDs include the StART-like domain-containing GRAMD1s, also known as Asters (GRAMD1a/Aster-A, GRAMD1b/Aster-B, and GRAMD1c/Aster-C), and two highly related proteins that lack a StART-like domain (GRAMD2 and GRAMD3). Lam/Ltc proteins and GRAMDs all possess an N-terminal GRAM domain, which may sense/bind lipids based on its structural similarity to the PH domain (Begley et al., 2003; Tong et al., 2018), as well as a C-terminal transmembrane domain, which anchors the proteins to the ER. Structural and biochemical studies of yeast and mammalian StART-like domains identified a hydrophobic cavity that can bind sterol (Gatta et al., 2018; Horenkamp et al., 2018; Jentsch et al., 2018; Sandhu et al., 2018; Tong et al., 2018). The StART-like domains of GRAMD1s bind and transport sterols *in vitro* (Horenkamp et al., 2018; Sandhu et al., 2018). Recent studies have demonstrated that some GRAMDs, including GRAMD1a, GRAMD1b, and GRAMD2, localize to ER-PM contact sites (Besprozvannaya et al., 2018; Sandhu et al., 2018). GRAMD2 facilitates STIM1 recruitment to ER-PM contacts and potentially regulates Ca²⁺ homeostasis (Besprozvannaya et al., 2018), whereas GRAMD1b facilitates transport of HDL-derived cholesterol to the ER in the adrenal glands of mice (Sandhu et al., 2018). In contrast, yeast Lam/Ltc proteins sense cellular stress and potentially regulate cholesterol exchange between the ER and other membranes (Gatta et al., 2015; Murley et al., 2015; Murley et al., 2017). However, the role of these proteins in PM cholesterol/sterol homeostasis has been elusive. In this study, we provide evidence that GRAMD1s sense a transient expansion of the accessible pool of PM cholesterol and facilitate its transport to the ER at ER-PM contact sites, thereby contributing to PM cholesterol homeostasis.

We found that GRAMDs form homo- and hetero-meric complexes via their transmembrane domains and predicted luminal amphipathic helices, and that GRAMD1s rapidly move to ER-PM contacts upon acute hydrolysis of sphingomyelin in the PM. We characterized the mechanisms of this acute recruitment and found that the GRAM domain acts as a coincidence detector of unsequestered/accessible cholesterol and anionic lipids in the PM, including phosphatidylserine, allowing the GRAMD1s to sense a transient expansion of the accessible pool of PM cholesterol once it reaches above a certain threshold. We generated HeLa cells that lacked GRAMD1a/1b/1c (i.e., all GRAMDs that contain a StART-like domain) and determined the effect on cholesterol metabolism using a combination of cholesterol-sensing

probes for live cell imaging, and lipidomics of membrane extracts. Upon treatment with sphingomyelinase, which liberates sphingomyelin-sequestered pool of PM cholesterol into the “accessible” pool and stimulates its PM to ER transport, GRAMD1 triple knockout (TKO) cells exhibited exaggerated accumulation of the accessible pool of PM cholesterol and reduced suppression of SREBP-2 cleavage compared to wild-type control due to less efficient transport of accessible cholesterol from the PM to the ER. Using structure-function analysis, we demonstrated that GRAMD1s couple their PM sensing property and cholesterol transport function via their GRAM and StART-like domains, and that GRAMD1 complex formation ensures their progressive recruitment to ER-PM contacts. Finally, we observed striking expansion of the accessible pool of PM cholesterol in GRAMD1 TKO cells at steady state. Drug-induced acute recruitment of GRAMD1b to ER-PM contacts was sufficient to facilitate removal of the expanded pool of accessible cholesterol from the PM in GRAMD1 TKO cells. Collectively, our findings provide evidence for novel cellular mechanisms by which GRAMD1s monitor and help maintain PM cholesterol homeostasis in mammalian cells as one of the key homeostatic regulators. GRAMD1s sense a transient expansion of the accessible pool of PM cholesterol and facilitate its transport to the ER, thereby contributing to PM cholesterol homeostasis at ER-PM contact sites.

RESULTS

GRAMD proteins form homo- and hetero-meric complexes

Previous studies identified GRAMD1s as ER-resident proteins that are distributed throughout ER structures in a punctate pattern (Sandhu et al., 2018). GRAMDs (namely GRAMD1a, GRAMD1b, GRAMD1c, GRAMD2, and GRAMD3) all possess an N-terminal GRAM domain and a C-terminal transmembrane domain. In addition, the three GRAMD1 proteins (GRAMD1s) possess a StART-like domain (**Figure 1A**). Some LTPs are known to form homo- and hetero-meric complexes. Thus, we reasoned that GRAMD1s may also interact with one another to form complexes. To further analyze dynamics of these proteins on the ER at high spatial resolution, we tagged the GRAMD1s, as well as GRAMD3, with fluorescent proteins and analyzed their localization using spinning disc confocal microscopy coupled with structured illumination (SDC-SIM). Analysis of COS-7 cells expressing individual EGFP-tagged GRAMD1s or GRAMD3 (EGFP-GRAMD1a, EGFP-GRAMD1b, EGFP-GRAMD1c, or EGFP-GRAMD3) and a general ER marker (RFP-tagged Sec61 β), revealed enrichment of GRAMD1s and GRAMD3 in similar discrete patches along ER tubules. In contrast, RFP-Sec61 β localized to all domains of the ER, including the nuclear envelope and the peripheral tubular ER network (Hoyer et al., 2018) (**Figure 1B and Figure1-figure supplement 1A**). When individual EGFP-GRAMD1s and either mRuby-tagged GRAMD1b (mRuby-GRAMD1b) (**Figure 1C**) or mCherry-tagged GRAMD3 (mCherry-GRAMD3) (**Figure1-figure supplement 1B**) were co-expressed in COS-7 cells, the patches of EGFP and mRuby/mCherry significantly overlapped, indicating potential complex formation between these proteins on tubular ER.

To test whether these proteins form complexes, we examined biochemical interactions between GRAMD1s and GRAMD3 using co-immunoprecipitation assays. HeLa cells co-transfected with individual EGFP-GRAMD1s together with either myc-tagged GRAMD1b (Myc-GRAMD1b) (**Figure 1D and Figure 1-figure supplement 1C**) or myc-tagged GRAMD3 (Myc-GRAMD3) (**Figure 1E and Figure 1-figure supplement 1D**) were lysed, and either anti-GFP (**Figure 1D,E**) or anti-Myc nanobodies (**Figure 1-figure supplement 1C,D**) were used to perform immunoprecipitation. Analysis of the resulting immunoprecipitates by western blotting revealed robust interaction between GRAMD1s and GRAMD1b (**Figure 1D and Figure 1-figure supplement 1C**), as well as between GRAMD1s and GRAMD3 (**Figure 1E and Figure 1-figure supplement 1D**). These results demonstrate that these proteins form both homo- and hetero-meric complexes.

Luminal helices and transmembrane domains of GRAMD proteins are important for their complex formation

The formation of homo- and hetero-meric complexes between GRAMD1s and GRAMD3 suggested the presence of amino acid sequence within these proteins that facilitate their interaction. Secondary structure predictions indicated the presence of a conserved alpha helix within the luminal region of GRAMD1s (**Figure 2A**). Furthermore, helical wheel analysis of the luminal helix from GRAMD1b predicted that it formed an amphipathic helix with charged and hydrophobic amino acids occupying opposite sides of the helix (**Figure 2B and Figure 2-figure supplement 1A,B**). It is known that some amphipathic helices mediate protein-protein interactions through their hydrophobic surfaces (Segrest et al., 1990). Therefore, we first asked whether the luminal helix was necessary for these proteins to form discrete patches on tubular ER. We focused on GRAMD1b as a model protein to analyze the properties of the GRAMD1 luminal helices, generating a version of GRAMD1b that lacked the luminal helix (Δ helix), and a second version in which the five hydrophobic residues within the luminal helix

were mutated to glutamic acid (5E) to disrupt its hydrophobic surface (**Figure 2B** and **Figure 2-figure supplement 1C**). Whereas GRAMD1b (wild-type control) formed patches on tubular ER, both GRAMD1b (Δ helix) and GRAMD1b (5E) exhibited diffuse localization patterns, with fewer discrete patches on tubular ER (**Figure 2C**). In contrast, a version of GRAMD1b in which the four hydrophobic residues preceding the luminal helix were mutated to glutamic acid (4E) formed patches similar to control (**Figure 2C**), demonstrating that the 5E mutation specifically disrupted patch formation.

The potential ability of the luminal helices to directly interact with one another was examined using cell-free assays. Wild-type luminal helices (GRAMD1b₆₇₄₋₇₁₈) and luminal helices with the 5E mutation (GRAMD1b₆₇₄₋₇₁₈ 5E) were purified individually as EGFP fusion proteins and analyzed by size exclusion chromatography (SEC). Whereas the predicted molecular weights of the fusion proteins were the same (~35 kDa), wild-type luminal helices (EGFP-helix: EGFP-GRAMD1b₆₇₄₋₇₁₈) eluted at a much lower elution volume compared to 5E mutant luminal helices [EGFP-helix (5E): EGFP-GRAMD1b₆₇₄₋₇₁₈ 5E] (**Figure 2D**). Blue native PAGE analysis (BN-PAGE) of the purified proteins revealed that wild-type helices migrated slower than the 5E mutants, indicating that interaction between luminal helices depended on its hydrophobic surface (**Figure 2E**). In contrast, the denatured forms of these proteins in the presence of SDS migrated similarly (SDS-PAGE). Slightly slower migration of 5E mutants on the gel was possibly due to the increased hydrophilicity of this fragment compared to wild-type (Guan et al., 2015) (**Figure 2E**). These results suggest that the luminal helix is likely amphipathic and important for the formation of GRAMD1b complexes through its hydrophobic surface.

Finally, the formation of GRAMD1 complexes was examined biochemically in cells using co-immunoprecipitation assays. Homomeric interactions between GRAMD1bs and heteromeric interactions between GRAMD1b and GRAMD1a were greatly reduced when the luminal helix of GRAMD1b was either removed (Δ helix) or mutated to the 5E version, supporting the important role of the luminal helix in homo- and hetero-meric interactions of the GRAMD1s (**Figure 2F,G**). Residual interactions were mediated by the transmembrane domain of GRAMD1b, as replacing it together with its luminal region with those from Sec61 β (TM swap) (**Figure 2J**) completely abolished the ability of GRAMD1b to form homo- and hetero-meric complexes (**Figure 2F,G**). Accordingly, GRAMD1b with the TM swap exhibited a diffuse localization pattern (**Figure 2H**) and failed to interact with wild-type GRAMD1b on tubular ER, compared to wild-type GRAMD1b (**Figure 2I**). Thus, both transmembrane domains and luminal helices contributed to the formation of GRAMD1 complexes (**Figure 2J**). Taken together, these results revealed the biochemical mechanisms by which GRAMDs form homo- and hetero-meric complexes. As key residues contributing to the hydrophobic surface of the luminal helix are conserved among GRAMD1s (**Figure 2A** and **Figure 2-figure supplement 1A**), they likely play a role in heteromeric interactions of all these proteins.

The GRAM domain of GRAMD1s acts as a coincidence detector of unsequestered/accessible cholesterol and anionic lipids and senses the accessibility of cholesterol

Recent studies demonstrated that “cholesterol loading” leads to the accumulation of GRAMD1s at ER-PM contact sites (Sandhu et al., 2018). Within 20 min of treating cells with a complex of cholesterol and methyl- β -cyclodextrin (cholesterol/MCD), GRAMD1b was indeed recruited to the PM (**Figure 3A,B; Video 1**). In addition, we found that GRAMD1a, GRAMD1c, and GRAMD3 were all recruited to ER-PM contacts upon cholesterol loading, with kinetics similar to GRAMD1b (**Figure 3B**). However, a version of GRAMD1b that lacked the GRAM domain (GRAMD1b Δ GRAM) failed to localize to the PM, even after 30 min, indicating the

essential role of this domain in sensing PM cholesterol (**Figure 3-figure supplement 1A; Video 2**). While these results suggest that PM cholesterol plays a critical role in recruiting GRAMDs to ER-PM contacts, all of the GRAMDs localize to tubular ER at rest, despite a significant amount of cholesterol already present in the PM (Lange et al., 1989; Ray et al., 1969). Thus, their GRAM domains may possess unique abilities to sense the accessibility of PM cholesterol, rather than detecting the total levels of PM cholesterol. However, if the GRAM domains are able to sense accessible cholesterol in the PM is unknown.

To elucidate the biochemical properties of the GRAMD1 GRAM domain, we first purified the GRAM domain of GRAMD1b and performed liposome sedimentation assays to test its ability to bind lipids. In this assay, purified GRAM domains were mixed with sucrose-loaded heavy liposomes in sucrose-free buffer. After incubation, free liposomes and the liposomes that bound to GRAM domains (P) were pelleted by centrifugation; the supernatant contained only unbound GRAM domains (S) (**Figure 3C, E, Figure 3-figure supplement 1B, D, and Figure 3-figure supplement 2A, B**). The GRAM domain did not bind liposomes when the liposome contained only phosphatidylcholine (**Figure 3C and Figure 3-figure supplement 1B**). In contrast, the GRAM domain bound liposomes that contained free cholesterol, although such binding was rather weak, and only ~25% of purified GRAM domains bound liposomes even when the liposome contained high levels of cholesterol (Chol) (60%) (**Figure 3-figure supplement 1B**). The GRAM domain also bound liposomes when the liposomes contained phosphatidylserine (PS), the predominant anionic phospholipid in the PM. However, such binding only occurred when the liposomes contained non-physiologically high levels of phosphatidylserine (50%, 80%) (**Figure 3-figure supplement 1B**). Thus, we explored the possibility that the GRAM domain may bind to membranes more efficiently in the presence of both lipids, acting as a coincidence detector of unsequestered/accessible cholesterol and phosphatidylserine.

Little binding was observed when the liposomes contained 50% cholesterol or 20% phosphatidylserine (**Figure 3C and Figure 3-figure supplement 1B**). However, strong binding was observed when 50% cholesterol and 20% phosphatidylserine were both present in the liposomes, with ~80% of the GRAM domains bound to liposomes (**Figure 3C**). Thus, the addition of free cholesterol dramatically enhanced binding of the GRAM domain to phosphatidylserine-containing membranes. Replacing cholesterol with a non-bilayer forming lipid, phosphatidylethanolamine (PE), abolished the binding of the GRAM domains to liposomes, confirming the specific effect of cholesterol (**Figure 3-figure supplement 2A**). Similar synergistic effects were observed with the GRAM domain of GRAMD1a (**Figure 3D**), suggesting the conserved function of GRAMD1 GRAM domains.

Despite the presence of phosphatidylserine (~10% of PM lipids) and high levels of cholesterol (~45% of PM lipids) in the PM of mammalian cells, GRAMD1s are not enriched at ER-PM contacts at rest (**Figure 1B, Figure 3A and Figure 4-figure supplement 3B**). The majority of cholesterol in the PM (~27% of PM lipids) is sequestered and “inaccessible” to cytosolic proteins, and only ~15% of PM lipids remain unsequestered and accessible (Das et al., 2014). Thus, interactions between GRAM domains and the PM could be suppressed by “the factors that sequester cholesterol” in this bilayer in cells.

One of the major factors that mediate direct sequestration of PM cholesterol is sphingomyelin, which forms a complex with cholesterol and makes it inaccessible (Endapally et al., 2019; Finean, 1953; McConnell and Radhakrishnan, 2003; Radhakrishnan and McConnell, 2000; Slotte, 1992). Sphingomyelin-sequestered pool of PM cholesterol consists of ~15% of PM lipids, while the rest of the inaccessible pool is sequestered by other membrane factors (Das

et al., 2014). To test if sequestration of cholesterol by sphingomyelin affects the binding of GRAM domains to artificial membranes, we incorporated increasing amounts of sphingomyelin (SM) (10%, 25%) into liposomes that contained 50% cholesterol and 20% phosphatidylserine (**Figure 3E**). When these liposomes contained 25% sphingomyelin, the percentage of GRAMD1b GRAM domains that bound to the liposomes decreased from ~80% to ~45% (**Figure 3E and Figure 3-figure supplement 1C**). Similar results were obtained with the GRAM domain of GRAMD1a (**Figure 3F**). Thus, binding of GRAM domains to artificial membranes that contain cholesterol and phosphatidylserine can be modulated by the presence of sphingomyelin (**Figure 3-figure supplement 1C**). These results suggest that sphingomyelin helps to suppress the binding of GRAM domains to the PM at rest by reducing the accessibility of cholesterol in this bilayer.

In addition to sphingomyelin, phospholipid acyl chain saturation has profound effects on the accessibility of cholesterol in membranes (Chakrabarti et al., 2017; Gay et al., 2015; Lange et al., 2013; Radhakrishnan and McConnell, 2000; Sokolov and Radhakrishnan, 2010). If the GRAM domain binds to the PM by sensing the accessibility of cholesterol, its binding to artificial membranes should also be influenced by acyl chain diversity of phospholipids. To test this possibility, we generated liposomes containing fixed amounts of phosphatidylserine (20%) with varying ratios of cholesterol and phosphatidylcholine (**Figure 3-figure supplement 2B**). We individually tested either one of the three types of phosphatidylcholine that possesses different acyl chain structures, namely POPC, DOPC, and DPhyPC (**Figure 3-figure supplement 2C**). Branched (DPhyPC) and more unsaturated (DOPC) acyl chains lower the tendency to form ordered conformation in the membranes, and thus, POPC has the strongest cholesterol sequestration effect among these three lipids, followed by DOPC and DPhyPC (Sokolov and Radhakrishnan, 2010). The binding of GRAM domain of GRAMD1b to liposomes shifted to lower cholesterol concentration as the ordering tendency of phosphatidylcholine is lowered (i.e. as cholesterol sequestration effect is reduced) (**Figure 3-figure supplement 2B**). These results are consistent with the ability of the GRAM domain to sense the accessibility of cholesterol in membranes.

Finally, to determine whether GRAM domains bind more broadly to other anionic lipids, we replaced phosphatidylserine with other anionic lipids, namely phosphatidic acid (PA), PI(4)P, and PI(4,5)P₂, and asked whether they similarly affected GRAM domain binding. In this assay we used 5% anionic lipids, including phosphatidylserine, as even 5% phosphatidylserine was sufficient to mediate binding of the GRAM domain to liposomes that also contained 50% free cholesterol, albeit less efficiently than 20% phosphatidylserine (**Figure 3-figure supplement 1D**). No or little binding was observed when GRAM domains were mixed with liposomes that contained 5% of these anionic lipids (each was tested individually) (**Figure 3-figure supplement 1D**). However, as seen when phosphatidylserine and cholesterol were combined, the addition of free cholesterol to these anionic lipid-containing liposomes enhanced the binding of GRAM domains to the liposomes (**Figure 3-figure supplement 1D**).

As anionic lipids, including phosphatidylserine, are enriched in the inner leaflet of the PM (Yeung et al., 2008), these results indicate that the recruitment of GRAMD1s to the PM is regulated by interactions between GRAM domains and anionic lipids, and that these interactions are enhanced by the additional presence of accessible/unsequestered cholesterol in the PM.

Liberation of sphingomyelin-sequestered pool of cholesterol induces acute recruitment of GRAMD1b to the PM

To examine the physiological role of sphingomyelin in GRAM domain-dependent recruitment of GRAMD1s to the PM, HeLa cells expressing either EGFP-GRAMD1b or EGFP-GRAMD1b Δ GRAM were treated with sphingomyelinase, which hydrolyzes PM sphingomyelin, and imaged under TIRF microscopy. Although sphingomyelin is enriched in the outer leaflet of the PM bilayer, it also contributes to the suppression of the accessibility of cholesterol in the inner leaflet of the PM as unsequestered cholesterol can spontaneously flip flop between outer and inner leaflets of this bilayer (Leventis and Silvius, 2001; Steck and Lange, 2018). Within 30 min of sphingomyelinase treatment, GRAMD1b was indeed recruited to the PM (**Figure 3G**), albeit less efficiently compared to cholesterol loading to the PM (**Figure 3B**). GRAMD1b Δ GRAM, however, failed to localize to the PM, even after 60 min (**Figure 3G**). EGFP-tagged GRAMD1 GRAM domains (namely EGFP-GRAM_{1a}, EGFP-GRAM_{1b}, and EGFP-GRAM_{1c}) were all recruited to the PM upon sphingomyelinase treatment (**Figure 3H**), revealing a direct role of the GRAM domain in detecting the unsequestered/accessible pool of PM cholesterol in cells. These results are also consistent with the lack of enrichment of GRAMD1s at ER-PM contact sites at rest (**Figure 1B**, **Figure 3A** and **Figure 4-figure supplement 3B**). Taken together, these data demonstrate that GRAMD1s are recruited to the PM by sensing increase in the accessibility of PM cholesterol (i.e. acute expansion of the accessible pool of PM cholesterol that reaches above a certain threshold for the GRAM domain to interact with the PM), and that this recruitment depends on the GRAM domain, which acts as a coincidence detector for both unsequestered/accessible cholesterol and anionic lipids in the PM (**Figure 3I**).

Deletion of GRAMD1s results in exaggerated accumulation of the accessible pool of cholesterol in the PM

As GRAMD1s move to ER-PM contact sites upon acute expansion of the accessible pool of PM cholesterol (**Figure 3G,H**), they may also contribute to the extraction of accessible PM cholesterol in order to maintain homeostasis. To investigate the potential functions of GRAMD1s in this process, we used the CRISPR/Cas9 system to disrupt GRAMD1 function by targeting all three GRAMD1 genes (GRAMD1A, GRAMD1B and GRAMD1C) in HeLa cells. Guide RNAs specific to exon 13 of GRAMD1A and GRAMD1B and to exon 11 of GRAMD1C were chosen, as they encode the lipid-harboring StART-like domains (**Figure 4A**). After transfection of plasmids expressing GRAMD1-specific guide RNAs and Cas9 protein, two independent isolates of GRAMD1a/1b double knockout cell clones (DKO #38 and DKO #40) and two independent isolates of GRAMD1a/1b/1c triple knockout cell clones (TKO #1 and TKO #15) were selected. The absence of GRAMD1a and GRAMD1b was confirmed by western blotting and genomic sequencing (**Figure 4B** and **Figure 4-figure supplement 1A-D**). Disruption of the GRAMD1C gene was validated by sequencing the targeted genomic region within the GRAMD1C locus (**Figure 4C** and **Figure 4-figure supplement 1E**). No obvious defects in cell viability or overall morphology were observed for these KO cells, with the exception that KO cells grew slightly slower than parental HeLa cells. Subsequent experiments were performed using GRAMD1a/1b/1c TKO #15 cells (hereafter referred to as GRAMD1 TKO cells).

Incubation of cells with sphingomyelinase reduces the sequestration of PM cholesterol, resulting in a transient expansion of the accessible pool of cholesterol in the PM (Das et al., 2014; Endapally et al., 2019). The newly expanded pool of accessible cholesterol is then extracted and transported to the ER (Das et al., 2014; Lange and Steck, 1997; Scheek et al., 1997; Slotte and Bierman, 1988). Based on the ability of the GRAM domain to sense expansion of the accessible pool of PM cholesterol (**Figure 3H,I**), EGFP-GRAM_{1b} was used as a probe to detect acute increases in the accessible pool of PM cholesterol. Without

stimulation, cytosolically expressed EGFP-GRAM_{1b} distributed throughout the cytoplasm without particular enrichment in the PM in both wild-type and GRAMD1 TKO HeLa cells (**Figure 4-figure supplement 2A**). Treatment with sphingomyelinase for 1 hour led to only modest recruitment of EGFP-GRAM_{1b} to the PM in wild-type HeLa cells (**Figure 4D**). In contrast, the same treatment led to much more prominent recruitment of EGFP-GRAM_{1b} to the PM in GRAMD1 TKO cells (**Figure 4D**). TIRF microscopy of cells expressing EGFP-GRAM_{1b} revealed that PM recruitment of EGFP-GRAM_{1b} upon sphingomyelinase treatment was significantly enhanced in GRAMD1 TKO cells compared to wild-type control cells over the entire 1-hour treatment (**Figure 4E**). Importantly, additional treatment of GRAMD1 TKO cells with methyl- β -cyclodextrin (MCD), which extracts cholesterol from cellular membranes, resulted in acute loss of the PM recruitment of EGFP-GRAM_{1b} within 2 minutes (**Figure 4-figure supplement 2B**). However, the same treatment resulted in only modest changes in the binding of phosphatidylserine biosensor (mCherry-tagged C2 domain of Lactadherin, mCherry-LactC2) or PI(4,5)P₂ biosensor (iRFP-tagged PH domain of PLC δ , iRFP-PH^{PLC δ}), confirming the specificity of EGFP-GRAM_{1b} in sensing the newly expanded pool of accessible cholesterol in the PM upon sphingomyelinase treatment (**Figure 4-figure supplement 2B**). Taken together, these results demonstrate an exaggerated accumulation of the accessible pool of PM cholesterol in GRAMD1 TKO cells upon sphingomyelinase treatment and suggest that extraction and transport of this acutely expanded accessible pool may be impaired in the absence of GRAMD1s.

We also assessed the role of GRAMD1s in regulating steady state PM cholesterol levels by separating and purifying PMs from cultured cells using poly-D-lysine-coated dextran beads (Saheki et al., 2016). Cultured cells were attached to the beads and osmotically lysed by vigorous vortexing. Brief sonication was used to remove most organelles, whereas PM sheets remained attached to the bead surface (visualized by BODIPY-labeled ceramide) (**Figure 4-figure supplement 3A**). As shown by western blotting, the PM sheets that remained bound to the beads were highly enriched for PM marker proteins (such as CD44) relative to the starting material. The endosomal marker, EEA1, was greatly depleted, whereas small amounts of ER proteins were recovered in the PM, such as VAPA and VAPB (**Figure 4-figure supplement 3B**). This likely reflected tightly attached cortical ER (Saheki et al., 2016). Importantly, the levels of endogenous GRAMD1a and GRAMD1b on bead-attached PM sheets were similar to those seen for the integral ER protein, VAP (**Figure 4-figure supplement 3B**). This confirmed that the majority of these two proteins are distributed throughout the ER, with only a very small fraction localizing to ER-PM contact sites at rest (**Figure 1B and Figure 3A**). Mass spectrometry analysis of whole-cell and purified PM lipid extracts of wild-type control and GRAMD1 TKO HeLa cells did not reveal significant changes in cholesterol and other major lipids, except for very minor increases in cholesterol esters (**Figure 4-figure supplement 3C,D**). Thus, GRAMD1s are not essential for maintaining total levels of PM cholesterol. This result is also consistent with very little enrichment of GRAMD1s at ER-PM contacts at the steady state. Collectively, these results indicate that GRAMD1s may contribute to PM cholesterol homeostasis by counteracting acute increases in the accessible pool of PM cholesterol via its extraction and transport to the ER.

The cholesterol transporting property of the StART-like domain of GRAMD1s is critical for the removal of an acutely expanded pool of accessible PM cholesterol

Although GRAMD1 StART-like domains transport cholesterol *in vitro*, it remains unclear whether this property is relevant to cellular physiology. Our live cell imaging analysis of EGFP-GRAM_{1b} (i.e., a novel biosensor for detecting acute expansion of the accessible pool of PM cholesterol that we identified in this study) allowed us for the first time to conduct structure-

function analysis of GRAMD1s in the context of cellular functions. We first asked whether the sterol-binding pocket of the StART-like domain is required for the cellular functions of GRAMD1s. As a first step, we characterized the cholesterol-transporting properties of individual StART-like domains *in vitro* and generated a series of structure-guided mutations to identify key amino acid residues that are essential for cholesterol transport. We purified StART-like domains from all three GRAMD1s and performed cell-free liposomes-based lipid transfer assays. In this assay, the amount of dehydroergosterol (DHE) (a fluorescent analog of cholesterol) in liposomes was quantitatively measured using fluorescence resonance energy transfer (FRET) between DHE and Dansyl-PE (DNS-PE) (**Figure 5A**). DHE was initially loaded only into donor liposomes, and its transfer from donor to DNS-PE containing acceptor liposomes was monitored over time by measuring FRET between transferred DHE and DNS-PE in acceptor liposomes (**Figure 5A, Figure 5-figure supplement 1A**). In the absence of StART-like domains, very little increases in the FRET signal were observed (**Figure 5-figure supplement 1B, buffer**). However, when GRAMD1 StART-like domains were mixed with donor and acceptor liposomes, a rapid increase in FRET signal was observed, indicating the efficient extraction of DHE from donor liposomes and its loading onto acceptor liposomes by the StART-like domains (**Figure 5E and Figure 5-figure supplement 1B**). Increasing amounts of purified proteins (0.5 μ M, 1 μ M, and 2 μ M) reduced the time required for the FRET signal to plateau (**Figure 5-figure supplement 1C-E**). GRAMD1a StART-like domains transferred DHE most efficiently, at a rate corresponding to \sim 8 DHE molecules per minute. In comparison, GRAMD1b and GRAMD1c transported \sim 1 DHE molecule per minute, as calculated using a standard curve (**Figure 5-figure supplement 1A,F**). Our results show the ability of GRAMD1 StART-like domains to transport cholesterol between membranes.

Guided by crystal structures of GRAMD1 StART-like domains in complex with 25-hydroxycholesterol (Laraia et al., 2019; Sandhu et al., 2018), we designed mutations that would potentially block the insertion of cholesterol into the GRAMD1b StART-like domain. Our mutagenesis strategy was to rigidify the loop that was predicted to open or close to capture or release sterol (5P) (**Figure 5B**). Purified GRAMD1a and GRAMD1b StART-like domains with 5P mutations were unable to transfer DHE *in vitro* (**Figure 5C,D and Figure 5-figure supplement 1G,H**). Similar result was also obtained with a version of the GRAMD1b StART-like domain with a point mutation (T469D) that was previously shown to be defective in DHE extraction *in vitro* (Horenkamp et al., 2018) (**Figure 5-figure supplement 1H**).

Building upon our newly designed 5P mutation, which eliminated the ability of StART-like domains to transport cholesterol, we asked whether exaggerated accumulation of the accessible pool of PM cholesterol observed in GRAMD1 TKO cells upon sphingomyelinase treatment (using the EGFP-GRAM_{1b} biosensor) could be rescued by re-expressing wild-type or mutant versions of GRAMD1b. Strikingly, the enhanced PM recruitment of EGFP-GRAM_{1b} was dramatically suppressed by expressing wild-type mRuby-GRAMD1b but not by expressing a mutant version of mRuby-GRAMD1b that is defective in cholesterol transport [mRuby-GRAMD1b (5P)] (**Figure 5E**). In contrast, PM recruitment of mRuby-GRAMD1b upon sphingomyelinase treatment in TKO cells was enhanced for the 5P mutant compared with wild-type GRAMD1b (**Figure 5F**). These results suggest that StART-like domain-dependent extraction and transport of accessible PM cholesterol to the ER facilitates the dissociation of GRAMD1b from the PM, as interaction of its GRAM domain with the PM is weakened, due to a reduction in accessible cholesterol in the PM.

Our results so far suggest that GRAMD1b may play a unique role in sensing and controlling movement of accessible PM cholesterol. To further support this notion, we examined whether overexpression of other known cholesterol transfer proteins, such as STARD4 (Iaea et al.,

2017; Mesmin et al., 2011) and some ORPs, including OSBP (Antonny et al., 2018), ORP4 (Charman et al., 2014), and ORP9 (Ngo and Ridgway, 2009), could substitute the function of GRAMD1s, using GRAMD1 TKO cells. Specifically, we examined if their overexpression rescue exaggerated accumulation of the accessible pool of PM cholesterol observed in GRAMD1 TKO cells, as monitored by EGFP-GRAM_{1b} biosensor, upon sphingomyelinase treatment (**Figure 4D,E**). Transiently transfected mCherry-tagged STARD4 (mCherry-STARD4) and mRuby-tagged ORPs (mRuby-OSBP, mRuby-ORP4, and mRuby-ORP9) were all well expressed in TKO cells (**Figure 5-figure supplement 2A**). However, their expression did not suppress the enhanced recruitment of EGFP-GRAM_{1b} to the PM in TKO cells upon sphingomyelinase treatment, being unable to substitute the function of GRAMD1s (**Figure 5-figure supplement 2B and D; compare with Figure 5E**). None of these proteins were recruited to the PM by sphingomyelinase treatment, demonstrating a unique property of GRAMD1s in sensing a transient expansion of the accessible pool of PM cholesterol (**Figure 5-figure supplement 2C and E**).

Taken together, our results suggest a critical role of the GRAMD1s in controlling the movement of the accessible pool of PM cholesterol between the PM and the ER via their StART-like domains.

GRAMD1s play a role in accessible cholesterol transport from the PM to the ER during acute expansion of the accessible pool of PM cholesterol

Acute expansion of the accessible pool of PM cholesterol results in the suppression of SREBP-2 cleavage and inhibition of cholesterol biosynthesis as a result of transport of accessible cholesterol from the PM to the ER. However, the intracellular transport machinery by which accessible cholesterol is transported from the PM to the ER remains unknown. GRAMD1s may play a role in this process, as they are able to sense and counteract the acute expansion of the accessible pool of PM cholesterol.

TIRF microscopy of cells expressing EGFP-GRAMD1b revealed that sphingomyelinase treatment led to sustained recruitment of GRAMD1b to the PM (during 3 hours of imaging) (**Figure 6A; Video 3**). As GRAMD1 TKO cells show exaggerated accumulation of the accessible pool of PM cholesterol upon sphingomyelinase treatment compared with wild-type cells (**Figure 4D,E**), GRAMD1s may be involved in PM to ER transport of the accessible pool of cholesterol via their GRAM and StART-like domains. To examine the role of GRAMD1s in this process, we determined a time-course for the suppression of SREBP-2 cleavage upon sphingomyelinase treatment in wild-type control and GRAMD1 TKO cells as an estimate of the efficiency of the transport of accessible cholesterol from the PM to the ER. In this assay, we first depleted most of accessible cholesterol from control and TKO cells by treating them with a combination of lipoprotein deficient serum (LPDS) and mevastatin, an HMG-CoA reductase inhibitor, for 16 hours (a treatment to induce maximum SREBP-2 cleavage by cholesterol starvation) and then stimulated the cells with sphingomyelinase and monitored the suppression of SREBP-2 cleavage, which results from PM to ER transport of accessible cholesterol in response to liberation of sphingomyelin-sequestered pool of PM cholesterol by sphingomyelinase, over time using total cell lysates. Cell lysates were collected at different time points (0, 30, 60, 90, 120, 150, and 180 min) and analyzed by SDS-PAGE followed by immuno-blotting against SREBP-2 (**Figure 6B**). At time 0, there were no detectable changes in the cleavage of SREBP-2 in GRAMD1 TKO cells compared to wild-type control cells. Suppression of SREBP-2 cleavage was observed in control cell lysates within 90 min; however, such suppression was delayed and reduced (but not eliminated) in TKO cells. Even

after 180 min, TKO cells were not able to suppress SREBP-2 cleavage to the similar levels as wild-type control cells (**Figure 6B,C**).

Importantly, re-expression of GRAMD1b in TKO cells was sufficient to suppress SREBP-2 cleavage to the similar extent to wild-type control cells at the 180 min time point, thereby rescuing the phenotype (**Figure 6D,E** and **Figure 6-figure supplement 1A,B**). We hypothesized that both the recruitment of GRAMD1s to ER-PM contact sites and their ability to transport cholesterol are critical for the suppression of the cleavage of SREBP-2 by facilitating transport of newly expanded pool of accessible PM cholesterol to the ER. To test this hypothesis, we used a GRAMD1b mutant that lacks the GRAM domain (GRAMD1b Δ GRAM), which cannot be recruited to the PM (**Figure 3G**), and a GRAMD1b with the mutated StART-like domain, which is defective in cholesterol transport (5P) (**Figure 5B-D**). The expression of GRAMD1b Δ GRAM or GRAMD1b 5P in TKO cells failed to rescue the phenotype (**Figure 6D** and **Figure 6-figure supplement 1A**). These data demonstrate that GRAMD1s play a role in the transport of accessible cholesterol from the PM to the ER upon acute expansion of the accessible pool of PM cholesterol and help suppress SREBP-2 activity, and that such functions require their recruitment to ER-PM contact sites, which is regulated by the ability of their GRAM domain to sense a transient expansion of the accessible pool of PM cholesterol, and their StART-like domain-dependent cholesterol transport.

In order to measure changes in the accessible pool of PM cholesterol, we took advantage of the cholesterol-binding domain 4 (D4) of bacterial Perfringolysin O (PFO), which has been widely used as a probe to measure the accessible pool of PM cholesterol (Das et al., 2013; Gay et al., 2015; Shimada et al., 2002; Sokolov and Radhakrishnan, 2010). Wild-type control and GRAMD1 TKO cells that had been pre-treated with a combination of LPDS and mevastatin for 16 hours were stimulated with sphingomyelinase for a fixed period of time (0, 30, 60, 90, 120, 150, and 180 min) and washed. Cells were then incubated with recombinant EGFP-tagged D4 (EGFP-D4) proteins for 15 min at room temperature. After wash, cell lysates were collected and analyzed by SDS-PAGE followed by immuno-blotting against GFP to detect EGFP-D4 proteins that were bound to accessible cholesterol in the PM (**Figure 6-figure supplement 2A**). At time 0, there were no detectable changes in EGFP-D4 signals in TKO cells compared to wild-type control cells. 30 min treatment with sphingomyelinase induced similar increase in the binding of EGFP-D4 to both control and TKO cells. Gradual decrease of EGFP-D4 signals was observed in control cell lysates over the time course of 180 min, similar to a previous report that utilized a mutant form of PFO to assess changes in accessible cholesterol in the PM upon sphingomyelinase treatment (Das et al., 2014). TKO cells, however, showed continuous increase in binding of EGFP-D4 to the PM even after 180 min (**Figure 6-figure supplement 2A,B**), suggesting sustained accumulation of accessible cholesterol in the PM compared to wild-type control cells due to less efficient transport of accessible cholesterol from the PM to the ER.

Together with the results obtained with cytosolically expressed EGFP-GRAM_{1b} biosensor (**Figure 4 D,E**), these data strongly indicate that extraction and transport of accessible PM cholesterol to the ER by GRAMD1s is able to counteract with acute expansion of the accessible pool of PM cholesterol (e.g. acute expansion induced by sphingomyelinase treatment) to prevent accumulation of accessible cholesterol in the PM in wild-type control cells and that such homeostatic response is impaired in GRAMD1 TKO cells. It is also important to note that there might be other intracellular cholesterol transport mechanisms that may act in parallel with GRAMD1s and facilitate accessible cholesterol extraction from the PM for its transport to the ER as suppression of SREBP-2 cleavage is not eliminated even in the total absence of GRAMD1s (see Discussion).

Efficient transport of the accessible pool of PM cholesterol to the ER requires GRAMD1 complex formation

A version of GRAMD1b with its transmembrane domain and luminal region both replaced by those of Sec61 β (TM swap) cannot form protein complexes (**Figure 2F-J**). Remarkably, GRAMD1b TM swap failed to rescue the reduced suppression of SREBP-2 cleavage observed in GRAMD1 TKO cells (**Figure 6E and Figure 6-figure supplement 1B**) and failed to suppress the enhanced recruitment of EGFP-GRAM1_b to the PM in TKO cells upon sphingomyelinase treatment, although the mutant protein was still recruited to the PM (**Figure 6-figure supplement 1C,D**). TIRF microscopic analysis of HeLa cells expressing the GRAMD1b TM swap mutant, however, revealed major differences in how it was recruited to the PM compared to wild-type GRAMD1b (**Figure 6F**). The GRAMD1b TM swap remained diffusely distributed on the tubular ER (which is closely attached to the PM) even at the end of the 180 min imaging period. In contrast, wild-type GRAMD1b progressively accumulated at ER-PM contacts as discrete patches with much stronger PM recruitment (**Figure 6F,G; Video 3**). These results support an important role for GRAMD1 complex formation in facilitating their progressive accumulation at ER-PM contacts, thereby supporting efficient accessible cholesterol transport at these contacts. Taken together, we conclude that GRAMD1s play a role in PM to ER transport of the accessible pool of PM cholesterol upon its acute expansion. Loss of GRAMD1 function leads to sustained accumulation of accessible cholesterol in the PM, resulting in less effective suppression of SREBP-2 cleavage and possibly dysregulation of cellular cholesterol homeostasis.

Chronic expansion of the accessible pool of PM cholesterol in GRAMD1 TKO cells

Distinct pools of cholesterol co-exist in the PM at steady state, as a major pool is “inaccessible” (i.e., sequestered or chemically inactive) and a smaller pool is “accessible” (i.e., unsequestered or chemically active). Given the role of GRAMD1s in facilitating the transport of accessible cholesterol from the PM to the ER, the impact of GRAMD1 deficiency on steady state levels of accessible PM cholesterol was examined.

We purified EGFP-tagged D4 mutant (D434S) proteins (EGFP-D4H), which have a lower threshold for binding to accessible cholesterol compared to D4 *in vitro* (Johnson et al., 2012; Maekawa and Fairn, 2015). Wild-type control and GRAMD1 TKO HeLa cells that express a PM marker (iRFP-PH^{PLC δ}) were incubated with buffer containing purified recombinant EGFP-D4H proteins for 15 min at room temperature and washed, and then imaged under spinning disc confocal microscopy. D4H binding was assessed by line scan analysis. Strikingly, EGFP-D4H proteins bound more strongly to the PM of GRAMD1 TKO cells compared to that of control cells (**Figure 7A, B**). Pre-treatment of GRAMD1 TKO cells with MCD for 30 min resulted in loss of the binding of EGFP-D4H to the PM (**Figure 7-figure supplement 1A,B**), validating the specificity of this probe in sensing accessible pool of PM cholesterol. As the total level of PM cholesterol was not elevated in GRAMD1 TKO cells in our lipidomics analysis (**Figure 4-figure supplement 3C,D**), these results indicate that the chronic expansion of the accessible pool of PM cholesterol occurs in the absence of GRAMD1s.

Re-expression of either one of the three GRAMD1s in TKO cells was sufficient to reduce the binding of EGFP-D4H to the PM, thereby rescuing the chronic expansion of the D4H accessible pool of PM cholesterol observed in TKO cells (**Figure 7-figure supplement 2A-C**). Versions of GRAMD1b in which the StART-like domain was mutated were systematically expressed in TKO cells to determine whether the ability of GRAMD1b to transport accessible cholesterol is required to rescue the phenotype (**Figure 7-figure supplement 2D**). All mutant

versions of GRAMD1b, including a newly designed mutant with the hydrophobicity of the surface of the sterol-binding pocket changed (Y430A, V445A), as well as 5P and T469D mutants, failed to reduce the binding of EGFP-D4H to the PM of TKO cells, being unable to rescue the chronic expansion of the D4H accessible pool of PM cholesterol in TKO cells (**Figure 7-figure supplement 2E-I**).

Taken together, these results suggest the importance of GRAMD1s in maintaining steady state levels of accessible PM cholesterol by facilitating its transport from the PM to the ER.

Acute recruitment of GRAMD1b to ER-PM contacts facilitates removal of the expanded pool of accessible PM cholesterol in GRAMD1 TKO cells

Chronic expansion of the accessible pool of PM cholesterol in GRAMD1 TKO cells at steady state, revealed by increased PM binding of the EGFP-D4H probe, indicates that GRAMD1s are important for maintaining PM cholesterol homeostasis through their functions in sensing a transient expansion of the accessible pool of PM cholesterol and facilitating its transport to the ER at ER-PM contact sites. If this is the case, artificial forced recruitment of re-expressed GRAMD1s to ER-PM contacts in GRAMD1 TKO cells should mediate extraction and transport of accessible cholesterol from the PM to the ER and reduce the binding of the EGFP-D4H probe to the PM.

To test whether GRAMD1s can directly act at ER-PM contact sites, rapamycin-induced dimerization of the FK506-binding protein (FKBP) and the FKBP-rapamycin-binding domain (FRB) (Muthuswamy et al., 1999) was used to acutely recruit GRAMD1b to these sites. In this assay, GRAMD1 TKO cells were co-transfected with a version of GRAMD1b where its N-terminus, which contains the GRAM domain, was replaced by a miRFP-tagged FKBP module (miRFP-FKBP-GRAMD1b), and a PM-targeted FRB module (PM-FRB-mCherry) (**Figure 7C**). TIRF microscopy revealed rapid recruitment of miRFP-FKBP-GRAMD1b to the PM within 10 min of rapamycin treatment (**Figure 7D and Figure 7-figure supplement 3A; Video 4**). To assess accessible pool of PM cholesterol after the acute recruitment of the chimeric GRAMD1b protein to the PM, cells that had been pre-treated with rapamycin for a fixed period of time (0 min, 30 min, and 60 min) were incubated with recombinant EGFP-D4H proteins for 15 min at room temperature and washed and imaged under spinning disc confocal microscopy.

Strikingly, rapamycin-induced PM recruitment of the chimeric GRAMD1b protein led to acute reduction in D4H accessible PM cholesterol in GRAMD1 TKO cells within 60 min, reducing the binding of EGFP-D4H proteins to the PM (**Figure 7E,F**). Mutant versions of miRFP-FKBP-GRAMD1b carrying a StART-like domain that cannot transport cholesterol (5P and T469D mutants; see also **Figure 5B-D, Figure 7-figure supplement 2D-I and Figure 5-figure supplement 1H**) were recruited to the PM with kinetics similar to the wild-type version (WT) (**Figure 7D and Figure 7-figure supplement 3B,C; Video 5**). However, recruitment of the mutant versions did not reduce the PM EGFP-D4H signal (**Figure 7F**), demonstrating a critical role for StART-like domain-dependent PM to ER cholesterol transport in the removal of the expanded accessible PM cholesterol by GRAMD1b at ER-PM contact sites.

Based on these results, we conclude that GRAMD1s play a direct role in facilitating transport of accessible PM cholesterol to the ER at ER-PM contact sites.

DISCUSSION

We have demonstrated that the evolutionarily conserved family of ER-anchored GRAMD1s contribute to PM cholesterol homeostasis by sensing a transient expansion of the accessible pool of PM cholesterol and facilitating its transport to the ER at ER-PM contact sites. We have also identified the molecular mechanisms by which GRAMD1s interact with one another to form a complex, and how they are recruited to the PM. Key findings of the current study are the following:

1) We found that GRAMD1s and GRAMD3 form homo- and hetero-meric complexes and localize to discrete patches on tubular ER in mammalian cells at rest. We identified that their transmembrane domains and luminal helices, which are predicted to form amphipathic surfaces, mediated the formation of protein-protein complexes and regulated their progressive recruitment to ER-PM contacts and their functions;

2) Using *in vitro* liposome sedimentation assays and live cell imaging, we found that the GRAM domain of GRAMD1s acts as a coincidence detector, tuned to the presence of both “unsequestered/accessible” cholesterol and anionic lipids, including phosphatidylserine, in the PM (**Figure 3I**). Importantly, the binding of the GRAM domain to membranes requires unsequestered/accessible cholesterol to reach above a certain threshold. As the majority of cholesterol in the PM is sequestered (i.e., inaccessible), this switch-like property allows GRAMD1s to move to ER-PM contact sites only when the accessible pool of PM cholesterol transiently expands, preventing GRAMD1s from accumulating at ER-PM contacts at rest;

3) We have deciphered the novel cellular mechanisms by which the accessibility of PM cholesterol is monitored by a LTP at ER-PM contacts. We found that GRAMD1s sense a transient expansion of the accessible pool of PM cholesterol by their GRAM domain and facilitate its transport by their StART-like domain. Disruption of their functions leads to less efficient transport of accessible PM cholesterol to the ER and reduced suppression of SREBP-2 cleavage. Importantly, we showed that the formation of GRAMD1 protein complexes, as well as their StART-like and GRAM domains, is critical for the cellular functions of GRAMD1s *in vivo*;

4) Our results demonstrate that removal of accessible PM cholesterol occurs within ~1 hour, when re-expressed GRAMD1 proteins are artificially recruited to ER-PM contact sites to facilitate transport of accessible cholesterol from the PM to the ER in GRAMD1 TKO cells. These experiments utilized a drug-induced dimerization approach. In addition, this GRAMD1 function requires the sterol-transporting StART-like domain. Previous studies of yeast mutants lacking Lam/Ltc proteins relied on genetic approaches (over a time scale of ~20 hours), making it difficult to interpret the significance of their lipid transfer functions *in vivo*.

Using the CRISPR/Cas9 gene editing system, we demonstrated that GRAMD1s are not essential for cell viability. Although cells that lack all three GRAMD1s grow more slowly than wild-type cells, they do not exhibit major abnormalities. Overlapping functions between mammalian GRAMD1s and other sterol-binding STARD proteins may explain the lack of major defects in these cells. Accordingly, PM lipidomics did not reveal major differences in PM cholesterol levels in GRAMD1 TKO cells. Our analyses, however, suggest that GRAMD1s facilitate the transport of accessible cholesterol from the PM to the ER in response to a transient expansion in the accessible pool of PM cholesterol, thereby contributing to PM cholesterol homeostasis. First, GRAMD1 TKO cells exhibited an exaggerated accumulation of the accessible pool of PM cholesterol in response to acute hydrolysis of sphingomyelin,

which liberates sphingomyelin-sequestered pool of cholesterol into the “accessible pool”. This was revealed by sustained binding of the PFO D4 probe to the PM and enhanced PM recruitment of the GRAM domain of GRAMD1b, a novel biosensor for detecting acute expansion of the accessible pool of PM cholesterol that we identified in this study, in GRAMD1 TKO cells. Second, GRAMD1 TKO cells showed reduced suppression of SREBP-2 cleavage upon hydrolysis of sphingomyelin, reflecting less efficient PM to ER transport of the newly expanded pool of accessible cholesterol in these cells. Third, GRAMD1 TKO cells exhibited a chronic expansion of the accessible pool of PM cholesterol, as detected by the D4H probe. All these phenotypes are consistent with defects in efficient PM to ER transport of the accessible pool of cholesterol. Importantly, re-expression of GRAMD1b rescued these phenotypes, with rescue depending on the sterol-binding property of its StART-like domain, the GRAM domain, and protein complex formation.

Although the transition of cholesterol between “inaccessible” and “accessible” pools in the PM plays crucial roles in controlling cellular cholesterol homeostasis (Das et al., 2014; Endapally et al., 2019), the molecular mechanisms by which these transitions are monitored, and the intracellular transport machinery responsible for the PM to ER transport of the accessible pool of cholesterol, have both remained elusive. Our results suggest that these two mechanisms can be coupled by non-vesicular cholesterol transport mediated by a LTP at ER-PM contact sites. We found that GRAMD1s sense a transient expansion of the accessible pool of PM cholesterol and facilitate its transport to the ER at ER-PM contact sites (**Figure 8A-C**). We found that interactions between purified GRAM domains of GRAMD1a/b and artificial membranes that contain phosphatidylserine, which is a major acidic phospholipid in the PM, are dramatically enhanced by the presence of unsequestered/accessible cholesterol when it reaches above a certain threshold, and such interactions are modulated by sphingomyelin and phospholipids, which sequester cholesterol by forming dynamic complexes. Thus, the GRAM domain allows GRAMD1s to sense increase in accessible PM cholesterol and facilitates the accumulation of GRAMD1s at ER-PM contacts only when the accessible pool of cholesterol transiently expands in this bilayer (**Figure 8B**). Importantly, such regulation prevents GRAMD1s from depleting PM cholesterol at steady state. Loss of their functions, however, leads to chronic and acute expansion of the accessible pool of PM cholesterol (**Figure 8B,C**). It has been known that accessible cholesterol, upon reaching a certain threshold, is extracted for transport to the ER and regulate cholesterol biosynthesis to maintain homeostasis. How intracellular transport machinery senses such sharp threshold has been unknown. The ability of the GRAMD1s to accumulate at ER-PM contacts in a switch-like fashion by sensing a transient expansion of the accessible pool of PM cholesterol through their GRAM domain provides a conceptual framework for this process. Importantly, GRAMD1s themselves directly facilitate the transport of the expanded pool of accessible PM cholesterol from the PM to the ER, thereby contributing to PM cholesterol homeostasis as a critical homeostatic regulator.

Levels of PM cholesterol are maintained at an equilibrium by balancing the efflux and influx of cholesterol out of and into the PM, respectively. Thus, inhibition of the efflux pathway only (e.g., by loss of GRAMD1s) disrupts this equilibrium, potentially increasing total levels of PM cholesterol. However, levels of PM cholesterol are unchanged in GRAMD1 TKO cells (**Figure 4-figure supplement 3C,D**). Thus, alternative backup systems may support the efflux of PM cholesterol (or reduce the influx of cholesterol to the PM) to maintain total cholesterol levels in the PM in the absence of GRAMD1s. For example, recent studies found that macrophages are able to dispose of accessible cholesterol by releasing PM-derived particles that are rich in cholesterol (He et al., 2018; Hu et al., 2019). It is also important to note that suppression of

SREBP-2 cleavage upon sphingomyelinase treatment (an estimate of the efficiency of PM to ER transport of accessible cholesterol) is reduced but not eliminated in the absence of GRAMD1s (**Figure 6B,C**). Thus, other intracellular cholesterol transport machineries might also participate in the transport of accessible cholesterol from the PM to the ER. Such robust parallel mechanisms may be partially mediated by other non-vesicular sterol transport systems, such as the ones mediated by STARDs or ORPs; vesicular transport may also be involved in maintaining total levels of PM cholesterol. Further studies are needed to better understand the interplay between GRAMD1s and other sterol efflux/transfer systems in the regulation of cellular cholesterol homeostasis.

GRAMD1s interact with each other through their transmembrane domains and predicted luminal amphipathic helices (e.g., GRAMD1b homomeric and GRAMD1b/GRAMD1a heteromeric interactions). Mutant GRAMD1b proteins that lack these regions fail to interact with one another and are diffusely distributed throughout the tubular ER. Other lipid transfer proteins known to localize to membrane contact sites also form complexes/oligomers. These proteins include E-Syts (Giordano et al., 2013; Saheki et al., 2016), ORP2 (Wang et al., 2018), ORP5/8 (Chung et al., 2015), as well as the yeast ERMES complex (AhYoung et al., 2015). ORP2 oligomerization and ERMES assembly enhance the ability of these proteins to transfer lipids (Kawano et al., 2018; Wang et al., 2018). Accordingly, mutant GRAMD1b proteins that lack the ability to form protein complexes accumulate less robustly at ER-PM contacts, and less effectively rescue phenotypes associated with GRAMD1 TKO cells. Thus, the formation of GRAMD1 complexes plays important roles in regulating their localization and function.

A recent study by Sandhu et al. reported that GRAMD1s facilitate the transport of PM cholesterol that is additionally loaded from external sources. In particular, they showed that GRAMD1b mediates PM to ER transport of HDL-derived cholesterol that is taken up by adrenal glands via the scavenger receptor SR-B1 in mice (Sandhu et al., 2018). Based on these results, they proposed that GRAMD1s might also play more general roles in intracellular cholesterol transport by sensing accessible cholesterol in the PM. Our findings support this notion and further demonstrate that GRAMD1s contribute to PM cholesterol homeostasis and cholesterol metabolism by sensing a transient expansion of the accessible pool of PM cholesterol by their GRAM domain and facilitate its transport to the ER by their StART-like domain. Interestingly, GRAMD1a is broadly expressed in many tissues with particular enrichment in the brain. Future studies will be needed to determine the physiological functions of GRAMD1s in other tissues in mammals.

In summary, our study has demonstrated that ER-localized GRAMD1s help to maintain PM cholesterol homeostasis *in trans* via their ability to transport accessible cholesterol from the PM to the ER at ER-PM contact sites. Our results show that GRAMD1s sense a transient expansion of the pool of accessible PM cholesterol and facilitate its transport to the ER through non-vesicular transport. These proteins likely perform additional functions, as yeast mutants that lack Lam/Ltc proteins show pleiotropic defects in cell signaling, including altered mTOR kinase signaling (Murley et al., 2017). Furthermore, the StART-like domain of GRAMD1b has been shown to transport PI(4,5)P₂ in addition to cholesterol (Horenkamp et al., 2018). Thus, potential changes in the properties of other organelles and the PM in GRAMD1 TKO cells deserve future investigations. Further elucidating the physiological functions of these proteins, as well as other sterol-transfer proteins, at membrane contact sites will be important to gain insight into how cellular cholesterol homeostasis is regulated.

MATERIALS AND METHODS

Antibodies and Chemicals

Primary and secondary antibodies, chemicals, lipids and other reagents used in this study are listed in Supplementary File 1.

DNA Plasmids

DNA plasmids used in this study are listed in Supplementary File 1; the sequences of oligos and primers used are listed in Supplementary File 2.

For mammalian expression:

Cloning of EGFP-GRAMD1a, EGFP-GRAMD1b, EGFP-GRAMD1c and EGFP-GRAMD3

cDNAs of GRAMD1a/Aster-A (NP_065946.2), GRAMD1b/Aster-B (NP_065767.1), GRAMD1c/Aster-C (NP_060047.3), and GRAMD3 (NP_001139791.1) were amplified by PCR using the following primer sets (GRAMD1a: GRAMD1a_F and GRAMD1a_Stop_R; GRAMD1b: GRAMD1b_F and GRAMD1b_Stop_R; GRAMD1c: GRAMD1c_F and GRAMD1c_Stop_R; GRAMD3: GRAMD3_F and GRAMD3_Stop_R). PCR products were ligated in XhoI and KpnI sites for GRAMD1a, GRAMD1b, and GRAMD1c, and Sall and KpnI sites for GRAMD3 in the pEGFP-C1 vector.

Cloning of Myc-GRAMD1a, Myc-GRAMD1b, mRuby-GRAMD1b, Myc-GRAMD3, and mCherry-GRAMD3

cDNAs corresponding to GRAMD1a of EGFP-GRAMD1a and GRAMD1b of EGFP-GRAMD1b were excised and ligated into pMyc-C1 and pmRuby-C1 vectors in the XhoI and KpnI sites to generate Myc-GRAMD1a, Myc-GRAMD1b, and mRuby-GRAMD1b, respectively.

cDNA corresponding to GRAMD3 of EGFP-GRAMD3 was excised and ligated into pMyc-C1 and pmCherry-C1 vectors in the Sall and KpnI sites to generate Myc-GRAMD3 and mCherry-GRAMD3, respectively.

Cloning of EGFP-GRAMD1b Δ GRAM and EGFP-GRAMD1b Δ Helix

cDNAs corresponding to the residues 164-738 (Δ GRAM) and 1-688 (Δ Helix) of GRAMD1b were PCR amplified and ligated into pEGFP-C1 vector in the XhoI and KpnI sites, using the following primer sets: GRAMD1b DeltaNterm F and GRAMD1b_Stop_R for generating EGFP-GRAMD1b (164-738) (Δ GRAM); GRAMD1b_F and 3'_KpnI-stop_GRAMD1b_683aa for generating EGFP-GRAMD1b (Δ Helix).

Cloning of EGFP-GRAMD1b (4E) and EGFP-GRAMD1b (5E)

Hydrophobic amino acid residues (W678, L681, L682 and Y688) present in the luminal region of GRAMD1b were mutated to glutamic acid using site-directed mutagenesis in EGFP-GRAMD1b with the primer set, GRAMD1b_Helix4E_F and GRAMD1b_Helix4E_R, to generate EGFP-GRAMD1b (4E).

Hydrophobic amino acid residues (L693, W696, I699, I700, and L707) present in the predicted luminal amphipathic helix of GRAMD1b were mutated to glutamic acid using site-directed

mutagenesis in EGFP-GRAMD1b with the primer set, GRAMD1b_Helix_2_5E_F and GRAMD1b_Helix_2_5E_R, to generate EGFP-GRAMD1b (5E).

Cloning of mRuby-GRAMD1b (T469D) and mRuby-GRAMD1b (Y430A, V445A)

The amino acid residue present in the StART-like domain that was reported to be important for transporting cholesterol (T469) (Horenkamp et al., 2018) was mutated to aspartic acid using site-directed mutagenesis in mRuby-GRAMD1b with the primer set, GRAMD1b_T469D_F and GRAMD1b_T469D_R, to generate mRuby-GRAMD1b (T469D).

The amino acid residues present in the StART-like domain that were predicted to be critical for binding cholesterol based on our structural modeling (Y430 and V445) were mutated to alanine using site-directed mutagenesis in mRuby-GRAMD1b, with the primer set, GRAMD1b_Y430A_V445A_F and GRAMD1b_Y430A_V445A_R, to generate mRuby-GRAMD1b (Y430A, V445A).

Cloning of mRuby-GRAMD1b (5P)

Four residues (L434, T435, N436, L438) on the loop of the StART-like domain of GRAMD1b were mutated to proline using site-directed mutagenesis in mRuby-GRAMD1b using the primer set, GRAMD1b_434LTNPL_F and GRAMD1b_434LTNPL_R, to generate mRuby-GRAMD1b (5P).

Cloning of miRFP-FKBP-GRAMD1b (WT), miRFP-FKBP-GRAMD1b (5P) and miRFP-FKBP-GRAMD1b (T469D)

The plasmid miRFP-FKBP-GRAMD1b (WT) was generated using mCherry-pMag(x3)-MTMR1 (Benedetti et al., 2018) as a backbone.

cDNA corresponding to the residues 164-738 (Δ GRAM) of GRAMD1b was amplified by PCR using the primer set, 5'-KpnI-GRAMD1b-164aa-S and 3'-BamHI-stop-GRAMD1b-C-AS, and ligated in the KpnI and BamHI sites of mCherry-pMag(x3)-MTMR1 vector. Subsequently, cDNA corresponding to miRFP of LAMP1-miRFP was amplified by PCR using the primer set, 5' _NheI_miRFP_S and 3' _NotI_miRFP_AS, and ligated in the NheI and NotI sites of the vector to generate miRFP-pMag(x3)-GRAMD1b (164-738). Finally, cDNA corresponding to a FKBP module of mCherry-FKBP-MTM1 was amplified by PCR using the primer set, 5' _NotI_FKBP_linker_S and 3' _KpnI_FKBP_linker_AS, and ligated in the NotI and KpnI sites of miRFP-pMag(x3)-GRAMD1b (164-738) to generate miRFP-FKBP-GRAMD1b (WT).

cDNA corresponding to GRAMD1b (164-738) of miRFP-FKBP-GRAMD1b (WT) was replaced with cDNA corresponding to either GRAMD1b (164-738:5P) or GRAMD1b (164-738:T469D) by digesting either mRuby-GRAMD1b (5P) or mRuby-GRAMD1b (T469D), respectively, and ligating the resulting fragments in the EcoRV and MluI sites of miRFP-FKBP-GRAMD1b (WT) to generate miRFP-FKBP-GRAMD1b (5P) and miRFP-FKBP-GRAMD1b (T469D).

Cloning of EGFP-GRAMD1a GRAM (EGFP-GRAM_{1a}), EGFP-GRAMD1b GRAM (EGFP-GRAM_{1b}), and EGFP-GRAMD1c GRAM (EGFP-GRAM_{1c})

cDNAs corresponding to the GRAM domain residues 81-220 of GRAMD1a, 92-207 of GRAMD1b, and 65-186 of GRAMD1c were PCR amplified and ligated into pEGFP-C1 vector in the XhoI and KpnI sites, using the following primer sets: GRAMD1a_GRAM Domain_F and

GRAMD1a_GRAM Domain_R for generating EGFP-GRAMD1a GRAM; GRAMD1b_Short GRAM Domain_F and GRAMD1b_Short GRAM Domain_R for generating EGFP-GRAMD1b GRAM; GRAMD1c_GRAM Domain_F and GRAMD1c_GRAM Domain_R for generating EGFP-GRAMD1c GRAM.

Cloning of EGFP-GRAMD1b (TM swap) and mRuby-GRAMD1b (TM swap)

cDNAs corresponding to the residues 404-621 of GRAMD1b and 67-96 of Sec61 β were individually amplified by PCR with the following primer sets: 5'_GRAMD1b_iEcoRV_Fw_HiFi and 3'_GRAMD1b_621_Rv_HiFi for GRAMD1b; 5'_GRAMD1b-Sec61b_TM_Fw_HiFi and 3'_pEGFP_Sec61b_TM_Rv_HiFi for Sec61 β . The two PCR products were simultaneously ligated in the EcoRV and KpnI sites of mRuby-GRAMD1b by DNA HiFi assembly kit (NEB) to generate mRuby-GRAMD1b (TM swap). cDNA corresponding to GRAMD1b (TM swap) was excised and ligated into pEGFP-C1 vector in the XhoI and KpnI sites to generate EGFP-GRAMD1b (TM swap).

Cloning of mRuby-OSBP and mRuby-ORP9

cDNAs of OSBP (BC011581) and ORP9 (BC025978) were amplified by PCR and ligated in HindIII and BamHI sites and XhoI and HindIII sites, respectively, in the pmRuby-C1 vector, using the following primer sets (5'_HindIII_OSBP_NS and 3'_BamHI_stop_OSBP_CAS for generating mRuby-OSBP; 5'_XhoI_ORP9_NS and 3'_HindIII_stop_ORP9_CAS for generating mRuby-ORP9)

Cloning of mRuby-ORP4 and mCherry-STAR4

gBlocks (IDT) containing cDNA of ORP4 (BC118914) and STAR4 (BC042956) were synthesized (ORP4_Frag_1_XhoI, ORP4_Frag_2_BamHI, and XhoI_STAR4_KpnI) and ligated in XhoI and BamHI sites of pmRuby-C1 vector for generating mRuby-ORP4 and in XhoI and KpnI sites of pmCherry-C1 vector for generating mCherry-STAR4, respectively, using DNA HiFi assembly kit (NEB).

Cloning of PM-FRB-mCherry

cDNA corresponding to PM targeting signal (the residues 1-20 of mouse GAP43) and FRB module was digested from PM-FRB-CFP (a gift from the De Camilli Lab) and ligated into NheI and AgeI sites of pmCherry-N1 vector.

For recombinant protein purification:

Cloning of StART-like and GRAM domains of human GRAMD1s

The cDNAs corresponding to StART-like and GRAM domains of human GRAMD1 proteins were ligated into the pNIC28-Bsa4 vector with an N-terminal His₆-tag and a TEV-protease cleavage site (residues 366-537 for GRAMD1a_{StART}; 375-545 for GRAMD1b_{StART}; 325-500 for GRAMD1c_{StART}; 81-220 for GRAM_{1a}; 70-231 for GRAM_{1b}) via ligation-independent cloning to generate pNIC28-Bsa4 GRAMD1a StART L366-S537, pNIC28-Bsa4 GRAMD1b StART Q375-E545, pNIC28-Bsa4 GRAMD1c StART L325-I500, pNIC28-Bsa4 GRAMD1a GRAM 81-220 and pNIC28-Bsa4 GRAMD1b GRAM 70-231, respectively.

Cloning of GRAMD1a StART-like domain mutant (5P)

4 residues (I429, S430, N431, L433) on the loop of the StART-like domain of GRAMD1a were mutated to proline using site-directed mutagenesis in pNIC28-Bsa4 GRAMD1a StART L366-S537 using the primer set, GRAMD1a_I429SNPL_F and GRAMD1a_I429SNPL_R, to generate pNIC28-Bsa4 GRAMD1a StART L366-S537 5P.

Cloning of GRAMD1b StART-like domain mutant (5P)

4 residues (L434, T435, N436, L438) on the loop of the StART-like domain of GRAMD1b were mutated to proline using site-directed mutagenesis in pNIC28-Bsa4 GRAMD1b StART Q375-E545 using the primer set, GRAMD1b_434LTNPL_F and GRAMD1b_434LTNPL_R, to generate pNIC28-Bsa4 GRAMD1b StART Q375-E545 5P.

Cloning of GRAMD1b StART-like domain mutant (T469D)

T469 was mutated to aspartate using site-directed mutagenesis in pNIC28-Bsa4 GRAMD1b StART Q375-E545 using the primer set, GRAMD1b_T469D_F and GRAMD1b_T469D_R, to generate pNIC28-Bsa4 GRAMD1b StART Q375-E545 T469D.

Cloning of EGFP-linker-GRAMD1b luminal helix and EGFP-linker-GRAMD1b luminal helix 5E

gBlocks (IDT) containing EGFP-(GGGS)₃-GRAMD1b luminal helix (674-718) and EGFP-(GGGS)₃-GRAMD1b luminal helix (674-718) carrying 5E mutations were synthesized (EGFP-GRAMD1b 674-718aa and EGFP-GRAMD1b_Helix_5E) and amplified by PCR using the primer set, 5'NcoI_eGFP_1b_Helix and 3'XhoI_eGFP_1b_Helix. The PCR products were then ligated in NcoI and XhoI sites in the pET28b(+) vector to generate EGFP-linker-luminal He and EGFP-linker-luminal He with 5E.

Cloning of EGFP-D4 and EGFP-D4H (D434S)

gBlock (IDT) containing EGFP-D4 was synthesized (BsrG1-D4_E.coli-BamHI) and ligated into the pNIC28-Bsa4 vector via ligation-independent cloning to generate EGFP-D4-CLOPF-ec01. D434 was mutated to serine (Maekawa and Fairn, 2015) using site-directed mutagenesis in EGFP-D4-CLOPF-ec01 using the primer set, D4_D434S_F and D4_D434S_R, to generate pNIC28-Bsa4 EGFP-D4H.

Cell Culture and Transfection

HeLa and COS-7 cells were cultured in Dulbecco's modified Eagle's medium (DMEM) containing 10% or 20% fetal bovine serum (FBS) and 1% penicillin/streptomycin at 37°C and 5% CO₂. Transfection of plasmids was carried out with Lipofectamine 2000 (Thermo Fisher Scientific). Wild-type as well as genome-edited HeLa cell lines were routinely verified as free of mycoplasma contamination at least every two months, using MycoGuard Mycoplasma PCR Detection Kit (Genecopoeia). No cell lines used in this study were found in the database of commonly misidentified cell lines that is maintained by ICLAC and NCBI Biosample.

Fluorescence Microscopy

For imaging experiments, cells were plated on 35 mm glass bottom dishes at low density (MatTek Corporation). All live cell imaging were carried out one day after transfection.

Spinning disc confocal (SDC) microscopy (Figures 3A, 4D, 7A,E, 4-figure supplement 2A, 4-figure supplement 3A, 5-figure supplement 2A, 7-figure supplement 1A, 7-figure supplement

2A,E,G) and superresolution SDC-structured illumination microscopy (SDC-SIM) (Figures 1B,C, 2C,H-I, 1-figure supplement 1A,B) were performed on a setup built around a Nikon Ti2 inverted microscope equipped with a Yokogawa CSU-W1 confocal spinning head, a Plan-Apo objective (100x1.45-NA), a back-illuminated sCMOS camera (Prime 95B; Photometrics), and a super resolution module (Live-SR; Gataca Systems) based on structured illumination with optical reassignment and image processing (Roth and Heintzmann, 2016). The method, known as multifocal structured illumination microscopy (York et al., 2012), allows combining the doubling of the resolution with the optical sectioning capability of confocal microscopy. The maximum resolution is 128 nm with a pixel size in super resolution mode of 64 nm. Excitation light was provided by 488-nm/150mW (Coherent) (for GFP), 561-nm/100mW (Coherent) (for mCherry/mRFP/mRuby) and 642-nm/110mW (Vortran) (for iRFP/miRFP) (power measured at optical fiber end) DPSS laser combiner (iLAS system; Gataca systems), and all image acquisition and processing was controlled by MetaMorph (Molecular Device) software. Images were acquired with exposure times in the 400-500 msec range.

Total internal reflection fluorescence (TIRF) microscopy (Figures 3B,G,H, 4E, 5E,F, 6A,F,G, 7D,3-figure supplement 1A, 4-figure supplement 2B, 5-figure supplement 2B-E, 6-figure supplement 1C,D, 7-figure supplement 3A-C) was performed on a setup built around a Nikon Ti2 inverted microscope equipped with a HP Apo-TIRF objective (100X1.49-NA), and a back-illuminated sCMOS camera (Prime 95B; Photometrics). Excitation light was provided by 445-nm/25mW (for CFP), 488-nm/70mW (for GFP), 561-nm/70mW (for mCherry/mRFP/mRuby) and 647-nm/125mW (for iRFP/miRFP) (power measured at optical fiber end) DPSS laser combiner (Nikon LU-NV laser unit), coupled to the motorized TIRF illuminator through an optical fiber cable. Critical angle was maintained at different wavelengths throughout the experiment from the motorized TIRF illuminator. Acquisition was controlled by Nikon NIS-Element software. For time-lapse imaging, images were sampled at 0.05 Hz with exposure times in the 200-500 msec range.

Cells were washed twice and incubated with Ca^{2+} containing buffer (140 mM NaCl, 5 mM KCl, 1 mM MgCl_2 , 10 mM HEPES, 10 mM glucose, and 2 mM CaCl_2 [pH 7.4]) before imaging with either a SDC microscope or a TIRF microscope. All types of microscopy were carried out at 37 °C except for the experiments with recombinant EGFP-D4H proteins that were performed at room temperature via SDC microscopy.

Drug stimulation for time-lapse TIRF imaging

For all time-lapse TIRF imaging experiments with drug stimulation, drugs were added to the cells 5 min after the initiation of the imaging except for methyl- β -cyclodextrin (MCD) treatment, where 10 mM MCD (Sigma-Aldrich/Merck) was added to the cells as indicated in a figure (Figure 4-figure supplement 2B). Other drugs were used with the following concentration: 200 μM cholesterol/MCD complex generated as described previously (Brown et al., 2002); 100 mU/ml sphingomyelinase (SMase) (Sigma-Aldrich/Merck); 200 nM rapamycin (Sigma-Aldrich/Merck).

Assays with recombinant EGFP-D4H proteins

For the assays with recombinant EGFP-D4H proteins (Figures 7A,B,E,F, 7-figure supplement 1A,B, 7-figure supplement 2A,B,E,F,G,H), transfected cells with or without drug treatment were washed once with Ca^{2+} containing buffer and subsequently incubated with the same buffer containing recombinant EGFP-D4H proteins (15 $\mu\text{g}/\text{ml}$) for 15 min at room temperature.

Cells were then washed twice with the same buffer without EGFP-D4H proteins and immediately imaged under SDC microscopy at room temperature.

For the experiments with MCD treatment (Figure 7-figure supplement 1A,B), GRAMD1 TKO cells were transfected with iRFP-PH-PLC δ . On the following day, cells were washed with Ca²⁺ containing buffer and incubated for 30 min at room temperature with the same buffer containing 10 mM MCD (Sigma-Aldrich/Merck) before staining with recombinant EGFP-D4H proteins for SDC microscopy.

For rescue experiments with mRuby-GRAMD1 constructs (Figure 7-figure supplement 2A,B,E,F,G,H), GRAMD1 TKO cells were transfected with iRFP-PH-PLC δ together with indicated mRuby-GRAMD1 constructs. On the following day, cells were stained with recombinant EGFP-D4H proteins and imaged under SDC microscopy.

For rapamycin-induced dimerization experiments (Figure 7E,F), GRAMD1 TKO cells were transfected with PM-FRB-mCherry and either one of the three miRFP-FKBP-GRAMD1b constructs (WT, 5P, or T469D). On the following day, 200 nM rapamycin (Sigma-Aldrich/Merck) was added to the culture media and further incubated for either 30 min or 60 min at 37 °C before staining with recombinant EGFP-D4H proteins for SDC microscopy.

Image analysis

All images were analyzed off-line using Fiji (<http://fiji.sc/wiki/index.php/Fiji>). Quantification of fluorescence signals was performed using Excel (Microsoft) and Prism 7 or 8 (GraphPad Software). All data are presented as mean \pm s.e.m. In dot plots, each dot represents value from a single cell with the black bar as the mean.

For time-lapse imaging via TIRF microscopy, changes in PM fluorescence over time were analyzed by manually selecting regions of interest covering the largest possible area of the cell foot-print. Mean fluorescence intensity values of the selected regions were obtained and normalized to the average fluorescence intensity before stimulation after background subtraction.

For analysis of the binding of recombinant EGFP-D4H proteins to the PM via SDC microscopy, line scan analysis was performed. A line of 5 μ m in length was manually drawn around the PM (see dashed white lines in Figure 7A and Figure 7-figure supplement 1A), and EGFP fluorescence intensity along the manually drawn line was measured. The minimum fluorescence intensity along the line was subtracted from the maximum fluorescence intensity (corresponding to the PM-bound EGFP-D4H fluorescence) and plotted for quantification.

Generation of GRAMD1 Knockout HeLa Cell Lines

The GRAMD1B, GRAMD1A and GRAMD1C genes were sequentially targeted to generate GRAMD1 triple knockout cells. The sequences of oligos and primers used are listed in Supplementary File 2.

For the generation of HeLa cells lacking GRAMD1b, control wild-type HeLa cells were transfected with a plasmid encoding spCas9 and the GRAMD1b-targeting guide RNA (Figure 4A) followed by isolation of individual clones by dilution cloning. Two clones (#10 and #17) were further characterized with sequencing and immunoblotting (i.e. western blotting). These analyses revealed deletions and insertions within the guide RNA-binding sites, frame-shift and

early termination in the open-reading frame of GRAMD1B gene, and the loss of GRAMD1b protein expression (Figure 4-figure supplement 1A, C). To generate GRAMD1a/1b double knockout (DKO) cell lines, a subclone of the GRAMD1b KO cell line #10 was transfected with a plasmid encoding spCas9 and the GRAMD1a-targeting guide RNA with ssDNA oligos containing stop codons and homology-arms (Figure 4A). These cells were followed by single cell sorting, and individually isolated clones, line #38 and #40 (hereafter GRAMD1a/1b DKO #38 and GRAMD1a/1b DKO #40), showed insertion of ssDNA within the guide RNA-targeted locus, resulting in the lack of GRAMD1a protein expression (Figures 4B and 4-figure supplement 1B, D).

To generate GRAMD1 triple knockout (TKO) cell lines, the GRAMD1a/1b DKO #40 cell line was transfected with two plasmids encoding spCas9 and each one of the two GRAMD1b-targeting guide RNAs (Figure 4A). Two clones (GRAMD1a/1b/1c TKO #1 and GRAMD1a/1b/1c TKO #15) that showed large deletions in the exon 11 of GRAMD1C by genomic PCR (Figure 4-figure supplement 1E) were isolated and knock-outs were confirmed by direct sequencing (Figure 4C). In all figures and texts, TKO denotes GRAMD1a/1b/1c TKO #15 unless stated.

GRAMD1b knockout:

The genomic sequence surrounding the exon 13, which encodes the amino acid stretch in the StART-like domain of human GRAMD1b, was analyzed for potential CRISPR/Cas9 targets *in silico* using the Cas9 design target tool (<http://crispr.mit.edu>) (Hsu et al., 2013). The GRAMD1B genomic sequence targeted by the predicted CRISPR gRNA is: TCGCTACACGCTCACCCGTGTGG (GRAMD1b-sgRNA)

The CRISPR targeting site was synthesized by annealing GRAMD1b-sgRNA#1_S and GRAMD1b-sgRNA#1_AS and sub-cloned into a human codon-optimized Cas9 and chimeric gRNA expression plasmid that carries puromycin resistance, pSpCas9(BB)-2A-Puro (PX459), obtained from Addgene (Plasmid 48139) (Ran et al., 2013) to generate PX459-GRAMD1B_Back.

HeLa cells were transiently transfected with the PX459-GRAMD1B_Back plasmid. 24 hours after transfection, cells were supplemented with growth media containing puromycin (1.5 µg/mL) and incubated for 72 hours. Cells resistant to puromycin selection were then incubated with puromycin-free medium for 24 hours before harvesting for dilution cloning and assessed by genotyping PCR using the primer set, Genotyping_1B_F2 and Genotyping_1B_R1, to obtain GRAMD1b knockout cells.

GRAMD1a knockout:

The genomic sequence surrounding the exon 13, which encodes the amino acid stretch in the StART-like domain of human GRAMD1a, was analyzed *in silico* using the Cas9 design target tool (<http://crispr.mit.edu>) (Hsu et al., 2013). The GRAMD1A genomic sequence targeted by the predicted CRISPR gRNA is: GGACTCCGAGGTGCTGACGCAGGG (GRAMD1a-sgRNA).

The CRISPR targeting site was synthesized by annealing GRAMD1a_sgRNA#1_S and GRAMD1a_sgRNA#1_AS and sub-cloned into PX459 (Ran et al., 2013) to generate PX459-GRAMD1A_V2_Front.

To knock-in the sequence with stop codons, ssDNA containing stop codons and homology-arms surrounding the guide RNA targeting site was designed. The ssDNA of the reverse complementary sequence was synthesized by IDT and used for the transfection with PX459-GRAMD1A_V2_Front plasmid. The sequence of ssDNA was :GTGGGCAGTGTAGAAGTAGTCCTGGTAGGGGATGCCCTGCGGATCCCGGGCCCGCGGTACCGAATTCTGAAGCTTGAGCTCGAGATCTActagttaatcaGTCAGCACCTCGGAGTCCACCACACACCCGCCGGCCTGGG, where homology arms are indicated by the underline (ssDNA_StopKI_HR_GRAMD1a_V2).

Control HeLa cells and GRAMD1b knockout cell line #10 were transiently transfected with the PX459-GRAMD1A_V2_Front plasmid with ssDNA. 24 hours after transfection, cells were supplemented with growth media containing puromycin (1.5 µg/mL) and incubated for 72 hours. Cells resistant to puromycin selection were then incubated with puromycin-free medium for 24 hours before harvesting for single cell sorting, and individually isolated cell clones were assessed by genotyping PCR using the primer set, GRAMD1a_Genotyping_V2V3_F2 and GRAMD1a_Genotyping_V2V3_R2, to obtain GRAMD1a knockout and GRAMD1a/1b DKO cell lines.

GRAMD1c knockout:

The genomic sequence surrounding the exon 11, which encodes the amino acid stretch in the StART-like domain of human GRAMD1c, was analyzed *in silico* using the Cas9 design target tool (<http://crispr.mit.edu>) (Hsu et al., 2013). The GRAMD1C genomic sequences targeted by the predicted CRISPR gRNAs are: TAGATGGTAGTATCTACCCCTTGG (GRAMD1c-sgRNA#1) and ACTATTAAGGACTATAGTGTAGG (GRAMD1c-sgRNA#2).

The two CRISPR targeting sites were synthesized by annealing GRAMD1c-sgRNA#1_S and GRAMD1c-sgRNA#1_AS for GRAMD1c-sgRNA#1, and GRAMD1c-sgRNA#2_S and GRAMD1c-sgRNA#2_AS for GRAMD1c-sgRNA#2, respectively, and individually sub-cloned into PX459 (Ran et al., 2013) to generate PX459-GRAMD1c_sgRNA_#1 and PX459-GRAMD1c_sgRNA_#2.

GRAMD1a/1b DKO cell line #40 was transiently transfected with the two GRAMD1c CRISPR/Cas9 plasmids, PX459-GRAMD1c_sgRNA_#1 and PX459-GRAMD1c_sgRNA_#2. 24 hours after transfection, cells were supplemented with growth media containing puromycin (1.5 µg/mL) and incubated for 72 hours. Cells resistant to puromycin selection were then incubated with puromycin-free medium for 24 hours before harvesting for single cell sorting, and individually isolated clones were assessed by genotyping PCR using the primer set, GRAMD1c_Genotyping_F1 and GRAMD1c_Genotyping_R1, to obtain GRAMD1a/1b/1c triple knockout cell lines.

Sequencing of mutant alleles:

For GRAMD1a and GRAMD1b knockout cells, sequencing of mutated alleles was carried out by cloning PCR products into the pCR4 Blunt-TOPO vector using the Zero Blunt TOPO PCR cloning Kit for sequencing (Thermo Fisher Scientific). Biallelic insertions/deletions were confirmed by sequencing at least 10 individual colonies. The same primers were used as genotyping primers. For GRAMD1c knockout cells, sequencing of mutated alleles was carried out by direct-sequencing of the genomic PCR products. The same primers were used as genotyping primers.

Biochemical Analyses

Plasma membrane isolation and protein extraction

The procedure was modified from (Cohen et al., 1977; Saheki et al., 2016). Briefly, 2g of Cytodex 3 microcarrier beads (Sigma-Aldrich/Merck) were reconstituted in 100 ml Phosphate-Buffered Saline (PBS), autoclaved and coated by incubation with a poly-D-lysine solution overnight at 37 °C. Cells were added to the reconstituted beads in sterile PETG flasks (Thermo Fisher Scientific), allowed to attach to the beads for 4 hours with a gentle stirring every 30 min and then further incubated overnight with continuous stirring on rotating incubator at 37 °C with 5% CO₂. Beads were subsequently collected by spontaneous sedimentation and incubated with 220 mM Sucrose, 40 mM Sodium Acetate, pH 5.0 for 5 min at room temperature (Cohen et al., 1977). After the acid treatment, beads were collected, incubated with a hypotonic solution (10 mM Tris-HCl, pH 8.0) and vortexed for 10 seconds. A 10 seconds sonication pulse was then applied to the beads with Vibra Cell VCX130 (Sonics & Materials, Inc.) in the same solution. Beads were finally washed three times with the same solution and once with PBS for lipidomic analysis and for protein extraction with SDS lysis buffer [10 mM Tris-HCl, 150 mM NaCl, 2% SDS, pH 8.0].

Lipidomics

Lipids were extracted from either total cells still attached to the beads (total lipids), or from beads-bound plasma membranes prepared as described above (PM lipids) according to the Bligh-Dyer method (Bligh and Dyer, 1959).

Samples were then spiked with a SPLASH LIPIDOMIX deuterated lipid internal standard solution (Avanti Polar Lipids) and lipidomic analyses were performed in shotgun mode, using a Nanomate nanoflow electrospray infusion device (Advion BioSciences) coupled to a QExactive mass spectrometer (Thermo Fisher Scientific) in both positive and negative polarity (Surma et al., 2015). For measurements of cholesterol, samples were spiked with cholesterol D₆, derivatized with acetyl chloride (Lyons et al., 1981) and analyzed in direct infusion positive ion mode. Lipids were identified with LipidXplorer (Sales et al., 2017), using the accurate mass of intact lipid ions for identification and characteristic masses of fragment ions for confirmation. Quantification of lipids was performed using class-specific internal standards. To ensure analytical quality, WT/KO samples, as well as PM/total lipids, were injected in alternating order and bracketed by replicate injections of a pooled quality control (QC) sample and solvent blanks. Only analytes which showed RSD<20% in the QC samples, and a blank/sample ratio of <10%, were reported.

Immunoblotting and immunoprecipitation

Immunoblotting

HeLa cells were lysed in buffer containing 2% SDS, 150 mM NaCl, 10 mM Tris (pH 8.0), and incubated at 60 °C for 20 min followed by additional incubation at 70 °C for 10 min. The lysates were treated with Benzonase Nuclease (Sigma-Aldrich/Merck or SantaCruz) for 10-15 min at room temperature. The bicinchoninic acid assay (BCA assay) kit (Thermo Fisher Scientific) was used to measure protein concentration. Cell lysates were processed for SDS-PAGE and immunoblotting with standard procedure. All immunoblotting were developed by chemiluminescence using the SuperSignal West Dura reagents (Thermo Fisher Scientific). For SMase treatment assay, cells were cultured in DMEM supplemented with 10% Lipoprotein

Deficient Serum (LPDS) (Sigma-Aldrich/Merck) and 50 μ M mevastatin (Santa Cruz) for 16 hours and then treated with 100 mU/ml SMase in the same culture media at 37 °C for the indicated time before cell lysis (Figures 6 B-E, 6-figure supplement 1A,B). For experiments with recombinant EGFP-D4 proteins, cells that had been treated in the same way as the SMase treatment assay were washed once with PBS and subsequently incubated with PBS containing recombinant EGFP-D4 proteins (10 μ g/ml) for 15 min at room temperature. Cells were then washed three times with PBS without EGFP-D4 proteins and immediately lysed (Figure 6-figure supplement 2A,B).

Immunoprecipitation

HeLa cells expressing the indicated constructs were washed in cold PBS and lysed on ice in lysis buffer [50 mM Tris, 150 mM NaCl, 1% NP-40, 0.5 mM EDTA, 10% glycerol, pH 7.4 and protease inhibitor cocktail (Complete, mini, EDTA-free; Roche)]. Cell lysates were then centrifuged at 21,000 g for 20 min at 4 °C. For anti-GFP and anti-Myc immunoprecipitation, supernatants were incubated with GFP-trap and Myc-trap agarose beads (Chromotek), respectively for 30 min at 4 °C under rotation. Subsequently, beads were washed in lysis buffer containing 1% NP-40 once and 0.2% NP-40 twice. Afterwards, immunoprecipitated proteins bound to the beads were incubated in PAGE sample loading buffer (containing 2% SDS) and then incubated at 60 °C for 20 min and 70 °C for 10 min. Immunoprecipitates were processed for SDS-PAGE and immunoblottings were carried out as described above.

Protein purification

Expression and purification of EGFP-D4, EGFP-D4H, GRAMD1_{CStART}, GRAM_{1a} and GRAM_{1b}

All proteins were overexpressed in *E. coli* BL21-DE3 Rosetta cells. Inoculation cultures were started in 20 ml Terrific Broth (TB) media supplemented with appropriate antibiotics. The cultures were incubated at 37 °C, 200 rpm overnight. The following morning, bottles of 750 ml TB supplemented with appropriate antibiotics and 100 μ l of antifoam 204 (Sigma-Aldrich/Merck) were inoculated with the inoculation cultures. The cultures were incubated at 37 °C in the large-scale expression (LEX) system with aeration and agitation through the bubbling of filtered air through the cultures. When the OD₆₀₀ reached ~2, the temperature was reduced to 18 °C and the cultures were induced with 0.5 mM IPTG. Protein expression was allowed to continue overnight. The following morning, cells were harvested by centrifugation at 4,200 rpm, 15 °C for 10 min and re-suspended in lysis buffer (100 mM HEPES, 500 mM NaCl, 10 mM Imidazole, 10 % glycerol, 0.5 mM TCEP, pH 8.0), supplemented with proteinase inhibitors (Protease Inhibitor Cocktail Set III, EDTA free; Calbiochem) together with Benzonase Nuclease (Sigma-Aldrich/Merck)]. The re-suspended cell pellet suspensions were sonicated on ice by Vibra Cell (Sonics & Materials, Inc.) (70% power, 3 seconds pulse on, 3 seconds pulse off for 3 min). The lysate was clarified by centrifugation at 47,000g, 4°C for 25min. The supernatants were filtered through 1.2 μ m syringe filters and loaded directly onto AKTA Xpress system (GE Healthcare). The lysates were loaded on immobilized metal affinity chromatography (IMAC) columns. The sample-loaded columns were washed with 20 column volumes (CV) of wash buffer 1 (20 mM HEPES, 500 mM NaCl, 10 mM Imidazole, 10% glycerol, 0.5 mM TCEP, pH 7.5) and 20 CV of wash buffer 2 (20 mM HEPES, 500 mM NaCl, 25 mM imidazole, 10% glycerol, 0.5 mM TCEP, pH 7.5) or until a stable baseline was obtained. 5 CV of elution buffer 1 (20 mM HEPES, 500 mM NaCl, 500 mM imidazole, 10% glycerol, 0.5 mM TCEP, pH 7.5) was used to elute proteins from IMAC columns and stored in sample loops on the system before injecting into gel filtration columns for further purification, using elution buffer 2 (20 mM HEPES, 300 mM NaCl, 10% glycerol, 0.5 mM TCEP, pH 7.5). Relevant peaks were pooled, and the protein sample was concentrated in Vivaspin 20 filter concentrators (VivaScience).

Expression and purification of EGFP-helix, EGFP-helix (5E), GRAMD1a_{START}, GRAMD1b_{START}, GRAMD1b_{START} T469D and 5P mutants of GRAMD1a_{START} and GRAMD1b_{START}

All proteins were overexpressed in *E. coli* BL21-DE3 Rosetta cells. The cell cultures were grown at 37 °C until OD₆₀₀ reaches ~0.5-0.7 with appropriate antibiotics. 0.1 mM IPTG (Thermo Fisher Scientific) was then added, and the culture was further grown at 18 °C for 14-18 hours to allow protein expression. Cells were harvested by centrifugation at 4,700 g, 4 °C for 15 min and re-suspended in lysis buffer (100 mM HEPES, 500 mM NaCl, 10 mM imidazole, 10% glycerol, 0.5 mM TCEP, pH 7.5), supplemented with protease inhibitors (Complete, EDTA-free; Roche) together with Benzonase Nuclease (Sigma-Aldrich/Merck) or the cocktail of 100 ug/ml lysozyme (Sigma-Aldrich/Merck) and 50 ug/ml DNase I (Sigma-Aldrich/Merck). Cells were lysed with sonication on ice by Vibra Cell (Sonics & Materials, Inc.) (70% power, 3 seconds pulse on, 3 seconds pulse off for 3 min for five rounds). The lysate was clarified by centrifugation at 47,000g, 4 °C for 20 min. The supernatants were incubated at 4 °C for 30 min with either 1 ml Co-TALON (Takara Bio Inc.) or Ni-NTA resin (Thermo Fisher Scientific), which had been equilibrated with 10 ml of wash buffer 1. The protein-resin mixtures were then loaded onto a column to be allowed to drain by gravity. The column was washed with 10 ml of wash buffer 1 twice and 10 ml of wash buffer 2 twice and eluted with 5 ml of elution buffer 1. The proteins were then concentrated using Vivaspin 20 MWCO 10 kDa (GE Healthcare) or Amicon ultra-15 MWCO 10 kDa (Merck) and further purified by gel filtration (Superdex 200 increase 10/300 GL, GE Healthcare) with elution buffer 2, using AKTA Pure system (GE Healthcare). Relevant peaks were pooled, and the protein sample was concentrated.

Blue native (BN)-PAGE analysis of the EGFP-helix and EGFP-helix (5E)

BN-PAGE was performed using Native Page™ Novex® Bis-Tris Gel System (Thermo Fisher Scientific) according to the manufacturer's instructions. Briefly, 1 µg of purified proteins [EGFP-helix and EGFP-helix (5E)] were loaded on a 3-12% Bis-Tris gel. Electrophoresis was performed at 4 °C at constant 150 V for 1 h and then at constant 250 V. The gel was stained by colloidal blue (Thermo Fisher Scientific) according to the manufacturer's instruction. Gel filtration calibration kit LMW (GE healthcare) was used as marker proteins.

Liposome-based Experiments

Liposome Preparation

Lipids in chloroform were dried under a stream of N₂ gas followed by further drying in the vacuum for 2 h. Mole percent of lipids used for the acceptor and donor liposomes in FRET-based lipid transfer assays were shown in Supplementary File 3. The dried lipid films were hydrated with HK buffer (50 mM HEPES, 120 mM potassium acetate, pH 7.5). Liposomes were then formed by five freeze-thaw cycles (liquid N₂ and 37 °C water bath) followed by extrusion using Nanosizer™ with a pore size of 100 nm (T&T Scientific Corporation). All liposomes except the ones in Figure 3-figure supplement 1D were subjected to extrusion.

FRET-based DHE Transfer Assays

Buffer of the purified proteins was exchanged to HK buffer prior to the FRET-based DHE transfer assay. Reactions were performed in 50 µl volumes. The final lipid concentration in the reaction was 1 mM, with donor and acceptor liposomes added at a 1:1 ratio (only acceptor liposomes contain 2.5% DNS-PE, see Supplementary File 3 for the lipid compositions). Reactions were initiated by the addition of protein to a final concentration of 0.5-2 µM in a 96-well plate (Corning). The fluorescence intensity of DNS-PE (i.e. FRET signals), resulting from FRET between DNS-PE and DHE (excited at 310 nm), was monitored at 525 nm every 15

seconds over 30 min at room temperature by using a Synergy H1 microplate reader (Biotek). The values of blank solution (buffer only) were subtracted from all the values from each time point, and data were presented by setting the first value to zero at $t = 0$.

In some experiments, data were expressed as the number of DHE molecules transferred using the calibration curve (Figure 5-figure supplement 1B-E). For the generation of the calibration curve, FRET signals were measured for the liposomes containing either 0%, 5% (1.25 nmole), 10% (2.5 nmole) or 15% (3.75 nmole) DHE and 2.5% DNS-PE (0.5 mM lipids in total: compositions of the liposomes can be found in Supplementary File 3). The mean of FRET signals at $t = 0$ from three replicates were plotted versus DHE mole number in liposomes (Figure 5-figure supplement 1A). Then, the mole number of the transferred DHE from the donor to acceptor liposomes in *in vitro* DHE transfer assay was obtained using the following formula: $y = 7649.6667 + 5946.61531x$ (derived from the linear fit of the calibration curve). To obtain x (the amount of transferred DHE in nmole shown in the y axis of Figure 5-figure supplement 1F), the FRET values from each time point of the *in vitro* lipid transfer assay was put in y of the equation. Transfer rates of individual StART-like domain were obtained from the slopes of the graphs using one phase association function of Prism 7 (GraphPad) (Figure 5-figure supplement 1F).

Liposome Sedimentation Assays

Heavy liposomes were prepared by hydrating 1.6 mM dried lipid films in HK buffer containing sucrose (50 mM HEPES, pH 7.5, 120 mM K-acetate and 0.75 M sucrose) and subjected to freeze-thaw cycles five times. Next, 200 μ l of heavy liposomes were pelleted and washed with HK buffer without sucrose twice to remove unencapsulated sucrose. Pelleted heavy liposomes were resuspended in 200 μ l HK buffer and incubated with 7.5-10 μ g of the indicated proteins for 1 h at room temperature. Unbound proteins (supernatant) were separated from liposome-bound proteins (pellet) by centrifugation at 21,000 \times g for 1 h at 25 ° C. After centrifugation, the supernatant was removed, and pellets were re-suspended in 200 μ l HK buffer. 20 μ l samples were taken from both fractions and run on SDS-PAGE followed by colloidal blue staining. Quantification of the bands was performed using Fiji.

Molecular Modeling

The modeled structure of GRAMD1b_{StART} was obtained by submitting the primary sequence (residues 375-545) to I-TASSER server and using GRAMD1a_{StART} structure (PDB: 6GQF) as the template.

Primary sequences of luminal helices of GRAMD1s (GRAMD1a, 657-706; GRAMD1b, 672-720; GRAMD1c, 599-647) were submitted to I-TASSER server without assigning any templates. Only the luminal amphipathic helix region, indicated in Figure 2A, is shown in Figure 2-figure supplement 1B-C.

Statistical Analysis

No statistical method was used to predetermine sample size, and the experiments were not randomized for live cell imaging. Sample size and information about replicates are described in the figure legends. The number of biological replicate for all cell-based experiments and the number of technical replicate for all other biochemical assays are shown as the number of independent experiment within figure legends for each figure. Comparisons of data were carried out by the two-tailed unpaired Student's t-test, Holm-Sidak's t-test or the one-way

ANOVA followed by Tukey or Dunnett corrections for multiple comparisons as appropriate with Prism 7 or 8 (GraphPad software). Unless $P < 0.0001$, exact P values are shown within figure legends for each figure. $P > 0.05$ was considered not significant.

ACKNOWLEDGEMENTS

We thank Pietro De Camilli, Min Wu, Luo Dahai, Darshini Jeyasimman, Jingbo Sun, Nur Raihanah Binte Mohd Harion and Dhakshenya Dhinakaran for discussion and/or sharing reagents. We thank the NTU Protein Production Platform (www.proteins.sg) for the cloning, expression tests and purification of wild-type StART-like domains of GRAMD1a, GRAMD1b, GRAMD1c and GRAM domains of GRAMD1a and GRAMD1b, and recombinant EGFP-D4 and EGFP-D4H proteins. This work was supported in part by the Singapore Ministry of Education Academic Research Fund Tier 2 (MOE2017-T2-2-001), a Nanyang Assistant Professorship (NAP), a Lee Kong Chian School of Medicine startup grant (LKCmedicine-SUG), and a Grant-in-Aid for Young Scientists (A) from the Japan Society for the Promotion of Science (17H05065) to Y.S. M.R.W., F.T.T. and A.T. were supported by grants from the National University of Singapore via the Life Sciences Institute (LSI) and the National Research Foundation (NRFI2015-05 and NRFSBP-P4). T.N. was supported by a fellowship from the Japanese Society for Promotion of Science.

CONFLICT OF INTERESTS

The authors declare no competing interests.

FIGURE LEGENDS

Figure 1. GRAMD proteins form homo- and hetero-meric complexes.

A. Domain structure of GRAMD proteins in comparison to yeast Lam6/Ltc1.

B. Confocal images of live COS-7 cells expressing the ER membrane marker RFP-Sec61 β and EGFP-GRAMD protein constructs as indicated. Insets show at higher magnification the regions indicated by white dashed boxes. Note the presence of the patches of EGFP-GRAMDs throughout the tubular ER. Scale bars, 10 μ m.

C. Confocal images of live COS-7 cells expressing mRuby-GRAMD1b and EGFP-GRAMD1s as indicated. Note the presence of mRuby-GRAMD1b patches that are partially overlapping with the patches of EGFP-GRAMD1s. Scale bars, 1 μ m.

D and E. Extracts of HeLa cells transfected with the indicated constructs were subjected to anti-GFP immunoprecipitation (IP) and then processed for SDS-PAGE and immunoblotting (IB) with anti-GFP and anti-Myc antibodies. Inputs are 1% of the total cell lysates. Note the strong biochemical interaction (**D**) between GRAMD1b and GRAMD1s and (**E**) between GRAMD3 and GRAMD1s. Immunoprecipitated EGFP-GRAMD1s, Myc-GRAMD1b and Myc-GRAMD3 are indicated by arrows.

Figure 2. Luminal helix and transmembrane domain of GRAMD1b are important for homo- and hetero-meric interaction.

A. Sequence alignment of the luminal region of GRAMD1s. This region is predicted to contain an amphipathic helix by Phyre2 (Kelley et al., 2015) as indicated. Blue and red asterisks mark partially conserved hydrophobic amino acid residues of GRAMD1s. The identity of the amino acid sequence of the predicted amphipathic helices: 75% (GRAMD1a v.s. GRAMD1b); 75% (GRAMD1a v.s. GRAMD1c); 80% (GRAMD1b v.s. GRAMD1c) by BLAST analysis. The effects of the mutations of these residues to glutamic acid (4E in the case of blue marked; 5E in the case of red marked) are tested in GRAMD1b. Black, red, blue, and pink/purple colors denote hydrophobic, acidic, basic, and hydrophilic amino acid residues, respectively.

B. Predicted luminal amphipathic helix region of wild-type GRAMD1b (left panel) and that with L693E, W696E, I699E, I700E and L707E (5E) mutations (right panel) are shown as helical wheel representation. Predictions were made with the Heliquest server (Gautier et al., 2008).

C. Confocal images of live COS-7 cells expressing RFP-Sec61 β and EGFP fusions of various GRAMD1b constructs [Control, wild-type GRAMD1b; Δ helix, GRAMD1b lacking the predicted luminal amphipathic helix; 4E, GRAMD1b with 4E mutations in the luminal region (W678E, L681E, L682E, Y688E); 5E, GRAMD1b with 5E mutations in the predicted luminal amphipathic helix]. Note the reduced formation of GRAMD1b patches in Δ helix and 5E mutants but not in 4E mutant. Scale bars, 2 μ m.

D. Overlay of the size exclusion chromatography (SEC) profiles of the recombinant EGFP-tagged luminal helix region of wild-type GRAMD1b (EGFP-helix) and EGFP-helix with the 5E mutations [EGFP-helix (5E)]. Note the difference in elution volumes, indicating the formation of complexes mediated by wild-type luminal helix.

E. Blue native (BN)-PAGE analysis (left panel) and SDS-PAGE analysis (right panel) of SEC-purified EGFP-helix and EGFP-helix (5E). Black and red arrows indicate the major bands for EGFP-helix and EGFP-helix 5E, respectively. Note the difference in their migration pattern in BN-PAGE. CB, Colloidal blue staining.

F. Extracts of HeLa cells transfected with the constructs as indicated were subjected to anti-GFP immunoprecipitation (IP) and then processed for SDS-PAGE and immunoblotting (IB) with anti-GFP and anti-Myc antibodies. Inputs are 5% of the total cell lysates. Note that the interaction of GRAMD1b or GRAMD1a is much reduced with GRAMD1b Δ helix or 5E mutant and abolished with GRAMD1b (TM swap) mutant (GRAMD1b with its transmembrane domain and luminal region replaced with those of Sec61 β) compared to wild-type GRAMD1b. Such reduction is less with GRAMD1b 4E mutant.

G. Quantification of the coimmunoprecipitation experiments shown in (F). The ratio of the band intensity of the coimmunoprecipitated Myc-GRAMD1b (left) or Myc-GRAMD1a (right) over that of indicated immunoprecipitated EGFP-tagged proteins were calculated. The values were then normalized by the ratio of the band intensity of Myc-GRAMD1b over that of EGFP-GRAMD1b (WT) (left) or by the ratio of the band intensity of Myc-GRAMD1a over that of EGFP-GRAMD1b (WT) (right) [mean \pm s.e.m., n=3 IPs for each sample].

H. Confocal images of a live COS-7 cell expressing RFP-Sec61 β and EGFP-tagged GRAMD1b (TM swap). Scale bars, 2 μ m.

I. Confocal images of live COS-7 cells expressing mRuby-GRAMD1b and EGFP fusions of GRAMD1b constructs [Control, wild-type GRAMD1b; TM swap, GRAMD1b (TM swap)]. Note the abolished formation of GRAMD1b patches in TM swap mutants. Scale bars, 2 μ m.

J. Model of the homo- and hetero-meric interactions of GRAMD1a/b. Their complex formation is facilitated primarily by their luminal amphipathic helices and additionally mediated by their transmembrane domains. These regions are important for GRAMD1s to form complexes and patches on the tubular ER network.

Figure 3. The GRAM domain of GRAMD1s acts as a coincidence detector of unsequestered/accessible cholesterol and anionic lipids and senses a transient expansion of the accessible pool of cholesterol in the PM.

A. Confocal images of live HeLa cells expressing EGFP-GRAMD1b with or without cholesterol loading [the treatment with cholesterol/MCD complex (200 μ M) for 30 min at 37 $^{\circ}$ C]. Note the extensive recruitment of GRAMD1b to the PM upon cholesterol loading. Scale bars, 10 μ m.

B. Time course of normalized EGFP signal, as assessed by TIRF microscopy, from HeLa cells expressing EGFP-GRAMD protein constructs as indicated. Cholesterol loading [the treatment with cholesterol/MCD complex (200 μ M)] is indicated [mean \pm s.e.m., n=24 cells (EGFP-GRAMD1a), n=29 cells (EGFP-GRAMD1b), n=25 cells (EGFP-GRAMD1c), n=28 cells (EGFP-GRAMD3)]. Data are pooled from one experiment for GRAMD1a and two experiments for GRAMD1b, GRAMD1c and GRAMD3].

C - F. Liposome sedimentation assays of the GRAM domain of GRAMD1b (GRAM_{1b}) and GRAMD1a (GRAM_{1a}). Liposomes containing the indicated mole % lipids were incubated with (C, E) purified GRAM_{1b} proteins or (D, F) purified GRAM_{1a} proteins. Bound proteins (pellet, P) were separated from the unbound proteins (supernatant, S) and run on SDS-PAGE and

visualized by colloidal blue staining (mean \pm s.e.m., n=3 independent experiments for all the conditions). DOPC, phosphatidylcholine (1,2-dioleoyl-sn-glycero-3-phosphocholine); DOPS, phosphatidylserine (1,2-dioleoyl-sn-glycero-3-phospho-L-serine); Chol, cholesterol; SM, sphingomyelin (N-oleoyl-D-erythro-sphingosylphosphorylcholine).

G. Left: Time course of normalized EGFP signal in response to sphingomyelinase (SMase), as assessed by TIRF microscopy of HeLa cells expressing EGFP-GRAMD1b or EGFP-GRAMD1b Δ GRAM. The treatment with SMase (100 mU/ml) is indicated. Right: Values of $\Delta F/F_0$ corresponding to the end of the experiment as indicated by the arrow [mean \pm s.e.m., n=72 cells (EGFP-GRAMD1b), n=64 cells (EGFP-GRAMD1b Δ GRAM)]; data are pooled from three independent experiments for each condition; two-tailed unpaired Student's t-test, ****P < 0.0001**].

H. Left: Time course of normalized EGFP signal in response to SMase, as assessed by TIRF microscopy of HeLa cells expressing the indicated EGFP-tagged GRAM domain of GRAMD1s. The treatment with SMase (100 mU/ml) is indicated. Right: Values of $\Delta F/F_0$ corresponding to the end of the experiment as indicated by the arrow [mean \pm s.e.m., n=48 cells (EGFP-GRAM_{1a}), n=50 cells (EGFP-GRAM_{1b}), n=58 cells (EGFP-GRAM_{1c}); data are pooled from two to three independent experiments for each condition].

I. Schematics showing the interaction of the GRAM domain of GRAMD1s with the plasma membrane (PM) before and after sphingomyelinase (SMase) treatment. Left: At rest, subthreshold levels of accessible cholesterol in the PM are not sufficient to induce interaction of the GRAM domain with the PM. Right: Liberation of sphingomyelin-sequestered pool of cholesterol by SMase treatment leads to increase in accessible cholesterol in the PM beyond the threshold and induces PM recruitment of the GRAM domain as it senses both increase in unsequestered/accessible cholesterol and the presence of anionic lipids in the PM.

Figure 4. Deletion of GRAMD1s results in exaggerated accumulation of the accessible pool of cholesterol in the PM.

A. Schematics of the Cas9/sgRNA targeting sites in human GRAMD1A, GRAMD1B and GRAMD1C loci. The targeting sequences are highlighted in red. The protospacer-adjacent motifs (PAMs) are labeled in green.

B. Lysates of control HeLa cells, two independently isolated GRAMD1a/1b DKO cell lines, and two independently isolated GRAMD1 TKO cell lines were processed by SDS-PAGE and immunoblotting (IB) with anti-GRAMD1a, anti-GRAMD1b and anti-actin antibodies. The arrows indicate the specific bands for GRAMD1a and GRAMD1b.

C. Nucleotide sequence analysis of the GRAMD1C gene of the GRAMD1 TKO cell lines. Guide RNA-targeting sites are highlighted in red.

D. Confocal images of live wild-type (Control) and GRAMD1 TKO (TKO) HeLa cells expressing EGFP-tagged GRAM domain of GRAMD1b (EGFP-GRAM_{1b}) with SMase treatment (100mU/ml for 1 hour at 37°C). Insets show at higher magnification the regions indicated by white dashed boxes. Note the strong recruitment of EGFP-GRAM_{1b} to the PM of GRAMD1 TKO cells compared to that of the control cells. Scale bars, 10 μ m.

E. Left: Time course of normalized EGFP signal, as assessed by TIRF microscopy, from wild-type (Control) and GRAMD1 TKO (TKO) HeLa cells expressing EGFP-GRAM_{1b}. SMase

treatment (100 mU/ml) is indicated. Right: Values of $\Delta F/F_0$ corresponding to the end of the experiment as indicated by the arrow [mean \pm s.e.m., n=62 cells (Control), n=58 cells (TKO); data are pooled from three independent experiments for each condition; two-tailed unpaired Student's t-test with equal variance, **P < 0.0001].

Figure 5. The cholesterol transporting property of the StART-like domain of GRAMD1s is critical for removal of an acutely expanded pool of accessible PM cholesterol.

A. Schematic showing the design of *in vitro* lipid transfer assay. Donor liposomes (10% DHE, 90% DOPC) and acceptor liposomes [2.5% Dansyl-PE (DNS-PE), 97.5% DOPC] were incubated with purified StART-like domain of GRAMD1s (GRAMD1_{aStART}, GRAMD1_{bStART}, GRAMD1_{cStART}). Transfer of DHE from donor to acceptor liposomes, which results in increase in fluorescence resonance energy transfer (FRET) between DHE and DNS-PE in acceptor liposomes, was monitored using a fluorometer (see Materials and Methods).

B. Design of the mutant StART-like domain defective in lipid harboring. Ribbon diagram of the modeled GRAMD1_{bStART} (see Materials and Methods) with designed mutations (5P) in the $\Omega 1$ loop of GRAMD1b predicted to open and close to capture sterol.

C and D. 5P mutations in the $\Omega 1$ loop of StART-like domain impairs DHE transfer activity. **(C)** Time course of fold increase in FRET signals. WT GRAMD1_{bStART} and GRAMD1_{bStART} with 5P mutation (2 μ M, top panel) and WT GRAMD1_{aStART} and GRAMD1_{aStART} with 5P mutation (0.5 μ M, bottom panel) was individually added at time 0. **(D)** Values of fold increase in FRET signals of acceptor liposomes by indicated proteins corresponding to the end of the experiments as shown by arrows in **(C)** (mean \pm s.e.m., n=3 independent experiments for all of the conditions; two-tailed unpaired Student's t-test, GRAMD1_{bStART} **P = 0.0003, GRAMD1_{aStART} **P < 0.0001).

E and F. Left: Time course of normalized **(E)** EGFP or **(F)** mRuby signal, as assessed by TIRF microscopy, from GRAMD1 TKO cells expressing EGFP-GRAM_{1b} and mRuby-tagged constructs as indicated. SMase treatment (100 mU/ml) is indicated. Right: Values of $\Delta F/F_0$ corresponding to the end of the experiment as indicated by the arrows [**E**: mean \pm s.e.m., n=84 cells (TKO), n=57 cells (TKO + mRuby-GRAMD1b), n=64 cells (TKO + mRuby-GRAMD1b (5P)); Tukey's multiple comparisons test, **P < 0.0001, **F**: mean \pm s.e.m., n=57 cells (TKO + mRuby-GRAMD1b), n=64 cells (TKO + mRuby-GRAMD1b (5P)); two-tailed unpaired Student's t-test, **P = 0.0003; data are pooled from three to four independent experiments for each condition]

Figure 6: GRAMD1s-mediated PM to ER cholesterol transport plays a role in suppression of SREBP-2 cleavage upon sphingomyelinase treatment.

A. Time course of normalized EGFP signal, as assessed by TIRF microscopy, from HeLa cells expressing EGFP-GRAMD1b in response to sphingomyelinase (SMase) treatment (100 mU/ml). Note the sustained recruitment of EGFP-GRAMD1b to the PM even after 3 hours of the SMase treatment (mean \pm s.e.m., n=74 cells; data are pooled from four independent experiments).

B. Wild-type (Control) and GRAMD1 TKO (TKO) HeLa cells were cultured in the medium supplemented with 10 % lipoprotein deficient serum (LPDS) and mevastatin (50 μ M) for 16 hours and then treated with SMase (100 mU/ml) for the indicated time at 37°C. Lysates of the cells were processed for SDS-PAGE and immunoblotting (IB) with anti-SREBP-2 and anti-

Actin antibodies. Arrows indicate precursor (P) and cleaved (C) forms of SREBP-2, respectively.

C. Quantification of the response rate of the suppression of SREBP-2 cleavage upon SMase treatment from the experiment shown in **(B)**. For each time point, the ratio of the band intensity of the cleaved SREBP-2 over the total band intensity of cleaved and precursor forms of SREBP-2 was normalized by the ratio obtained from time 0 and plotted as response rate. Note that the suppression of SREBP-2 cleavage is attenuated in GRAMD1 TKO cells. [mean \pm s.e.m., n=5 lysates (independent experiments) for each time point, multiple comparisons with the Holm-Sidak method. *P = 0.0461 (120 min), *P = 0.0238 (150 min), **P = 0.0052 (180 min)].

D and E. Wild-type (Control) and GRAMD1 TKO (TKO) HeLa cells transfected with the EGFP-tagged GRAMD1s constructs as indicated were cultured in the medium supplemented with 10 % lipoprotein deficient serum (LPDS) and mevastatin (50 μ M) for 16 hours and then treated with SMase (100 mU/ml) for 3 hours at 37°C. Top: Lysates of the cells were processed for SDS-PAGE and IB with anti-SREBP-2 and anti-actin antibodies. Arrows indicate precursor (P) and cleaved (C) forms of SREBP-2, respectively. Bottom: the response rate was calculated as in **(C)** except that the ratio obtained from the cells with SMase treatment was normalized by the ratio obtained from the cells without SMase treatment for each condition. Note the rescue by expression of EGFP-GRAMD1b but not by mutant versions of EGFP-GRAMD1b (5P, Δ GRAM, TM swap) [**D**: mean \pm s.e.m., n=6 lysates (independent experiments) for each condition, Dunnett's multiple comparisons test, *P = 0.0162; **E**: mean \pm s.e.m., n=5 lysates (independent experiments) for each condition, Dunnett's multiple comparisons test, **P < 0.0001; n.s. denotes not significant]

F. Representative TIRF images of live HeLa cells expressing EGFP-GRAMD1b (Wild-type) and EGFP-GRAMD1b TM swap (TM swap) as treated in **(G)**. Note the differences in how they are recruited to the PM. While wild-type GRAMD1b accumulated progressively at ER-PM contacts, forming patches by the end of the 3-hour imaging period, the GRAMD1b TM swap mutant remained diffuse on the tubular ER even at the end of the 3-hour imaging period. Scale bars, 1 μ m.

G. Left: Time course of normalized EGFP signal, as assessed by TIRF microscopy, from HeLa cells expressing EGFP-GRAMD1b or EGFP-GRAMD1b TM swap in response to SMase treatment (100 mU/ml). Note the reduced recruitment of EGFP-GRAMD1b TM swap to the PM compared to EGFP-GRAMD1b after 3 hours of the SMase treatment. Right: Values of $\Delta F/F_0$ corresponding to the end of the experiment as indicated by the arrow [mean \pm s.e.m., n=72 cells (GRAMD1b), n=69 cells (GRAMD1b TM swap); data are pooled from three independent experiments for each condition; two-tailed unpaired Student's t-test, **P < 0.0001]

Figure 7. Acute recruitment of GRAMD1b to ER-PM contacts facilitates removal of the expanded pool of accessible PM cholesterol in GRAMD1 triple knockout (TKO) cells.

A. Left: Confocal images of live wild-type (Control) and GRAMD1 TKO (TKO) HeLa cells expressing a PI(4,5)P₂ probe/PM marker (iRFP-PH-PLC δ) that are stained with recombinant EGFP-D4H proteins (15 μ g/ml) for 15 min at room temperature. Scale Bars, 10 μ m. Note the increased D4H accessible PM cholesterol in GRAMD1 TKO cells compared to control cells as

detected by the presence of strong EGFP-D4H signals at the PM visualized by iRFP-PH-PLC δ . Scale Bars, 10 μ m.

B. Left: Line scan analysis of the regions indicated by white dotted lines in the images shown in **(A)**, showing the increase of EGFP-D4H signals at the PM (near the peak of iRFP-PH-PLC δ signals). Right: Schematics showing the D4H accessible pool of cholesterol on the outer leaflet of the PM (view from extracellular side) in wild-type (Control) and GRAMD1 TKO (TKO) HeLa cells. Green stars indicate D4H accessible cholesterol, while yellow stars indicate D4H inaccessible cholesterol.

C. Schematic representation of the rapamycin-induced GRAMD1b PM recruitment strategy. GRAMD1b was rapidly recruited to the PM by rapamycin-induced dimerization of FRB and FKBP. A version of GRAMD1b with its N-terminal region, including the GRAM domain, replaced by a miRFP-tagged FKBP module (miRFP-FKBP-GRAMD1b) was expressed in GRAMD1 TKO cells together with mCherry-tagged FRB module that is targeted to the PM (PM-FRB-mCherry).

D. Left: Time course of normalized miRFP signal in response to rapamycin, as assessed by TIRF microscopy of GRAMD1 TKO cells expressing indicated miRFP-FKBP-GRAMD1b constructs and PM-FRB-mCherry [wild-type (WT) and mutant versions with a StART-like domain that lacks cholesterol transport activity (5P or T469D)]. Rapamycin addition (200 nM) is indicated. [mean \pm s.e.m., n=29 cells (WT), n=29 cells (5P), n=27 cells (T469D). All data are pooled from two independent experiments]. Right: Values of $\Delta F/F_0$ corresponding to the end of the experiments as shown by arrows. Dunnet's multiple comparisons test, n.s. denotes not significant.

E. Confocal images of GRAMD1 TKO (TKO) HeLa cells expressing miRFP-FKBP-GRAMD1b and PM-FRB-mCherry that were treated with or without rapamycin (200nM) for 60 min at 37 $^\circ$ C and then stained with recombinant EGFP-D4H proteins (15 μ g/ml) for 15 min at room temperature. Insets show at higher magnification the regions indicated by white dashed boxes. Scale Bars, 10 μ m.

F. Values of EGFP-D4H signals at the PM after background subtraction, as assessed by confocal microscopy and line scan analysis, from GRAMD1 TKO HeLa cells expressing indicated miRFP-FKBP-GRAMD1b constructs and PM-FRB-mCherry that are stained with recombinant EGFP-D4H protein after rapamycin addition (200nM) for either 30 min or 60 min, as shown in **E**. Peak EGFP-D4H signals around the PM marked by peak PM-FRB-mCherry signals were quantified (see Materials and Methods) [mean \pm s.e.m., n=40 cells for each condition; all data are pooled from two independent experiments; Tukey's multiple comparisons test, **P < 0.0001, n.s. denotes not significant].

Figure 8. GRAMD1s facilitate the transport of the accessible pool of cholesterol from the PM to the ER, thereby contributing to PM cholesterol homeostasis.

A. Distinct pools of cholesterol co-exists in PM bilayers at steady state, as a major pool is inaccessible (i.e. sequestered or chemically inactive) and a smaller pool is accessible (i.e. unsequestered or chemically active). Sequestration is in part mediated by sphingomyelin. Compositions of phospholipids also influence the overall accessibility of PM cholesterol. Top: at rest, GRAMD1 complexes localize on the tubular ER network with little enrichment at ER-PM contact sites. Bottom: a transient expansion of the accessible pool of PM cholesterol (e.g. hydrolysis of sphingomyelin, cholesterol loading to the PM etc.) induces acute recruitment of

GRAMD1 complexes to ER-PM contacts once the levels of accessible PM cholesterol reach above a certain threshold. Red arrow denotes expansion of the accessible pool; blue arrow denotes transport of the newly expanded pool of accessible PM cholesterol to the ER by GRAMD1s and other, yet to be identified, intracellular cholesterol transport systems.

B. Top: in wild-type cells, the GRAM domain of GRAMD1s only weakly interacts with the PM at rest due to sequestration of the majority of cholesterol in this bilayer. Bottom: upon reaching a certain threshold of the accessibility (i.e. a transient expansion in the accessible pool of PM cholesterol), the interaction of the GRAM domain with the PM is enhanced, and GRAMD1s are recruited to ER-PM contacts. Supporting this model, the binding of the purified GRAM domains of GRAMD1a and GRAMD1b to liposomes containing phosphatidylserine, a major anionic lipid in the PM, is dramatically enhanced by the presence of unsequestered/accessible cholesterol in dose-dependent manner with a switch-like response (**Figure 3C-F, and Figure 3-figure supplement 2B**). Upon recruitment of GRAMD1s to ER-PM contacts, the StART-like domain initiates extraction of accessible PM cholesterol and facilitates its transport to the ER, contributing to the suppression of SREBP-2 cleavage and to PM cholesterol homeostasis.

C. Top: in GRAMD1 TKO cells at rest, D4H binding to the PM increases, indicating chronic expansion of the accessible pool of PM cholesterol due to the absence of GRAMD1s-mediated transport of accessible cholesterol from the PM to the ER (**Figure 7A,B**). Bottom: upon a transient expansion of the accessible pool of PM cholesterol, GRAMD1 TKO cells show exaggerated accumulation of the accessible pool of PM cholesterol due to the absence of GRAMD1s-mediated transport of accessible PM cholesterol to the ER. Consistent with this model, sphingomyelinase treatment leads to enhanced recruitment of the GRAM domain of GRAMD1b, a novel biosensor for detecting acute expansion of the accessible pool of PM cholesterol that we identified in this study, to the PM in GRAMD1 TKO cells (**Figure 4D,E**). Reduced transport of accessible cholesterol from the PM to the ER in GRAMD1 TKO cells also results in less efficient suppression of SREBP-2 cleavage and continuous increase in the binding of recombinant D4 proteins to the PM (**Figure 6B,C and Figure 6-figure supplement 2A,B**). Other parallel cholesterol transport and regulatory systems, yet to be identified, may operate to maintain the total levels of PM cholesterol in the absence of GRAMD1s.

FIGURE SUPPLEMENT LEGENDS

Figure 1-figure supplement 1. GRAMD proteins form homo- and hetero-meric complexes.

A. Confocal images of live COS-7 cells expressing the ER membrane marker RFP-Sec61 β and EGFP-GRAMD protein constructs as indicated (compare with **Figure 1B**). Insets show at higher magnification the regions indicated by white dashed boxes. Note that the overexpression of EGFP-GRAMD1s does not affect tubular ER structure. Scale bars, 10 μ m.

B. Confocal images of live COS-7 cells expressing mCherry-GRAMD3 and EGFP-GRAMD1s as indicated. Note the presence of mCherry-GRAMD3 patches that are partially overlapping with the patches of EGFP-GRAMD1s. Scale bars, 1 μ m.

C and D. Extracts of HeLa cells transfected with the constructs as indicated were subjected to anti-Myc immunoprecipitation (IP) and then processed for SDS-PAGE and immunoblotting (IB) with anti-Myc and anti-GFP antibodies. Inputs are 1% of the total cell lysates. Note the strong biochemical interaction (**C**) between GRAMD1b and GRAMD1s and (**D**) between GRAMD3 and GRAMD1s. EGFP-GRAMD1s that are present in the anti-Myc immunoprecipitates are indicated by arrows.

Figure 2-figure supplement 1. Luminal helix of GRAMD1b is important for homo- and hetero-meric interaction.

A. Predicted luminal amphipathic helix regions of GRAMD1s are shown as helical wheel representation. Predictions were made with the Heliquest server (Gautier et al., 2008).

B. Hydrophobic surface representation of the predicted luminal amphipathic helices of GRAMD1s (see Materials and Methods). The red color indicates the hydrophobicity of the amino acid residues.

C. A magnified image of a region of the predicted amphipathic helix of GRAMD1b indicated in a dashed box in (**B**) showing five amino acid residues (L693, W696, I699, I700 and L707) that were mutated to glutamic acid in the 5E mutant. Images were generated using PyMol Molecular Graphics System.

Figure 3-figure supplement 1. The GRAM domain of GRAMD1s acts as a coincidence detector of unsequestered/accessible cholesterol and anionic lipids.

A. Left: Time course of normalized EGFP signal, as assessed by TIRF microscopy, from HeLa cells expressing EGFP-GRAMD1b or EGFP-GRAMD1b Δ GRAM. Cholesterol loading [the treatment with cholesterol/methyl- β -cyclodextrin (MCD) complex (200 μ M)] is indicated. Right: Values of $\Delta F/F_0$ corresponding to the end of the experiment as indicated by the arrow [mean \pm s.e.m., n=35 cells (EGFP-GRAMD1b), n=41 cells (EGFP-GRAMD1b Δ GRAM); data are pooled from two independent experiments for each condition; two-tailed unpaired Student's t-test, **P < 0.0001].

B and D. Liposome sedimentation assays of the GRAM domain of GRAMD1b (GRAM_{1b}). Liposomes containing the indicated mole % lipids were incubated with purified GRAM_{1b} proteins. Bound proteins (pellet, P) were separated from the unbound proteins (supernatant, S) and run on SDS-PAGE and visualized by colloidal blue staining. Note that the GRAM

domain binds only weakly to liposomes when the liposomes contain high levels of cholesterol (50%, 60%, indicated by blue). Note also that the GRAM domain does not bind liposomes that contain physiological levels of PS (10%, 20%, indicated by red) (mean \pm s.e.m., n=3 independent experiments for all the conditions). DOPC, phosphatidylcholine (1,2-dioleoyl-sn-glycero-3-phosphocholine); DOPS, phosphatidylserine (1,2-dioleoyl-sn-glycero-3-phospho-L-serine); PA, phosphatidic acid (1,2-dioleoyl-sn-glycero-3-phosphate); POPE, phosphatidylethanolamine (1-palmitoyl-2-oleoyl-sn-glycero-3-phosphoethanolamine); SM, sphingomyelin (N-oleoyl-D-erythro-sphingosylphosphorylcholine); Chol, cholesterol; PI(4)P, phosphatidylinositol 4-phosphate; PI(4,5)P₂, phosphatidylinositol 4,5-bisphosphate.

C. Schematics showing the interaction of the GRAM domain of GRAMD1s to artificial membranes with or without sphingomyelin (SM) incorporation in our liposome sedimentation assays. Left: The presence of both free cholesterol and anionic lipids in artificial membranes results in strong binding of the GRAM domain when mole percentage of free cholesterol reaches above a certain threshold. Right: Incorporation of sphingomyelin into the artificial membranes reduces the accessibility of cholesterol in dose-dependent manner (due to complex formation between sphingomyelin and cholesterol) and suppresses the binding of the GRAM domain to the artificial membranes.

Figure 3-figure supplement 2. The GRAM domain of GRAMD1s binds to membranes by sensing cholesterol accessibility.

A and B. Liposome sedimentation assays of the GRAM domain of GRAMD1b (GRAM_{1b}). Liposomes containing the indicated mole % lipids were incubated with purified GRAM_{1b} proteins. Bound proteins (pellet, P) were separated from the unbound proteins (supernatant, S) and run on SDS-PAGE and visualized by colloidal blue staining. Note that the GRAM domain no longer binds to phosphatidylserine-containing liposomes when cholesterol was replaced with phosphatidylethanolamine (compare with Figure 3C). Note also that the acyl chain diversity of phosphatidylcholine (PC) affects the binding of GRAM_{1b} to liposomes containing phosphatidylserine and cholesterol. POPC has the strongest cholesterol sequestration effect in the membranes, followed by DOPC and DPhyPC (Sokolov and Radhakrishnan, 2010) (mean \pm s.e.m., n=3 independent experiments for all the conditions). DOPC, 1,2-dioleoyl-sn-glycero-3-phosphocholine; DPhyPC, 1,2-diphytanoyl-sn-glycero-3-phosphocholine; POPC, 1-palmitoyl-2-oleoyl-glycero-3-phosphocholine; DOPS, 1,2-dioleoyl-sn-glycero-3-phospho-L-serine; Chol, cholesterol; POPE, 1-palmitoyl-2-oleoyl-sn-glycero-3-phosphoethanolamine.

C. Chemical structures of phosphatidylcholines tested in the assay. Note the differences in acyl chain saturation and branching.

Figure 4-figure supplement 1. Generation of GRAMD1 triple knockout (TKO) HeLa cells.

A. Lysates of control HeLa cells (WT), nine independently isolated GRAMD1b knockout (KO) cell lines were processed by SDS-PAGE and immunoblotting (IB) with anti-GRAMD1b and anti-actin antibodies. #10 and #17 were further analyzed by nucleotide sequencing (see **C**).

B. Lysates of control HeLa cells (WT), four independently isolated GRAMD1a KO cell lines, one GRAMD1b KO cell line, and five GRAMD1a/1b double knockout (DKO) cell lines were processed by SDS-PAGE and immunoblotting (IB) with anti-GRAMD1a, anti-GRAMD1b and anti-actin antibodies. #40 was further analyzed by nucleotide sequencing (see **D**).

C. Nucleotide sequence analysis of the GRAMD1B gene of the GRAMD1b KO cell lines (#10 and #17). Guide RNA-targeting sites are highlighted in red. GRAMD1b KO #10 was used for generating GRAMD1a/1b DKO cell lines and subsequently for generating GRAMD1 triple knockout (TKO) cell lines.

D. Nucleotide sequence analysis of the GRAMD1A gene of the GRAMD1a/1b DKO cell line (#40). Guide RNA-targeting sites are highlighted in red. GRAMD1a/1b DKO #40 was used for generating GRAMD1 TKO cell lines.

E. Electrophoresis analysis of genomic DNA fragments of the GRAMD1C gene of the GRAMD1 TKO cell lines after genomic PCR. WT control cells show 513 bp bands, while TKO cells, such as #1 and #15, show smaller bands (464 bp).

Figure 4-figure supplement 2. Recruitment of the EGFP-tagged GRAM domain of GRAMD1b (EGFP-GRAM_{1b}) to the PM requires cholesterol.

A. Confocal images of live wild-type (Control) and GRAMD1 TKO (TKO) HeLa cells expressing EGFP-tagged GRAM domain of GRAMD1b (EGFP-GRAM_{1b}) before sphingomyelinase (SMase) treatment. Insets show at higher magnification the regions indicated by white dashed boxes. Scale bars, 10 μ m.

B. Left: Time course of normalized fluorescent signal, as assessed by TIRF microscopy, from GRAMD1 TKO HeLa cells expressing EGFP-GRAM_{1b}, a phosphatidylserine probe (mCherry-LactC2) and a PI(4,5)P₂ probe (iRFP-PH-PLC δ). SMase treatment (100 μ M/ml) and methyl- β -cyclodextrin (MCD) treatment (10mM) are indicated. Right: Values of $\Delta F/F_0$ corresponding to 65 min and 67 min time points of the experiment as indicated by the arrows [mean \pm s.e.m., n=32 cells; data are pooled from two independent experiments; Tukey's multiple comparisons test, **P < 0.0001, *P = 0.0225, n.s. denotes not significant].

Figure 4-figure supplement 3. Isolation and characterization of PM sheets of GRAMD1 triple knockout (TKO) HeLa cells

A. Confocal images of HeLa cells attached to a bead. Top: Bead without cells. Bottom: Bead coated with HeLa cells. Maximum projections of the serial Z-stack of confocal images are shown. The bead-attached PMs were stained with BODIPYTM TR Ceramide (BODIPY-Cer: green). Scale bars, 50 μ m.

B. Bead-attached material [total lysate (Total) and PM sheets (PM)] was processed by SDS-PAGE and immunoblotting (IB) with the indicated antibodies. Note the enrichment of PM proteins and depletion of ER and endosomal proteins in the PM fractions.

C and D. Quantitative analysis of lipids by mass spectrometry. **(C)** Comparisons of PM lipid profiles of wild-type (Control) and GRAMD1 TKO (TKO) HeLa cells. PM enrichment plots the ratio of indicated lipids present in the PM sheets over those present in the total lysate. **(D)** Comparisons of the mole % of cholesterol over total lipids for whole cell extracts (Total) and PM extracts (PM). Chol, cholesterol, CE, cholesterol esters, SM, sphingomyelin, PS, phosphatidylserine; PC, phosphatidylcholine; PE, phosphatidylethanolamine; PtdIns, phosphatidylinositol [mean \pm s.e.m., n=4 extracts (Control), n=4 extracts (TKO) (four biologically independent samples for each condition), two-tailed unpaired Student's t-test, **P = 0.0036, n.s. denotes not significant]

Figure 5-figure supplement 1. Characterization of the cholesterol transporting property of the StART-like domain of GRAMD1s.

A. Calibration curve showing the linear relationship between FRET signals and the various amount of DHE present in liposomes that contains 2.5 mole % of DNS-PE. This calibration curve was used to quantitatively measure the amount of transferred DHE from donor to acceptor liposomes overtime [mean \pm s.d., n=3 for all different DHE concentrations].

B - E. Time course of DHE transfer from donor to acceptor liposomes with the StART-like domains of GRAMD1s as indicated. Purified StART-like domains of GRAMD1s (0.5 μ M, 1 μ M or 2 μ M) were added at time 0. Control indicates buffer addition only. Data were fit to one phase association equation built-in the GraphPad Prism 7.

F. Values of DHE transfer rate of GRAMD1_{aStART}, GRAMD1_{bStART}, and GRAMD1_{cStART}, as estimated by the FRET-based lipid transfer assay (see Materials and Methods).

G. SDS-PAGE analysis of purified StART-like domains from wild-type GRAMD1a and GRAMD1b [GRAMD1_{aStART}, GRAMD1_{bStART}] and those with 5P mutations [GRAMD1_{aStART} (5P), GRAMD1_{bStART}(5P)]. CB, Colloidal blue staining.

H. Left: Time course of fold increase in FRET signals. Wild-type GRAMD1_{bStART} (WT), GRAMD1_{bStART} with 5P mutation (5P) and GRAMD1_{bStART} with T469D mutation (T469D) were individually added (2 μ M) at time 0. Right: Values of fold increase in FRET signals by indicated proteins corresponding to the end of the experiment as indicated by an arrow are shown (mean \pm s.e.m., n=3 independent experiments for all of the conditions; Tukey's multiple comparisons test, WT vs. 5P, **P < 0.0001; WT vs. T469D, **P < 0.0001).

Figure 5-figure supplement 2. Overexpression of STARD4 and selected ORPs does not rescue the exaggerated accumulation of the accessible pool of PM cholesterol in GRAMD1 TKO cells upon sphingomyelinase treatment.

A. Confocal images of live GRAMD1 TKO (TKO) HeLa cells expressing the indicated constructs. Scale bars, 10 μ m

B and C. Left: Time course of normalized (**B**) EGFP or (**C**) mCherry or mRuby signal, as assessed by TIRF microscopy, from GRAMD1 TKO cells co-expressing EGFP-GRAM_{1b} and either mCherry-STARD4 or mRuby-GRAMD1b. Sphingomyelinase (SMase) treatment (100 mU/ml) is indicated. Right: Values of $\Delta F/F_0$ corresponding to the end of the experiment as indicated by the arrows [**B**: mean \pm s.e.m., n=24 cells (TKO), n=28 cells (TKO + mRuby-GRAMD1b), n=25 cells (TKO + mCherry-STARD4); Tukey's multiple comparisons test, TKO vs. TKO + mRuby-GRAMD1b **P = 0.0002; TKO + mRuby-GRAMD1b vs. mCherry-STARD4, **P < 0.0001. **C**: mean \pm s.e.m., n=28 cells (TKO + mRuby-GRAMD1b), n=25 cells (TKO + mCherry-STARD4); two-tailed unpaired Student's t-test, **P < 0.0001; all data are pooled from two independent experiments].

D and E. Left: Time course of normalized (**D**) EGFP or (**E**) mRuby signal, as assessed by TIRF microscopy, from GRAMD1 TKO cells expressing EGFP-GRAM_{1b} and mRuby-tagged constructs as indicated. SMase treatment (100 mU/ml) is indicated. Right: Values of $\Delta F/F_0$ corresponding to the end of the experiment as indicated by the arrows [**D**: mean \pm s.e.m., n=27 cells (TKO), n=27 cells (TKO + mRuby-GRAMD1b), n=24 cells (TKO + mRuby-OSBP), n=22 cells (TKO + mRuby-ORP4), n=23 cells (TKO + mRuby-ORP9); Tukey's multiple

comparisons test, $**P < 0.0001$, n.s. denotes not significant. **E**: mean \pm s.e.m., n=27 cells (TKO + mRuby-GRAMD1b), n=24 cells (TKO + mRuby-OSBP), n=22 cells (TKO + mRuby-ORP4), n=23 cells (TKO + mRuby-ORP9); Dunnett's multiple comparisons test, TKO + mRuby-GRAMD1b vs. TKO + mRuby-OSBP, $**P = 0.0031$; TKO + mRuby-GRAMD1b vs. TKO + mRuby-ORP4, $**P = 0.0001$; TKO + mRuby-GRAMD1b vs. TKO + mRuby-ORP9, $**P = 0.0004$; all data are pooled from two independent experiments]

Figure 6-figure supplement 1. GRAMD1s-mediated PM to ER cholesterol transport requires their StART-like and GRAM domains as well as their complex formation.

A and B. Left: Quantification of the ratio of the band intensity of the cleaved SREBP-2 over the total band intensity of cleaved and precursor forms of SREBP-2 from the experiments shown in **Figure 6D,E**. [**A**: mean \pm s.e.m., n=6 lysates (independent experiments) for each condition, Dunnett's multiple comparisons test, $*P = 0.0111$; **B**: mean \pm s.e.m., n=5 lysates (independent experiments) for each condition, Dunnett's multiple comparisons test, $**P = 0.0074$; n.s. denotes not significant] Right: Lysates of wild-type control (Control) and GRAMD1 TKO (TKO) HeLa cells expressing the indicated EGFP-tagged constructs were processed by SDS-PAGE and immunoblotting (IB) with anti-GFP antibodies.

C and D. Left: Time course of normalized (**C**) EGFP or (**D**) mRuby signal, as assessed by TIRF microscopy, from GRAMD1 TKO (TKO) HeLa cells expressing EGFP-GRAM_{1b} and mRuby-tagged constructs as indicated. Sphingomyelinase (SMase) treatment (100 mU/ml) is indicated. Right: Values of $\Delta F/F_0$ corresponding to the end of the experiment as indicated by the arrow [**C**: mean \pm s.e.m., n=50 cells (TKO), n=45 cells (TKO + mRuby-GRAMD1b), n=43 cells (TKO + mRuby-GRAMD1b (TM swap)); data are pooled from three independent experiments for each condition; Tukey's multiple comparisons test; TKO vs. TKO + GRAMD1b and TKO + GRAMD1b vs. TKO + GRAMD1b (TM swap), $**P < 0.0001$, **D**: mean \pm s.e.m., n=45 cells (TKO + mRuby-GRAMD1b), n=43 cells (TKO + mRuby-GRAMD1b (TM swap)); data are pooled from three independent experiments for each condition; n.s. denotes not significant].

Figure 6-figure supplement 2. Deletion of GRAMD1s results in sustained D4 binding to the PM upon sphingomyelinase treatment.

A. Wild-type (Control) and GRAMD1 TKO (TKO) HeLa cells were cultured in the medium supplemented with 10 % lipoprotein deficient serum (LPDS) and mevastatin (50 μ M) for 16 hours and then treated with sphingomyelinase (SMase) (100 mU/ml) for the indicated time at 37 °C. Cells were then washed and incubated with Phosphate-Buffered Saline (PBS) containing recombinant EGFP-D4 proteins (10 μ g/ml) for 15 min at room temperature. After washing with PBS, lysates of the cells (10 μ g protein for each lane) were processed for SDS-PAGE and immunoblotting (IB) with anti-GFP and anti-actin antibodies.

B. Quantification of the binding of EGFP-D4 proteins to the PM upon SMase treatment from the experiment shown in (**A**). For each time point, the ratio of the band intensity of EGFP-D4 over the band intensity of EGFP-D4 at time 0 was calculated, and Δ Intensity/Intensity₀ was plotted to show the changes in D4 accessible PM cholesterol over time. Note the sustained increase in the binding of EGFP-D4 in GRAMD1 TKO cells compared to control cells. [mean \pm s.e.m., n=5 lysates (independent experiments) for each time point, multiple comparisons with the Holm-Sidak method, $**P = 0.0082$ (150 min), $*P = 0.0240$ (180 min)].

Figure 7-figure supplement 1. Increased D4H binding to the PM of GRAMD1 triple knockout (TKO) cells is dependent on the presence of cholesterol.

A. Left: Confocal images of live GRAMD1 TKO HeLa cells expressing a PI(4,5)P₂ probe/PM marker (iRFP-PH-PLC δ) with or without methyl- β -cyclodextrin (MCD) treatment (10 mM for 30 min at 37°C) that are stained with recombinant EGFP-D4H proteins (15 μ g/ml) for 15 min at room temperature. Scale Bars, 10 μ m. Right: Line scan analysis of the regions indicated by white dotted lines in the images shown in confocal images. Note the loss of EGFP-D4H signals from the PM after MCD treatment.

B. Values of EGFP-D4H signals at the PM after background subtraction, as assessed by confocal microscopy and line scan analysis from GRAMD1 TKO HeLa cells that are stained with recombinant EGFP-D4H proteins as shown in **A**. [mean \pm s.e.m., n=20 cells for each condition; data are pooled from two independent experiments; two-tailed unpaired Student's t-test, **P <0.0001.]

Figure 7-figure supplement 2. The cholesterol transporting property of the StART-like domain is essential for removal of the expanded pool of D4H accessible PM cholesterol in GRAMD1 knockout cells.

A, E, and G. Confocal images of live GRAMD1 TKO HeLa cells expressing either mRuby control or mRuby-tagged GRAMD1 constructs as indicated together with a PI(4,5)P₂ probe/PM marker (iRFP-PH-PLC δ) that are stained with recombinant EGFP-D4H proteins (15 μ g/ml) for 15 min at room temperature. Note that re-expression of wild-type mRuby-GRAMD1s but not the mutant versions of mRuby-GRAMD1b in TKO cells reduced the EGFP-D4H accessibility on the PM of TKO cells, rescuing the phenotype (see **B, F, and H** for quantification). Scale bars, 10 μ m.

D. Design of the mutant StART-like domain defective in lipid harboring. Ribbon diagram of the modeled GRAMD1b_{StART} (see Materials and Methods) with designed mutations in the sterol-binding pocket (T469D and V445A, Y430A) and in the Ω 1 loop of GRAMD1b predicted to open and close to capture sterol (5P).

B, F, and H. Values of EGFP-D4H signals at the PM after background subtraction, as assessed by confocal microscopy and line scan analysis, from GRAMD1 TKO HeLa cells that are stained with recombinant EGFP-D4H protein as shown in **A, E, and G**. Peak EGFP-D4H signals around the PM marked by peak iRFP-PH-PLC δ signals were quantified (see Materials and Methods). [mean \pm s.e.m., (**B**) n=40 cells for all the conditions; Tukey's multiple comparisons test, **P <0.0001; (**F**) n=40 cells for each condition except n=20 for control; Tukey's multiple comparisons test, **P <0.0001; n.s. denotes not significant. (**H**) n=40 cells for all the conditions; Tukey's multiple comparisons test, **P <0.0001; n.s. denotes not significant. Control denotes wild-type HeLa cells. All data are pooled from two independent experiments.]

C and I. Lysates of wild-type (Control) and GRAMD1 TKO (TKO) HeLa cells expressing the indicated mRuby-tagged constructs were processed by SDS-PAGE and immunoblotting (IB) with anti-mCherry and anti-actin antibodies as indicated. Note that our anti-mCherry antibodies are able to detect mRuby-tagged proteins.

Figure 7-figure supplement 3. Rapamycin-induced acute recruitment of FKBP-tagged GRAMD1b to the PM in GRAMD1 triple knockout (TKO) cells.

A - C. Snapshots of the cortical regions of the GRAMD1 TKO HeLa cells expressing PM-FRB-mCherry and indicated miRFP-FKBP-GRAMD1b constructs, imaged under TIRF microscopy, at different times are shown. Images were taken every 20 seconds. Rapamycin (200 nM) addition is indicated. Scale bars, 20 μm .

Video 1. GRAMD1b is recruited to ER-PM contacts upon cholesterol loading.

HeLa cells expressing EGFP-GRAMD1b were imaged under TIRF microscopy. Images were taken every 20 seconds, and 200 μM cholesterol/MCD were added at 5 min time point. Image size, 66.1 μm x 66.1 μm .

Video 2. GRAMD1b Δ GRAM is not recruited to ER-PM contacts upon cholesterol loading.

HeLa cells expressing EGFP-GRAMD1b Δ GRAM were imaged under TIRF microscopy. Images were taken every 20 seconds, and 200 μM cholesterol/MCD were added at 5 min time point. Image size, 66.1 μm x 66.1 μm .

Video 3. Comparison of the recruitment to the PM of a wild-type GRAMD1b and a mutant version of GRAMD1b that is defective in complex formation upon sphingomyelinase treatment.

HeLa cells expressing (left) EGFP-GRAMD1b or (right) EGFP-GRAMD1b TM swap were imaged under TIRF microscopy. Images were taken every 20 seconds, and 100 mU/ml of sphingomyelinase (SMase) was added at 10 min time point. Image size, 66.1 min time point.

Video 4. Rapamycin-induced acute recruitment of GRAMD1b to the PM in GRAMD1 triple knockout (TKO) cells.

GRAMD1 TKO HeLa cells expressing PM-FRB-mCherry and miRFP-FKBP-GRAMD1b (WT) were imaged under TIRF microscopy. Images were taken every 20 seconds, and 200 nM rapamycin were added at 5 min time point. Note the rapamycin-induced recruitment of miRFP-FKBP-GRAMD1b to the PM. Image size, 66.1 μm x 66.1 μm .

Video 5. Rapamycin-induced acute recruitment of a mutant version of GRAMD1b (5P) to the in GRAMD1 triple knockout (TKO) cells.

GRAMD1 TKO HeLa cells expressing PM-FRB-mCherry and miRFP-FKBP-GRAMD1b (5P) were imaged under TIRF microscopy. Images were taken every 20 seconds, and 200 nM rapamycin were added at 5 min time point. Note the rapamycin-induced recruitment of miRFP-FKBP-GRAMD1b (5P) to the PM. Image size, 66.1 μm x 66.1 μm .

SUPPLEMENTARY FILE LEGENDS

Supplementary File 1. Key Resources Table.

Supplementary File 2. Table 1. A list of sequence-based reagents.

DNA sequences for oligos and primers used in this study are described.

Supplementary File 3. Table 2. Lipid compositions of liposomes used for lipid transfer assays.

Moles percent of lipids used for the acceptor and donor liposomes in FRET-based lipid transfer experiments is described.

REFERENCES

- Acton, S., A. Rigotti, K.T. Landschulz, S. Xu, H.H. Hobbs, and M. Krieger. 1996. Identification of scavenger receptor SR-BI as a high density lipoprotein receptor. *Science*. 271:518-520.
- AhYoung, A.P., J. Jiang, J. Zhang, X. Khoi Dang, J.A. Loo, Z.H. Zhou, and P.F. Egea. 2015. Conserved SMP domains of the ERMES complex bind phospholipids and mediate tether assembly. *Proceedings of the National Academy of Sciences of the United States of America*. 112:E3179-3188.
- Alpy, F., A. Rousseau, Y. Schwab, F. Legueux, I. Stoll, C. Wendling, C. Spiegelhalter, P. Kessler, C. Mathelin, M.C. Rio, T.P. Levine, and C. Tomasetto. 2013. STARD3 or STARD3NL and VAP form a novel molecular tether between late endosomes and the ER. *Journal of cell science*. 126:5500-5512.
- Alpy, F., and C. Tomasetto. 2014. START ships lipids across interorganelle space. *Biochimie*. 96:85-95.
- Antonny, B., J. Bigay, and B. Mesmin. 2018. The Oxysterol-Binding Protein Cycle: Burning Off PI(4)P to Transport Cholesterol. *Annual review of biochemistry*. 87:809-837.
- Baumann, N.A., D.P. Sullivan, H. Ohvo-Rekila, C. Simonot, A. Pottekat, Z. Klaassen, C.T. Beh, and A.K. Menon. 2005. Transport of newly synthesized sterol to the sterol-enriched plasma membrane occurs via nonvesicular equilibration. *Biochemistry*. 44:5816-5826.
- Begley, M.J., G.S. Taylor, S.A. Kim, D.M. Veine, J.E. Dixon, and J.A. Stuckey. 2003. Crystal structure of a phosphoinositide phosphatase, MTMR2: insights into myotubular myopathy and Charcot-Marie-Tooth syndrome. *Molecular cell*. 12:1391-1402.
- Benedetti, L., A.E.S. Barentine, M. Messa, H. Wheeler, J. Bewersdorf, and P. De Camilli. 2018. Light-activated protein interaction with high spatial subcellular confinement. *Proceedings of the National Academy of Sciences of the United States of America*. 115:E2238-E2245.
- Besprozvannaya, M., E. Dickson, H. Li, K.S. Ginburg, D.M. Bers, J. Auwerx, and J. Nunnari. 2018. GRAM domain proteins specialize functionally distinct ER-PM contact sites in human cells. *eLife*. 7.
- Bligh, E.G., and W.J. Dyer. 1959. A rapid method of total lipid extraction and purification. *Can J Biochem Physiol*. 37:911-917.
- Brown, A.J., L. Sun, J.D. Feramisco, M.S. Brown, and J.L. Goldstein. 2002. Cholesterol addition to ER membranes alters conformation of SCAP, the SREBP escort protein that regulates cholesterol metabolism. *Molecular cell*. 10:237-245.
- Brown, M.S., A. Radhakrishnan, and J.L. Goldstein. 2018. Retrospective on Cholesterol Homeostasis: The Central Role of Scap. *Annual review of biochemistry*. 87:783-807.
- Chakrabarti, R.S., S.A. Ingham, J. Kozlitina, A. Gay, J.C. Cohen, A. Radhakrishnan, and H.H. Hobbs. 2017. Variability of cholesterol accessibility in human red blood cells measured using a bacterial cholesterol-binding toxin. *eLife*. 6.
- Charman, M., T.R. Colbourne, A. Pietrangelo, L. Kreplak, and N.D. Ridgway. 2014. Oxysterol-binding protein (OSBP)-related protein 4 (ORP4) is essential for cell proliferation and survival. *The Journal of biological chemistry*. 289:15705-15717.
- Chung, J., F. Torta, K. Masai, L. Lucast, H. Czapla, L.B. Tanner, P. Narayanaswamy, M.R. Wenk, F. Nakatsu, and P. De Camilli. 2015. INTRACELLULAR TRANSPORT. PI4P/phosphatidylserine countertransport at ORP5- and ORP8-mediated ER-plasma membrane contacts. *Science*. 349:428-432.
- Cohen, C.M., D.I. Kalish, B.S. Jacobson, and D. Branton. 1977. Membrane isolation on polylysine-coated beads. Plasma membrane from HeLa cells. *The Journal of cell biology*. 75:119-134.
- Das, A., M.S. Brown, D.D. Anderson, J.L. Goldstein, and A. Radhakrishnan. 2014. Three pools of plasma membrane cholesterol and their relation to cholesterol homeostasis. *eLife*. 3.
- Das, A., J.L. Goldstein, D.D. Anderson, M.S. Brown, and A. Radhakrishnan. 2013. Use of mutant 125I-perfringolysin O to probe transport and organization of cholesterol in membranes of animal cells. *Proceedings of the National Academy of Sciences of the United States of America*. 110:10580-10585.
- de Duve, C. 1971. Tissue fraction-past and present. *The Journal of cell biology*. 50:20.
- Drin, G. 2014. Topological regulation of lipid balance in cells. *Annual review of biochemistry*. 83:51-77.
- Elbaz, Y., and M. Schuldiner. 2011. Staying in touch: the molecular era of organelle contact sites. *Trends in biochemical sciences*. 36:616-623.

- Endapally, S., D. Frias, M. Grzemska, A. Gay, D.R. Tomchick, and A. Radhakrishnan. 2019. Molecular Discrimination between Two Conformations of Sphingomyelin in Plasma Membranes. *Cell*. 176:1040-1053 e1017.
- Finean, J.B. 1953. Phospholipid-cholesterol complex in the structure of myelin. *Experientia*. 9:17-19.
- Gatta, A.T., A.C. Sauerwein, A. Zhuravleva, T.P. Levine, and S. Matthews. 2018. Structural insights into a StART-like domain in Lam4 and its interaction with sterol ligands. *Biochemical and biophysical research communications*. 495:2270-2274.
- Gatta, A.T., L.H. Wong, Y.Y. Sere, D.M. Calderon-Norena, S. Cockcroft, A.K. Menon, and T.P. Levine. 2015. A new family of StART domain proteins at membrane contact sites has a role in ER-PM sterol transport. *eLife*. 4.
- Gautier, R., D. Douguet, B. Antony, and G. Drin. 2008. HELIQUEST: a web server to screen sequences with specific alpha-helical properties. *Bioinformatics*. 24:2101-2102.
- Gay, A., D. Rye, and A. Radhakrishnan. 2015. Switch-like responses of two cholesterol sensors do not require protein oligomerization in membranes. *Biophysical journal*. 108:1459-1469.
- Giordano, F., Y. Saheki, O. Idevall-Hagren, S.F. Colombo, M. Pirruccello, I. Milosevic, E.O. Gracheva, S.N. Bagriantsev, N. Borgese, and P. De Camilli. 2013. PI(4,5)P2-Dependent and Ca(2+)-Regulated ER-PM Interactions Mediated by the Extended Synaptotagmins. *Cell*. 153:1494-1509.
- Goldstein, J.L., and M.S. Brown. 1990. Regulation of the mevalonate pathway. *Nature*. 343:425-430.
- Goldstein, J.L., and M.S. Brown. 2015. A century of cholesterol and coronaries: from plaques to genes to statins. *Cell*. 161:161-172.
- Guan, Y., Q. Zhu, D. Huang, S. Zhao, L. Jan Lo, and J. Peng. 2015. An equation to estimate the difference between theoretically predicted and SDS PAGE-displayed molecular weights for an acidic peptide. *Sci Rep*. 5:13370.
- Hao, M., S.X. Lin, O.J. Karylowski, D. Wustner, T.E. McGraw, and F.R. Maxfield. 2002. Vesicular and non-vesicular sterol transport in living cells. The endocytic recycling compartment is a major sterol storage organelle. *The Journal of biological chemistry*. 277:609-617.
- He, C., X. Hu, T.A. Weston, R.S. Jung, J. Sandhu, S. Huang, P. Heizer, J. Kim, R. Ellison, J. Xu, M. Kilburn, S.J. Bensinger, H. Riezman, P. Tontonoz, L.G. Fong, H. Jiang, and S.G. Young. 2018. Macrophages release plasma membrane-derived particles rich in accessible cholesterol. *Proceedings of the National Academy of Sciences of the United States of America*. 115:E8499-E8508.
- Heino, S., S. Lusa, P. Somerharju, C. Ehnholm, V.M. Olkkonen, and E. Ikonen. 2000. Dissecting the role of the golgi complex and lipid rafts in biosynthetic transport of cholesterol to the cell surface. *Proceedings of the National Academy of Sciences of the United States of America*. 97:8375-8380.
- Holthuis, J.C., and A.K. Menon. 2014. Lipid landscapes and pipelines in membrane homeostasis. *Nature*. 510:48-57.
- Horenkamp, F.A., D.P. Valverde, J. Nunnari, and K.M. Reinisch. 2018. Molecular basis for sterol transport by StART-like lipid transfer domains. *The EMBO journal*. 37.
- Hoyer, M.J., P.J. Chitwood, C.C. Ebmeier, J.F. Striepen, R.Z. Qi, W.M. Old, and G.K. Voeltz. 2018. A Novel Class of ER Membrane Proteins Regulates ER-Associated Endosome Fission. *Cell*. 175:254-265 e214.
- Hsu, P.D., D.A. Scott, J.A. Weinstein, F.A. Ran, S. Konermann, V. Agarwala, Y. Li, E.J. Fine, X. Wu, O. Shalem, T.J. Cradick, L.A. Marraffini, G. Bao, and F. Zhang. 2013. DNA targeting specificity of RNA-guided Cas9 nucleases. *Nature biotechnology*. 31:827-832.
- Hu, X., T.A. Weston, C. He, R.S. Jung, P.J. Heizer, B.D. Young, Y. Tu, P. Tontonoz, J.A. Wohlschlegel, H. Jiang, S.G. Young, and L.G. Fong. 2019. Release of cholesterol-rich particles from the macrophage plasma membrane during movement of filopodia and lamellipodia. *eLife*. 8.
- Iaea, D.B., S. Mao, F.W. Lund, and F.R. Maxfield. 2017. Role of STARD4 in sterol transport between the endocytic recycling compartment and the plasma membrane. *Molecular biology of the cell*. 28:1111-1122.
- Ikonen, E. 2008. Cellular cholesterol trafficking and compartmentalization. *Nature reviews. Molecular cell biology*. 9:125-138.
- Infante, R.E., and A. Radhakrishnan. 2017. Continuous transport of a small fraction of plasma membrane cholesterol to endoplasmic reticulum regulates total cellular cholesterol. *eLife*. 6.
- Jentsch, J.A., I. Kiburu, K. Pandey, M. Timme, T. Ramlall, B. Levkau, J. Wu, D. Eliezer, O. Boudker, and A.K. Menon. 2018. Structural basis of sterol binding and transport by a yeast StArkin domain. *The Journal of biological chemistry*. 293:5522-5531.

- Jeyasimman, D., and Y. Saheki. 2019. SMP domain proteins in membrane lipid dynamics. *Biochim Biophys Acta Mol Cell Biol Lipids*.
- Johnson, B.B., P.C. Moe, D. Wang, K. Rossi, B.L. Trigatti, and A.P. Heuck. 2012. Modifications in perfringolysin O domain 4 alter the cholesterol concentration threshold required for binding. *Biochemistry*. 51:3373-3382.
- Johnson, K.A., S. Endapally, D.C. Vazquez, R.E. Infante, and A. Radhakrishnan. 2019. Ostreolysin A and anthrolysin O use different mechanisms to control movement of cholesterol from the plasma membrane to the endoplasmic reticulum. *The Journal of biological chemistry*.
- Kawano, S., Y. Tamura, R. Kojima, S. Bala, E. Asai, A.H. Michel, B. Kornmann, I. Riezman, H. Riezman, Y. Sakae, Y. Okamoto, and T. Endo. 2018. Structure-function insights into direct lipid transfer between membranes by Mmm1-Mdm12 of ERMES. *The Journal of cell biology*. 217:959-974.
- Kelley, L.A., S. Mezulis, C.M. Yates, M.N. Wass, and M.J. Sternberg. 2015. The Phyre2 web portal for protein modeling, prediction and analysis. *Nature protocols*. 10:845-858.
- Kumar, N., M. Leonzino, W. Hancock-Cerutti, F.A. Horenkamp, P. Li, J.A. Lees, H. Wheeler, K.M. Reinisch, and P. De Camilli. 2018. VPS13A and VPS13C are lipid transport proteins differentially localized at ER contact sites. *The Journal of cell biology*. 217:3625-3639.
- Lahiri, S., A. Toulmay, and W.A. Prinz. 2015. Membrane contact sites, gateways for lipid homeostasis. *Current opinion in cell biology*. 33:82-87.
- Lange, Y., and T.L. Steck. 1997. Quantitation of the pool of cholesterol associated with acyl-CoA:cholesterol acyltransferase in human fibroblasts. *The Journal of biological chemistry*. 272:13103-13108.
- Lange, Y., M.H. Swaisgood, B.V. Ramos, and T.L. Steck. 1989. Plasma membranes contain half the phospholipid and 90% of the cholesterol and sphingomyelin in cultured human fibroblasts. *The Journal of biological chemistry*. 264:3786-3793.
- Lange, Y., S.M. Tabei, J. Ye, and T.L. Steck. 2013. Stability and stoichiometry of bilayer phospholipid-cholesterol complexes: relationship to cellular sterol distribution and homeostasis. *Biochemistry*. 52:6950-6959.
- Lange, Y., J. Ye, and T.L. Steck. 2004. How cholesterol homeostasis is regulated by plasma membrane cholesterol in excess of phospholipids. *Proceedings of the National Academy of Sciences of the United States of America*. 101:11664-11667.
- Lange, Y., J. Ye, and T.L. Steck. 2014. Essentially all excess fibroblast cholesterol moves from plasma membranes to intracellular compartments. *PloS one*. 9:e98482.
- Laraia, L., A. Friese, D.P. Corkery, G. Konstantinidis, N. Erwin, W. Hofer, H. Karatas, L. Klewer, A. Brockmeyer, M. Metz, B. Scholermann, M. Dwivedi, L. Li, P. Rios-Munoz, M. Kohn, R. Winter, I.R. Vetter, S. Ziegler, P. Janning, Y.W. Wu, and H. Waldmann. 2019. The cholesterol transfer protein GRAMD1A regulates autophagosome biogenesis. *Nature chemical biology*. 15:710-720.
- Lev, S. 2012. Nonvesicular lipid transfer from the endoplasmic reticulum. *Cold Spring Harbor perspectives in biology*. 4.
- Leventis, R., and J.R. Silvius. 2001. Use of cyclodextrins to monitor transbilayer movement and differential lipid affinities of cholesterol. *Biophysical journal*. 81:2257-2267.
- Lin, D., T. Sugawara, J.F. Strauss, 3rd, B.J. Clark, D.M. Stocco, P. Saenger, A. Rogol, and W.L. Miller. 1995. Role of steroidogenic acute regulatory protein in adrenal and gonadal steroidogenesis. *Science*. 267:1828-1831.
- Luo, J., L.Y. Jiang, H. Yang, and B.L. Song. 2018. Intracellular Cholesterol Transport by Sterol Transfer Proteins at Membrane Contact Sites. *Trends in biochemical sciences*.
- Lyons, E.T., R.D. Hemken, and F.S. Button, Jr. 1981. Overwintering of larvae of the cattle lungworm (*Dictyocaulus viviparus*) on pasture in Kentucky. *J Am Vet Med Assoc*. 179:456-457.
- Maekawa, M., and G.D. Fairn. 2015. Complementary probes reveal that phosphatidylserine is required for the proper transbilayer distribution of cholesterol. *Journal of cell science*. 128:1422-1433.
- McConnell, H.M., and A. Radhakrishnan. 2003. Condensed complexes of cholesterol and phospholipids. *Biochimica et biophysica acta*. 1610:159-173.
- Mesmin, B., N.H. Pipalia, F.W. Lund, T.F. Ramlall, A. Sokolov, D. Eliezer, and F.R. Maxfield. 2011. STARD4 abundance regulates sterol transport and sensing. *Molecular biology of the cell*. 22:4004-4015.
- Murley, A., R.D. Sarsam, A. Toulmay, J. Yamada, W.A. Prinz, and J. Nunnari. 2015. Ltc1 is an ER-localized sterol transporter and a component of ER-mitochondria and ER-vacuole contacts. *The Journal of cell biology*. 209:539-548.

- Murley, A., J. Yamada, B.J. Niles, A. Toulmay, W.A. Prinz, T. Powers, and J. Nunnari. 2017. Sterol transporters at membrane contact sites regulate TORC1 and TORC2 signaling. *The Journal of cell biology*.
- Muthuswamy, S.K., M. Gilman, and J.S. Brugge. 1999. Controlled dimerization of ErbB receptors provides evidence for differential signaling by homo- and heterodimers. *Molecular and cellular biology*. 19:6845-6857.
- Ngo, M., and N.D. Ridgway. 2009. Oxysterol binding protein-related Protein 9 (ORP9) is a cholesterol transfer protein that regulates Golgi structure and function. *Molecular biology of the cell*. 20:1388-1399.
- Nishimura, T., and C.J. Stefan. 2019. Specialized ER membrane domains for lipid metabolism and transport. *Biochim Biophys Acta Mol Cell Biol Lipids*.
- Ohvo-Rekila, H., B. Ramstedt, P. Leppimaki, and J.P. Slotte. 2002. Cholesterol interactions with phospholipids in membranes. *Prog Lipid Res*. 41:66-97.
- Petrunaro, C., and B. Kornmann. 2019. Lipid exchange at ER-mitochondria contact sites: a puzzle falling into place with quite a few pieces missing. *Current opinion in cell biology*. 57:71-76.
- Phillips, M.C. 2014. Molecular mechanisms of cellular cholesterol efflux. *The Journal of biological chemistry*. 289:24020-24029.
- Phillips, M.J., and G.K. Voeltz. 2016. Structure and function of ER membrane contact sites with other organelles. *Nature reviews. Molecular cell biology*. 17:69-82.
- Radhakrishnan, A., and H.M. McConnell. 2000. Chemical activity of cholesterol in membranes. *Biochemistry*. 39:8119-8124.
- Ran, F.A., P.D. Hsu, J. Wright, V. Agarwala, D.A. Scott, and F. Zhang. 2013. Genome engineering using the CRISPR-Cas9 system. *Nature protocols*. 8:2281-2308.
- Ray, T.K., V.P. Skipski, M. Barclay, E. Essner, and F.M. Archibald. 1969. Lipid composition of rat liver plasma membranes. *The Journal of biological chemistry*. 244:5528-5536.
- Roth, S., and R. Heintzmann. 2016. Optical photon reassignment with increased axial resolution by structured illumination. *Methods Appl Fluoresc*. 4:045005.
- Saheki, Y., X. Bian, C.M. Schauder, Y. Sawaki, M.A. Surma, C. Klose, F. Pincet, K.M. Reinisch, and P. De Camilli. 2016. Control of plasma membrane lipid homeostasis by the extended synaptotagmins. *Nature cell biology*. 18:504-515.
- Saheki, Y., and P. De Camilli. 2017a. Endoplasmic Reticulum-Plasma Membrane Contact Sites. *Annual review of biochemistry*. 86:659-684.
- Saheki, Y., and P. De Camilli. 2017b. The Extended-Synaptotagmins. *Biochimica et biophysica acta*. 1864:1490-1493.
- Sales, S., O. Knittelfelder, and A. Shevchenko. 2017. Lipidomics of Human Blood Plasma by High-Resolution Shotgun Mass Spectrometry. *Methods Mol Biol*. 1619:203-212.
- Sandhu, J., S. Li, L. Fairall, S.G. Pfisterer, J.E. Gurnett, X. Xiao, T.A. Weston, D. Vashi, A. Ferrari, J.L. Orozco, C.L. Hartman, D. Strugatsky, S.D. Lee, C. He, C. Hong, H. Jiang, L.A. Bentolila, A.T. Gatta, T.P. Levine, A. Ferng, R. Lee, D.A. Ford, S.G. Young, E. Ikonen, J.W.R. Schwabe, and P. Tontonoz. 2018. Aster Proteins Facilitate Nonvesicular Plasma Membrane to ER Cholesterol Transport in Mammalian Cells. *Cell*. 175:514-529 e520.
- Scheek, S., M.S. Brown, and J.L. Goldstein. 1997. Sphingomyelin depletion in cultured cells blocks proteolysis of sterol regulatory element binding proteins at site 1. *Proceedings of the National Academy of Sciences of the United States of America*. 94:11179-11183.
- Segrest, J.P., H. De Loof, J.G. Dohlman, C.G. Brouillette, and G.M. Anantharamaiah. 1990. Amphipathic helix motif: classes and properties. *Proteins*. 8:103-117.
- Shimada, Y., M. Maruya, S. Iwashita, and Y. Ohno-Iwashita. 2002. The C-terminal domain of perfringolysin O is an essential cholesterol-binding unit targeting to cholesterol-rich microdomains. *European journal of biochemistry / FEBS*. 269:6195-6203.
- Slotte, J.P. 1992. Enzyme-catalyzed oxidation of cholesterol in mixed phospholipid monolayers reveals the stoichiometry at which free cholesterol clusters disappear. *Biochemistry*. 31:5472-5477.
- Slotte, J.P., and E.L. Bierman. 1988. Depletion of plasma-membrane sphingomyelin rapidly alters the distribution of cholesterol between plasma membranes and intracellular cholesterol pools in cultured fibroblasts. *The Biochemical journal*. 250:653-658.
- Soccio, R.E., R.M. Adams, M.J. Romanowski, E. Sehayek, S.K. Burley, and J.L. Breslow. 2002. The cholesterol-regulated StarD4 gene encodes a StAR-related lipid transfer protein with two closely related homologues, StarD5 and StarD6. *Proceedings of the National Academy of Sciences of the United States of America*. 99:6943-6948.

- Sokolov, A., and A. Radhakrishnan. 2010. Accessibility of cholesterol in endoplasmic reticulum membranes and activation of SREBP-2 switch abruptly at a common cholesterol threshold. *The Journal of biological chemistry*. 285:29480-29490.
- Steck, T.L., and Y. Lange. 2018. Transverse distribution of plasma membrane bilayer cholesterol: Picking sides. *Traffic*. 19:750-760.
- Stocco, D.M. 2001. StAR protein and the regulation of steroid hormone biosynthesis. *Annual review of physiology*. 63:193-213.
- Surma, M.A., R. Herzog, A. Vasilj, C. Klose, N. Christinat, D. Morin-Rivron, K. Simons, M. Masoodi, and J.L. Sampaio. 2015. An automated shotgun lipidomics platform for high throughput, comprehensive, and quantitative analysis of blood plasma intact lipids. *Eur J Lipid Sci Technol*. 117:1540-1549.
- Tong, J., M.K. Manik, and Y.J. Im. 2018. Structural basis of sterol recognition and nonvesicular transport by lipid transfer proteins anchored at membrane contact sites. *Proceedings of the National Academy of Sciences of the United States of America*. 115:E856-E865.
- Urbani, L., and R.D. Simoni. 1990. Cholesterol and vesicular stomatitis virus G protein take separate routes from the endoplasmic reticulum to the plasma membrane. *The Journal of biological chemistry*. 265:1919-1923.
- van Meer, G., D.R. Voelker, and G.W. Feigenson. 2008. Membrane lipids: where they are and how they behave. *Nature reviews. Molecular cell biology*. 9:112-124.
- Vance, J.E. 2015. Phospholipid synthesis and transport in mammalian cells. *Traffic*. 16:1-18.
- Wang, H., Q. Ma, Y. Qi, J. Dong, X. Du, J. Rae, J. Wang, W.F. Wu, A.J. Brown, R.G. Parton, J.W. Wu, and H. Yang. 2018. ORP2 Delivers Cholesterol to the Plasma Membrane in Exchange for Phosphatidylinositol 4, 5-Bisphosphate (PI(4,5)P2). *Molecular cell*.
- Wilhelm, L.P., C. Wendling, B. Védie, T. Kobayashi, M.P. Chenard, C. Tomasetto, G. Drin, and F. Alpy. 2017. STARD3 mediates endoplasmic reticulum-to-endosome cholesterol transport at membrane contact sites. *The EMBO journal*. 36:1412-1433.
- Wong, L.H., A.T. Gatta, and T.P. Levine. 2018. Lipid transfer proteins: the lipid commute via shuttles, bridges and tubes. *Nature reviews. Molecular cell biology*.
- Wu, H., P. Carvalho, and G.K. Voeltz. 2018. Here, there, and everywhere: The importance of ER membrane contact sites. *Science*. 361.
- Yeung, T., G.E. Gilbert, J. Shi, J. Silvius, A. Kapus, and S. Grinstein. 2008. Membrane phosphatidylserine regulates surface charge and protein localization. *Science*. 319:210-213.
- York, A.G., S.H. Parekh, D. Dalle Nogare, R.S. Fischer, K. Temprine, M. Mione, A.B. Chitnis, C.A. Combs, and H. Shroff. 2012. Resolution doubling in live, multicellular organisms via multifocal structured illumination microscopy. *Nature methods*. 9:749-754.

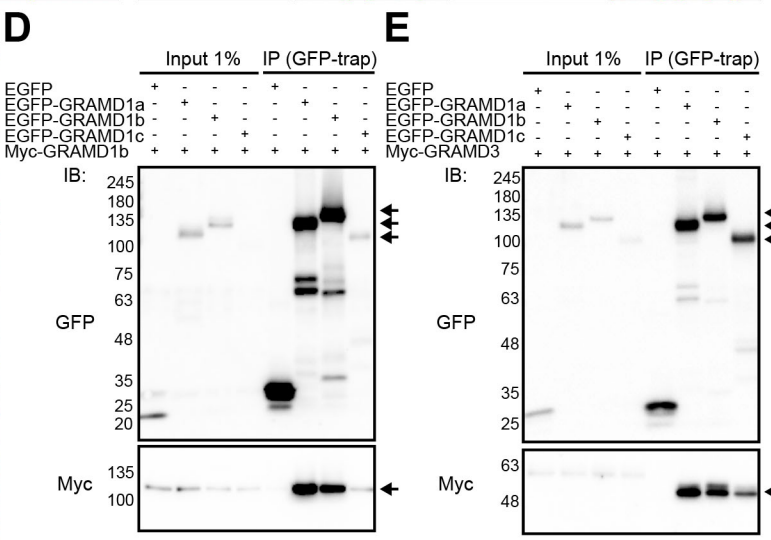
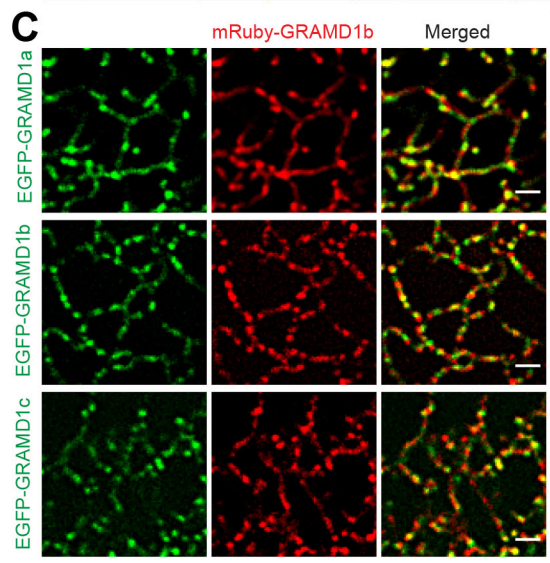
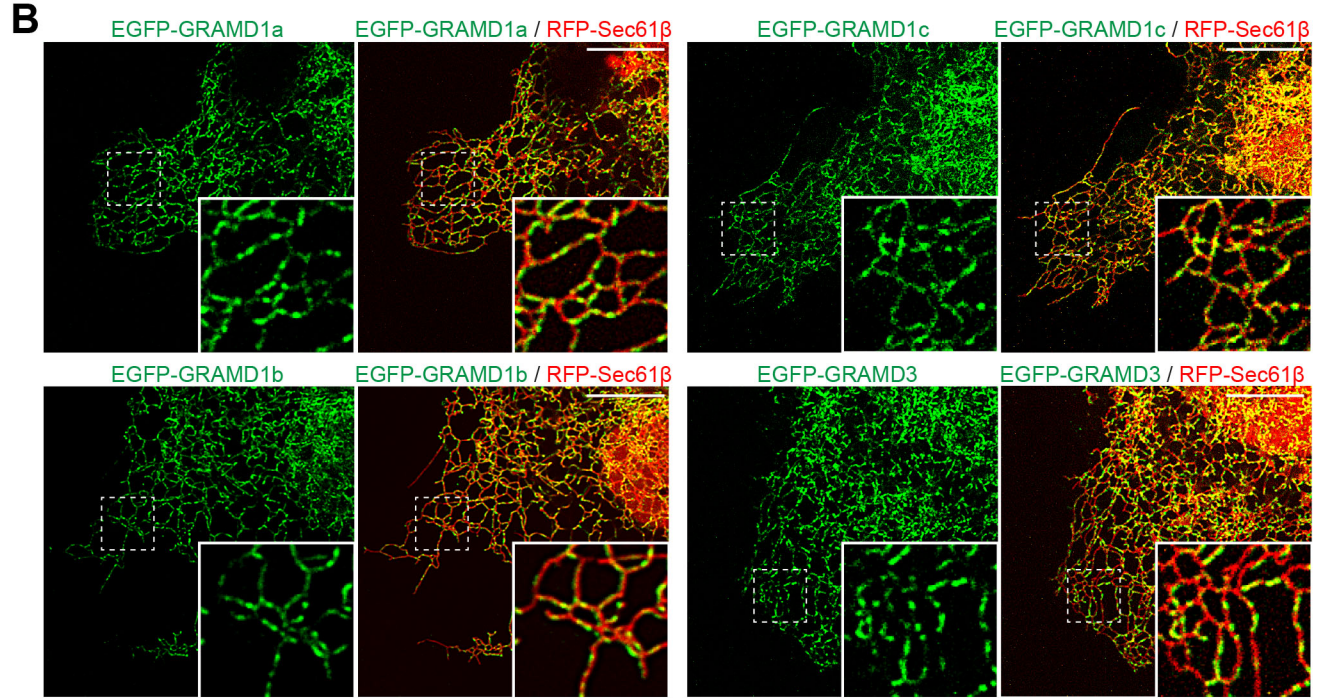
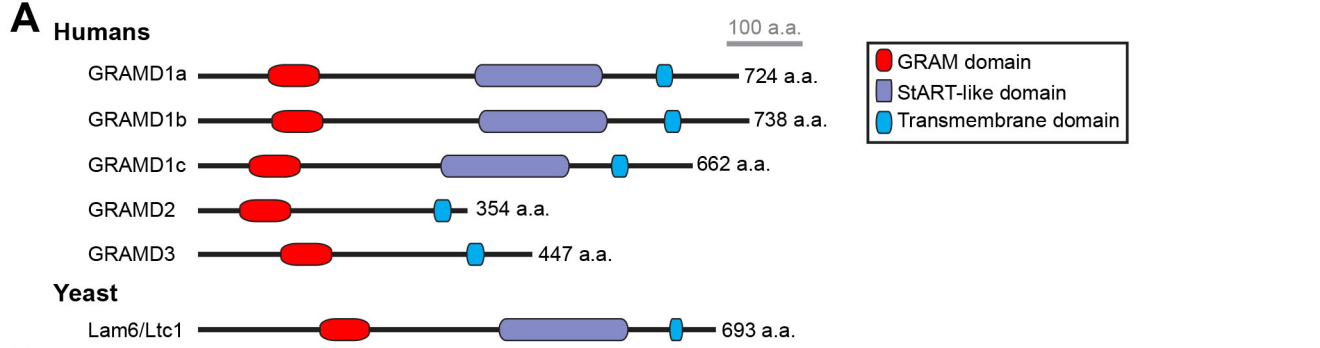


Figure 1

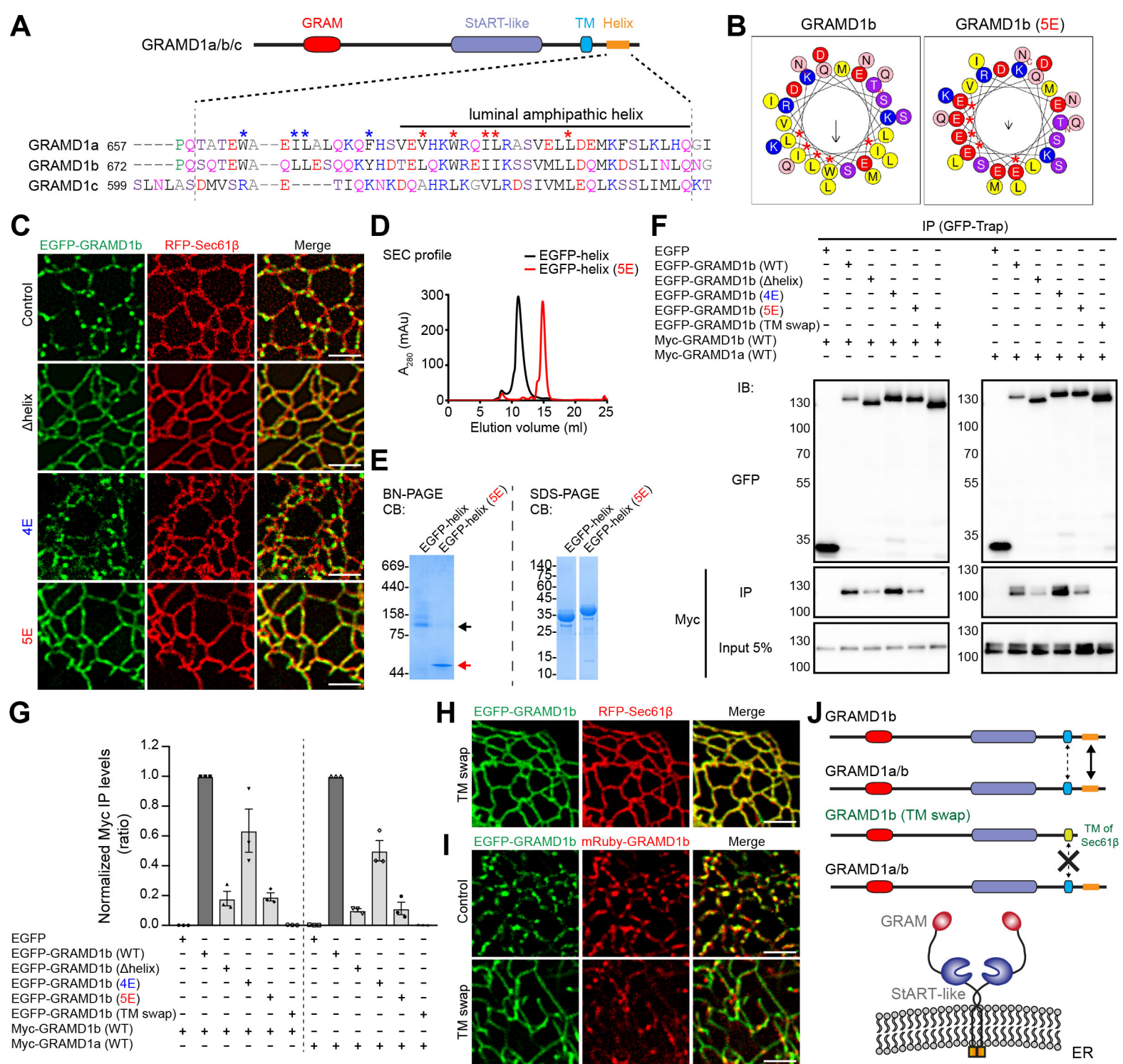


Figure 2

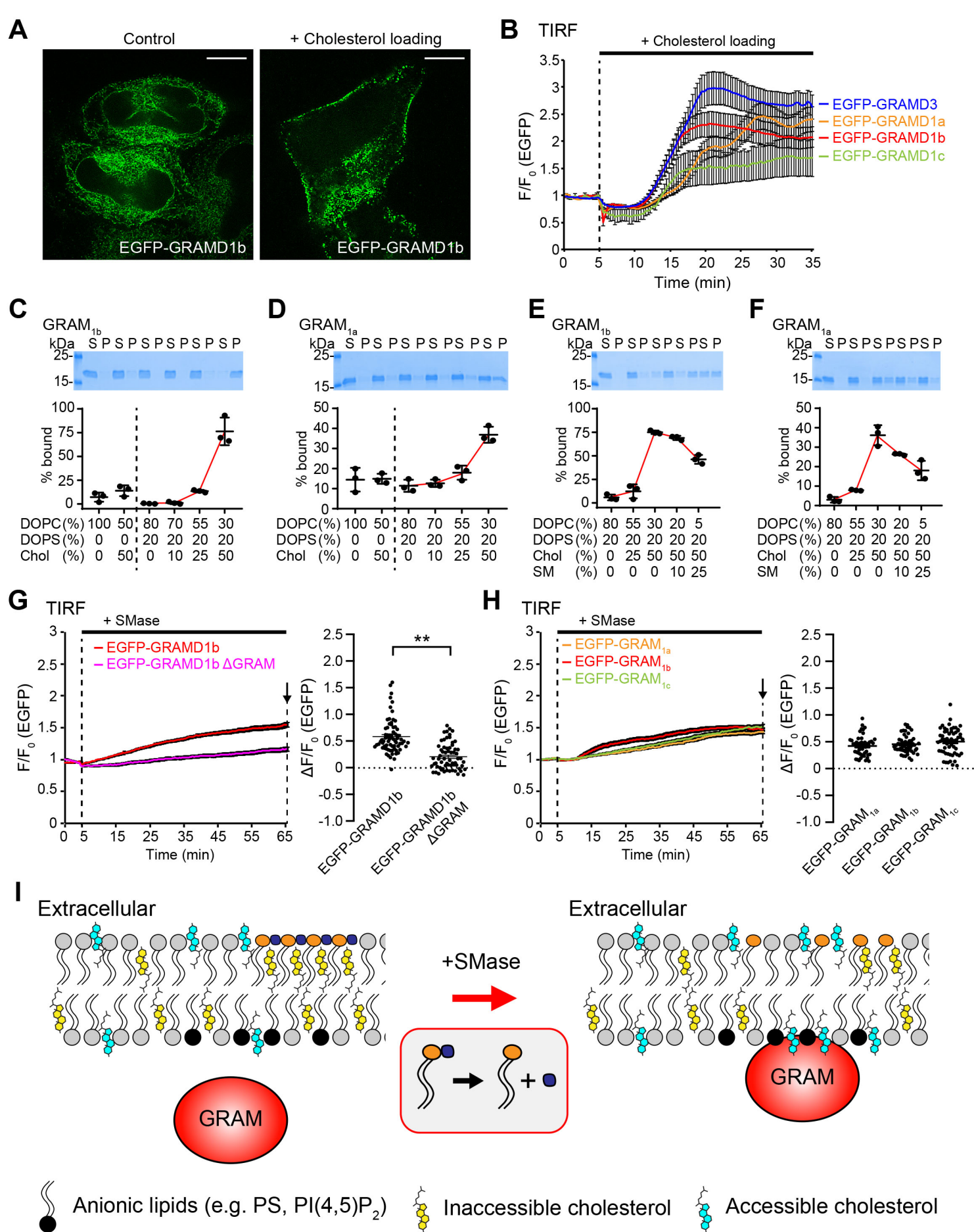


Figure 3

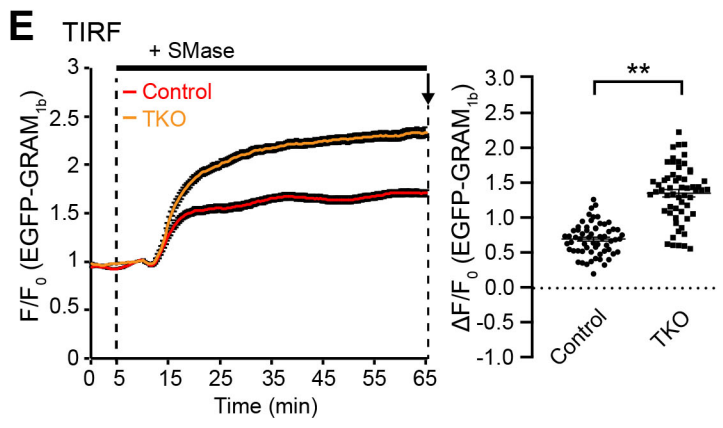
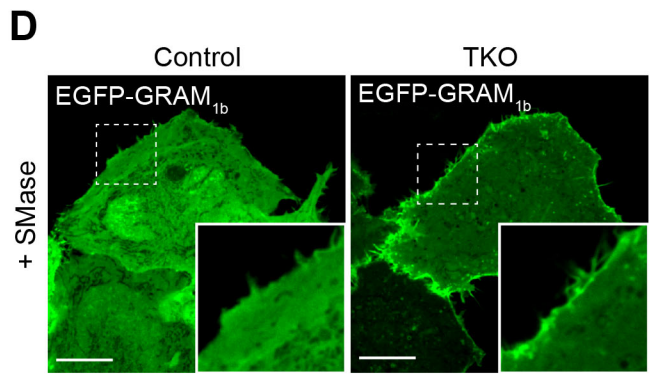
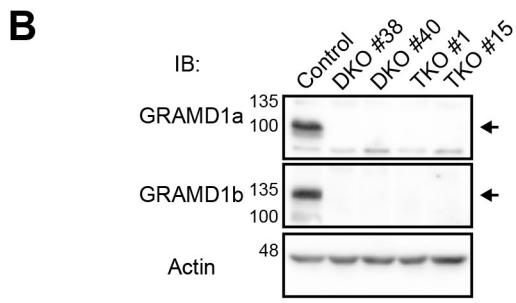
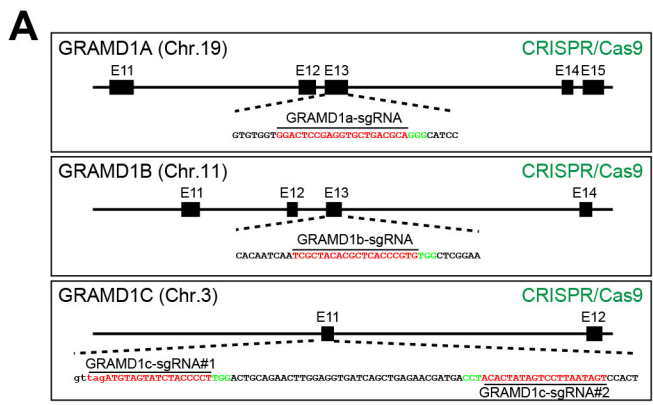


Figure 4

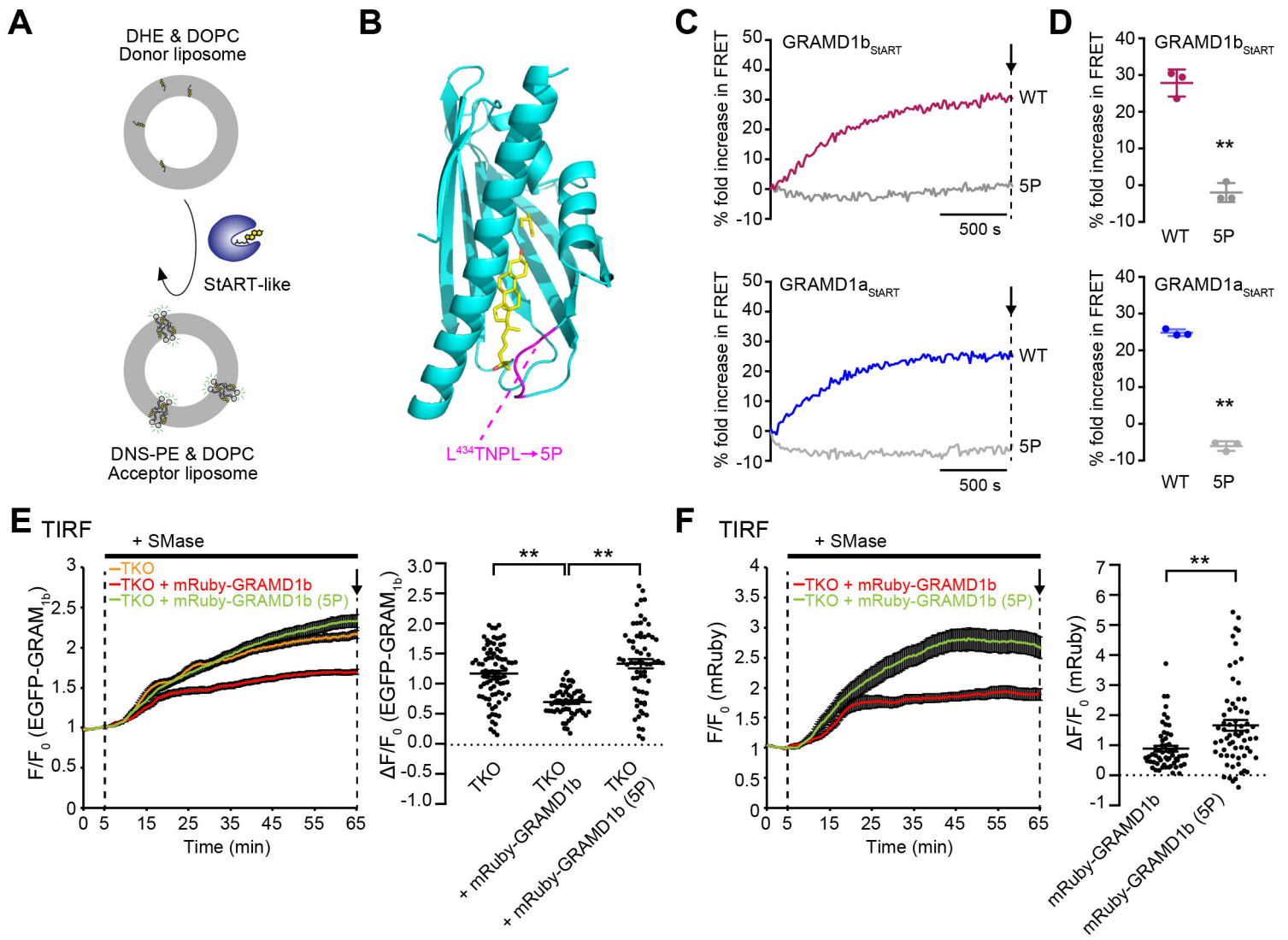


Figure 5

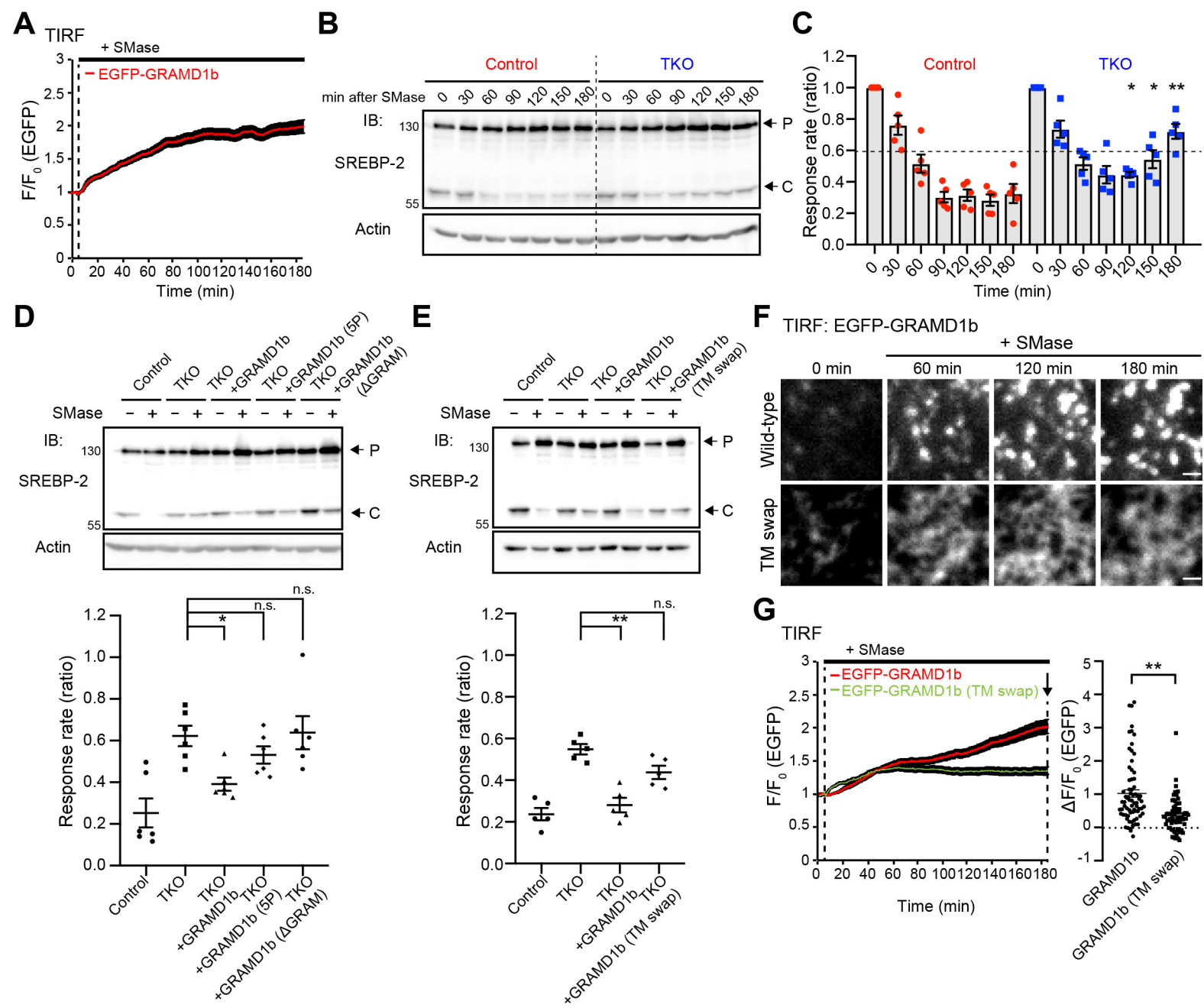


Figure 6

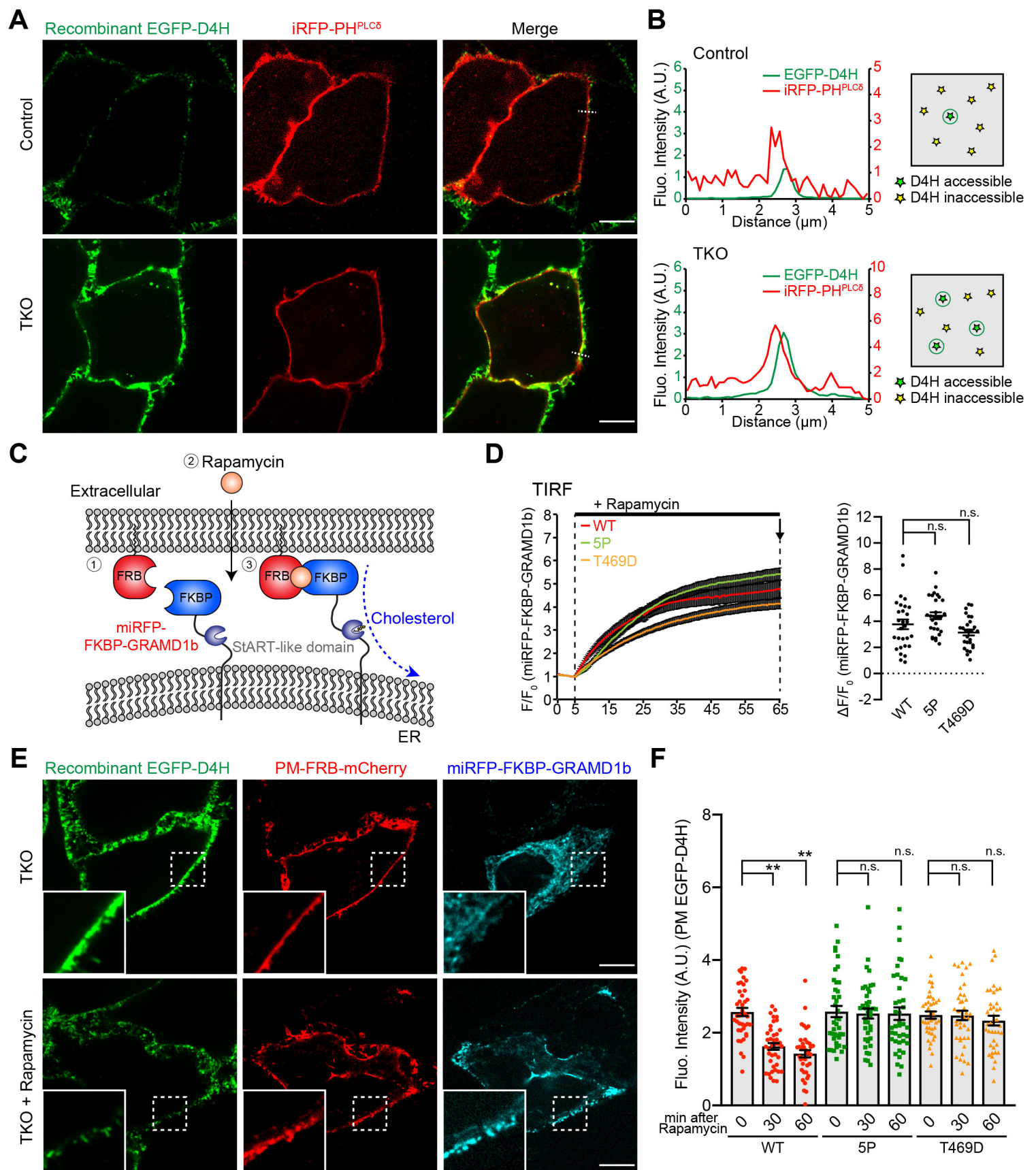
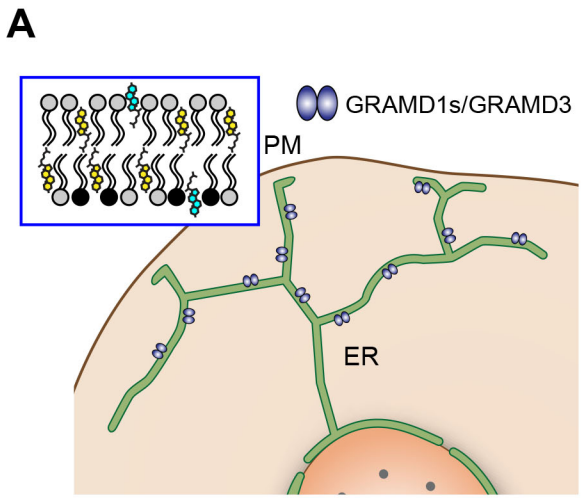
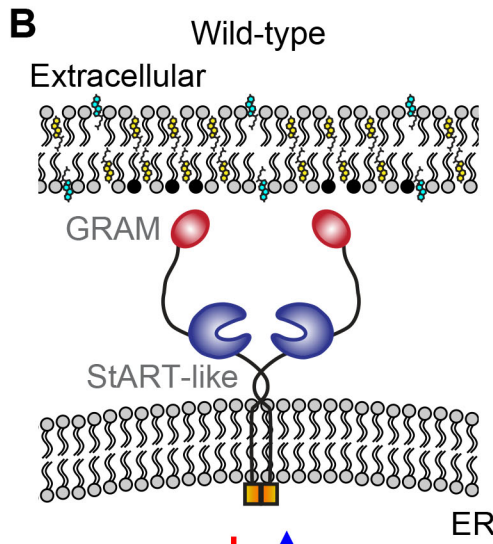
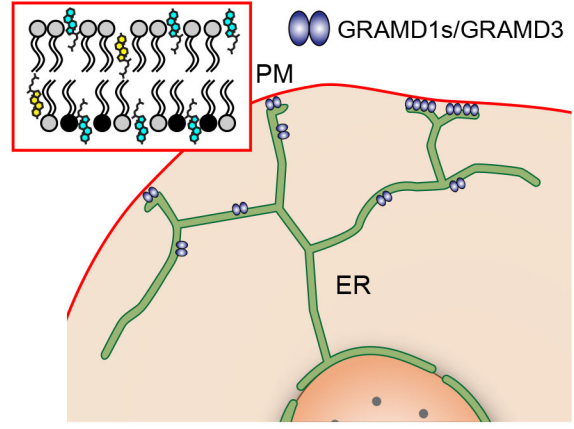


Figure 7

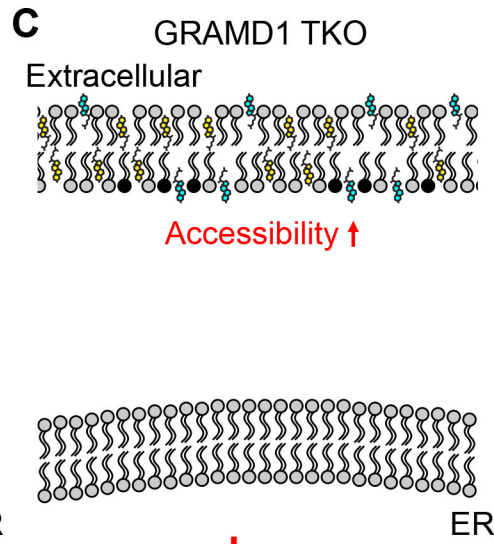
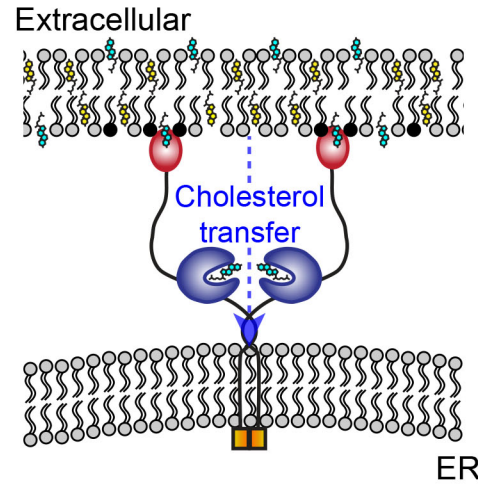


+SMase
+Cholesterol

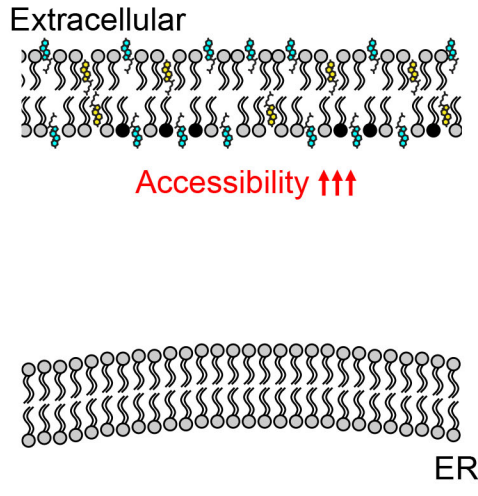
↓ ↑



↓ ↑



↓ ↑



Anionic lipids (e.g. PS, PI(4,5)P₂)
 Inaccessible cholesterol
 Accessible cholesterol

Figure 8

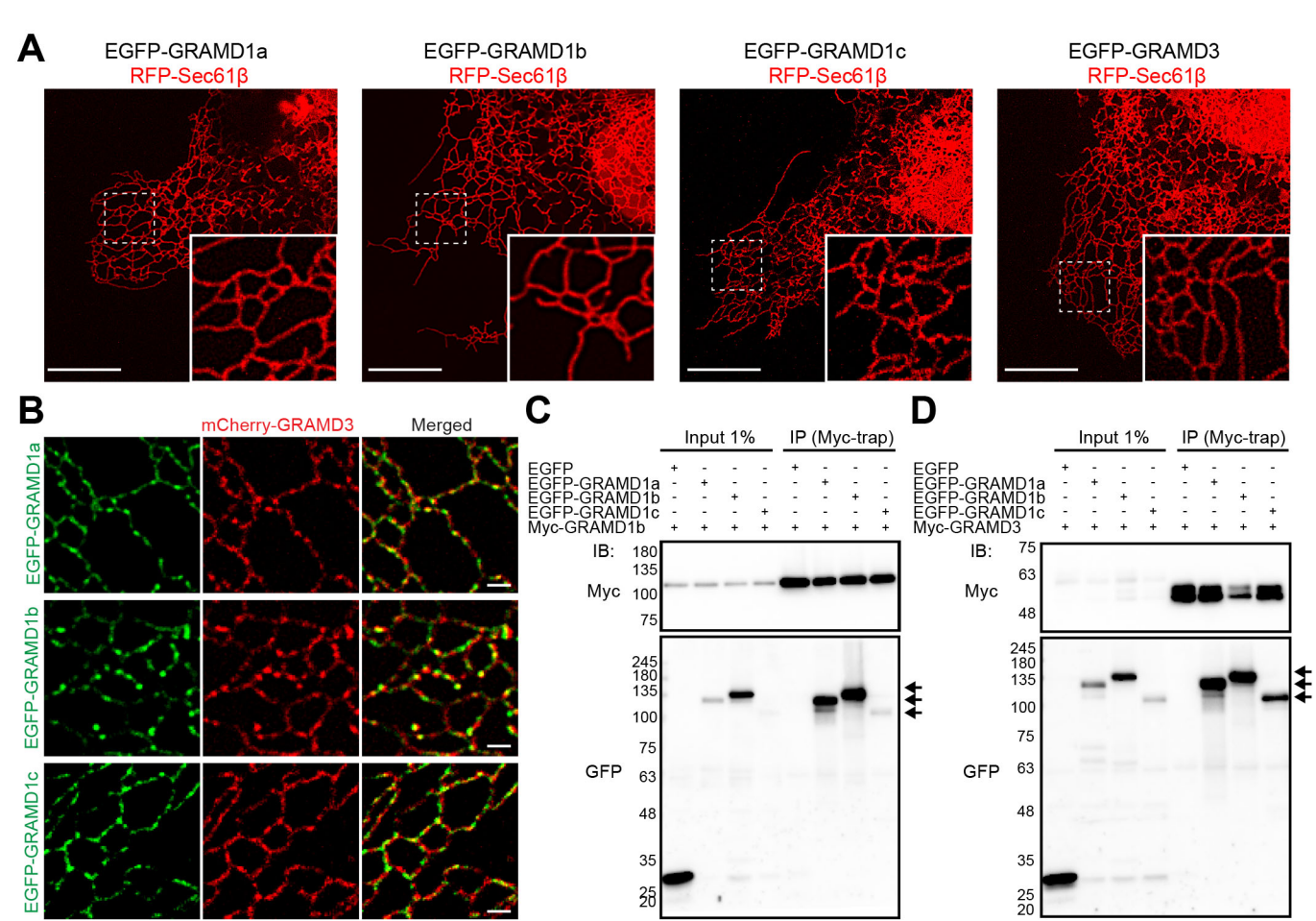
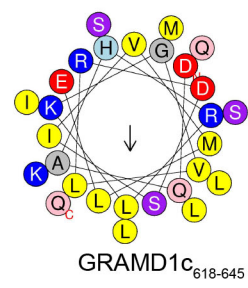
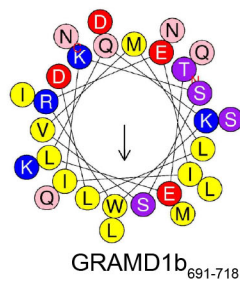
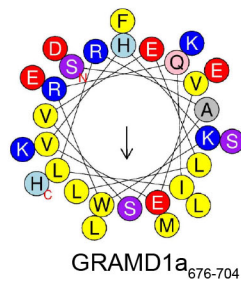
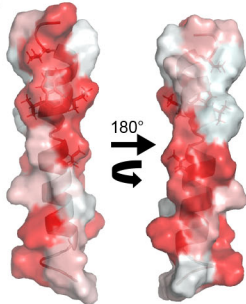
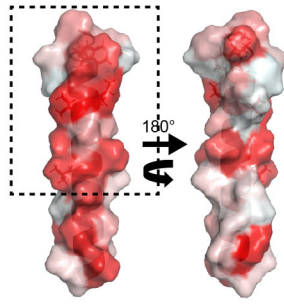
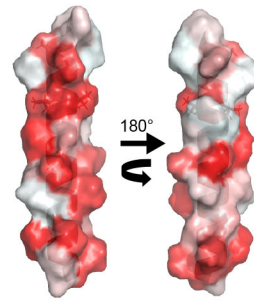


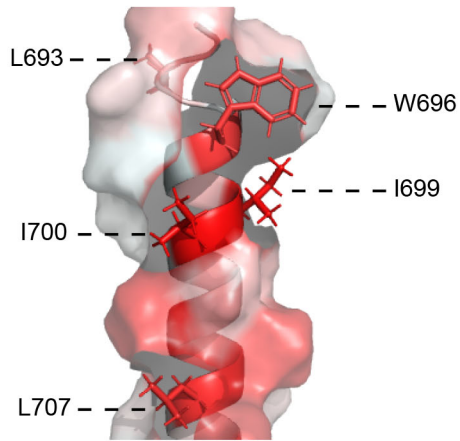
Figure 1-figure supplement 1

A**B**

N-term

GRAMD1a₆₇₆₋₇₀₃GRAMD1b₆₉₁₋₇₁₈GRAMD1c₆₁₈₋₆₄₅

C-term

C

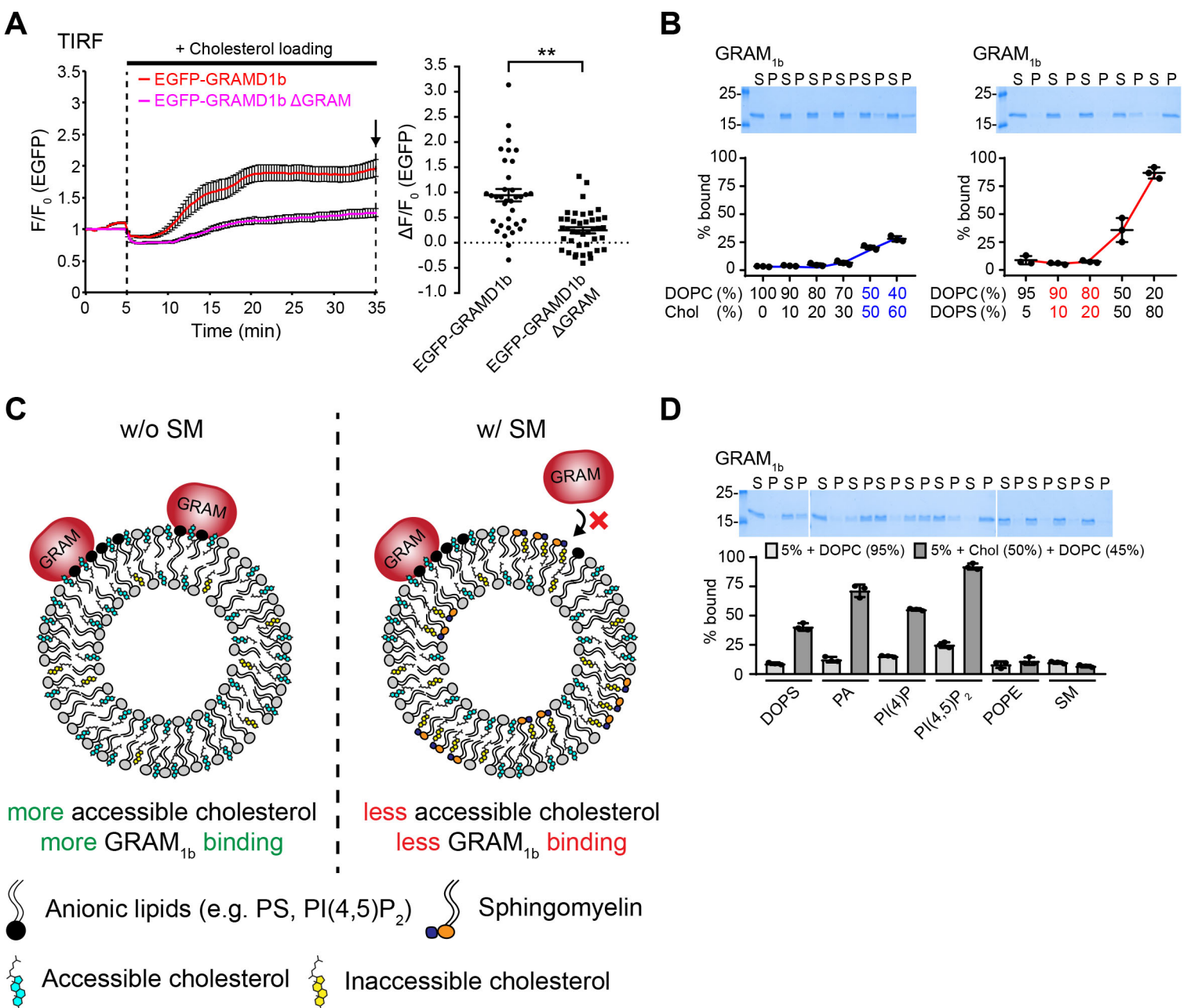


Figure 3-figure supplement 1

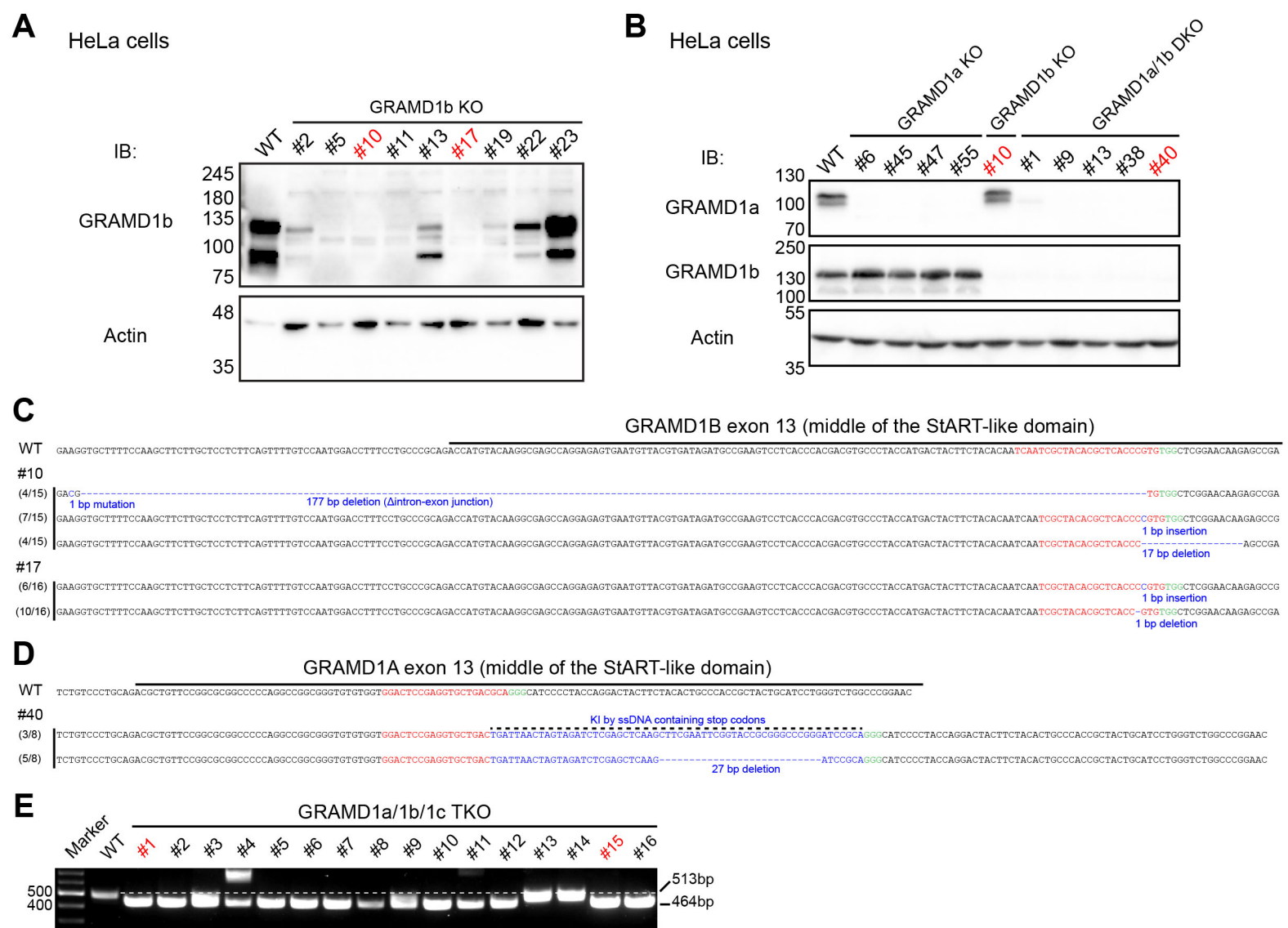


Figure 4-figure supplement 1

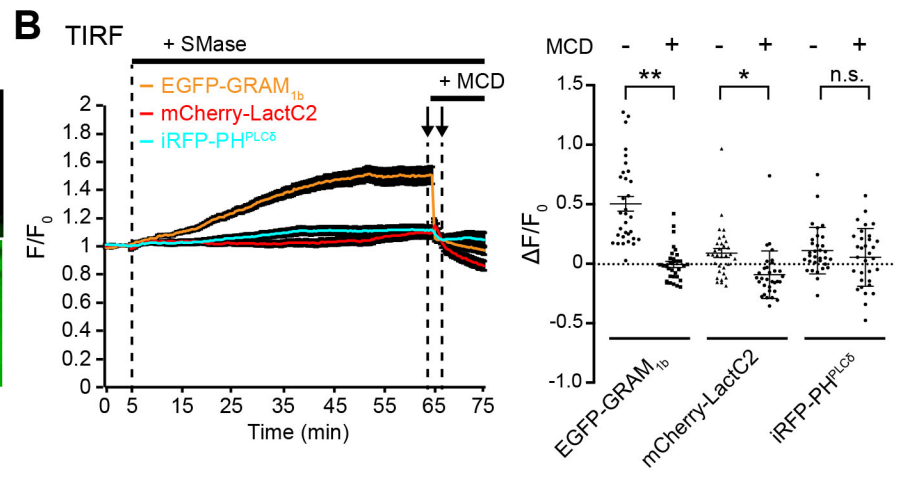
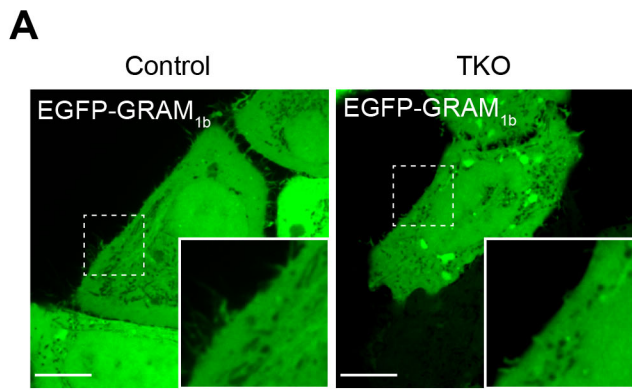


Figure 4-figure supplement 2

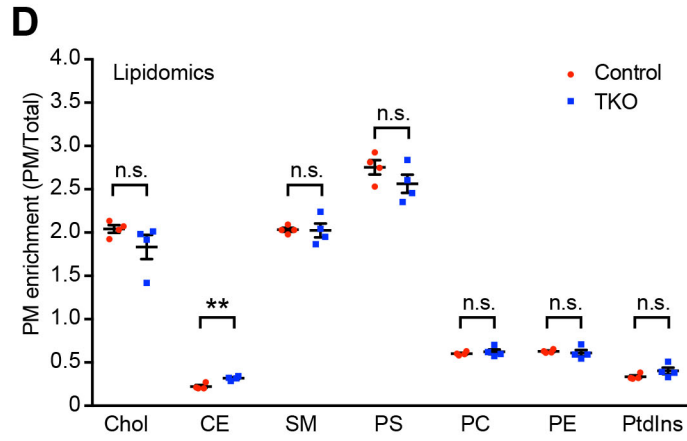
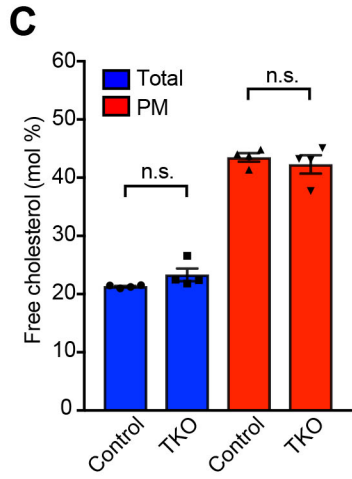
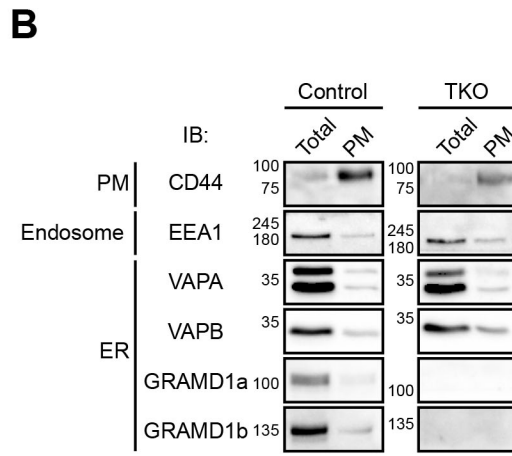
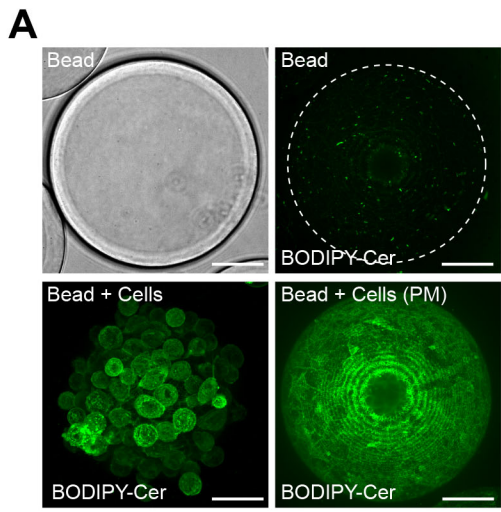


Figure 4-figure supplement 3

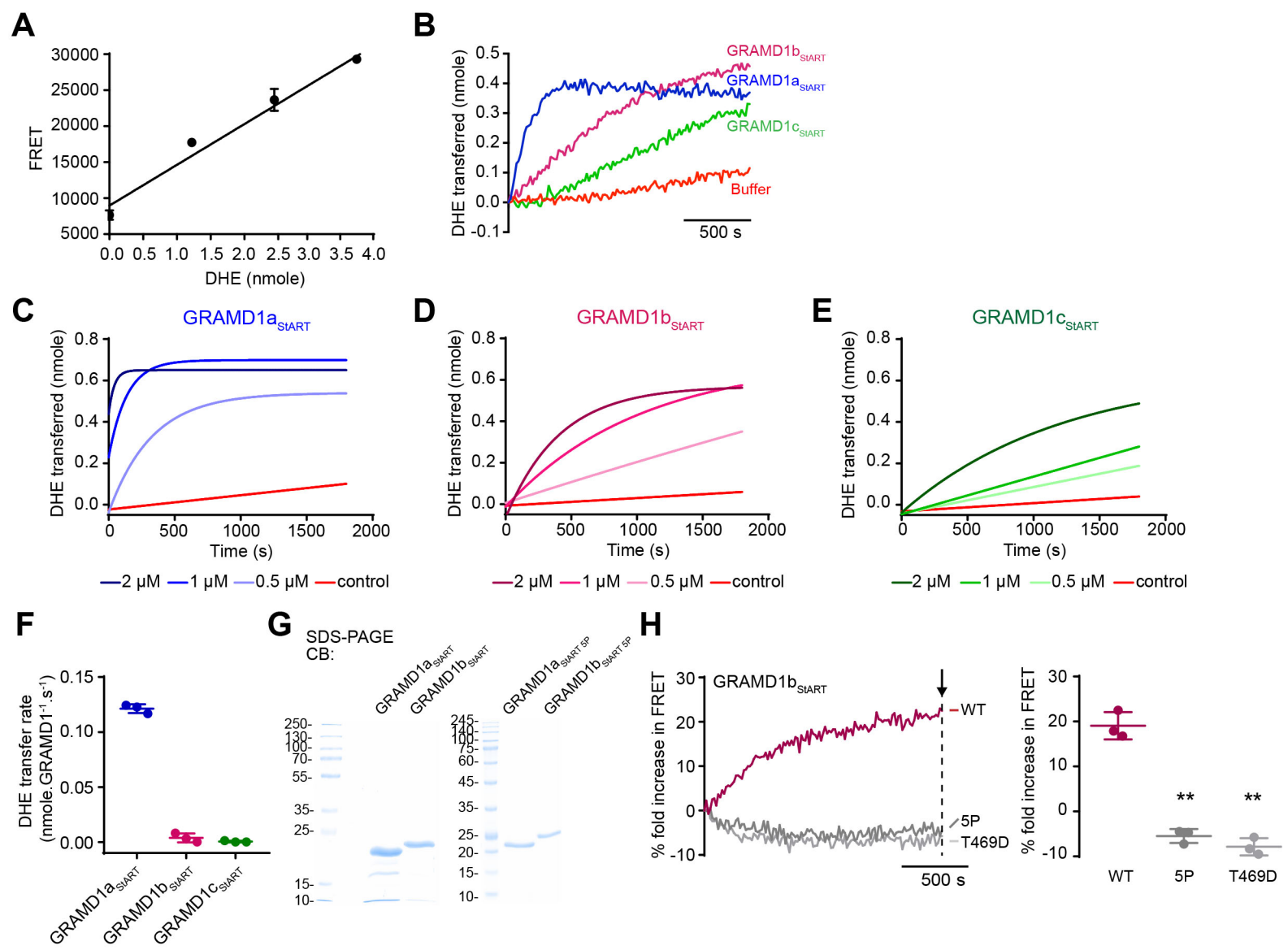


Figure 5-figure supplement 1

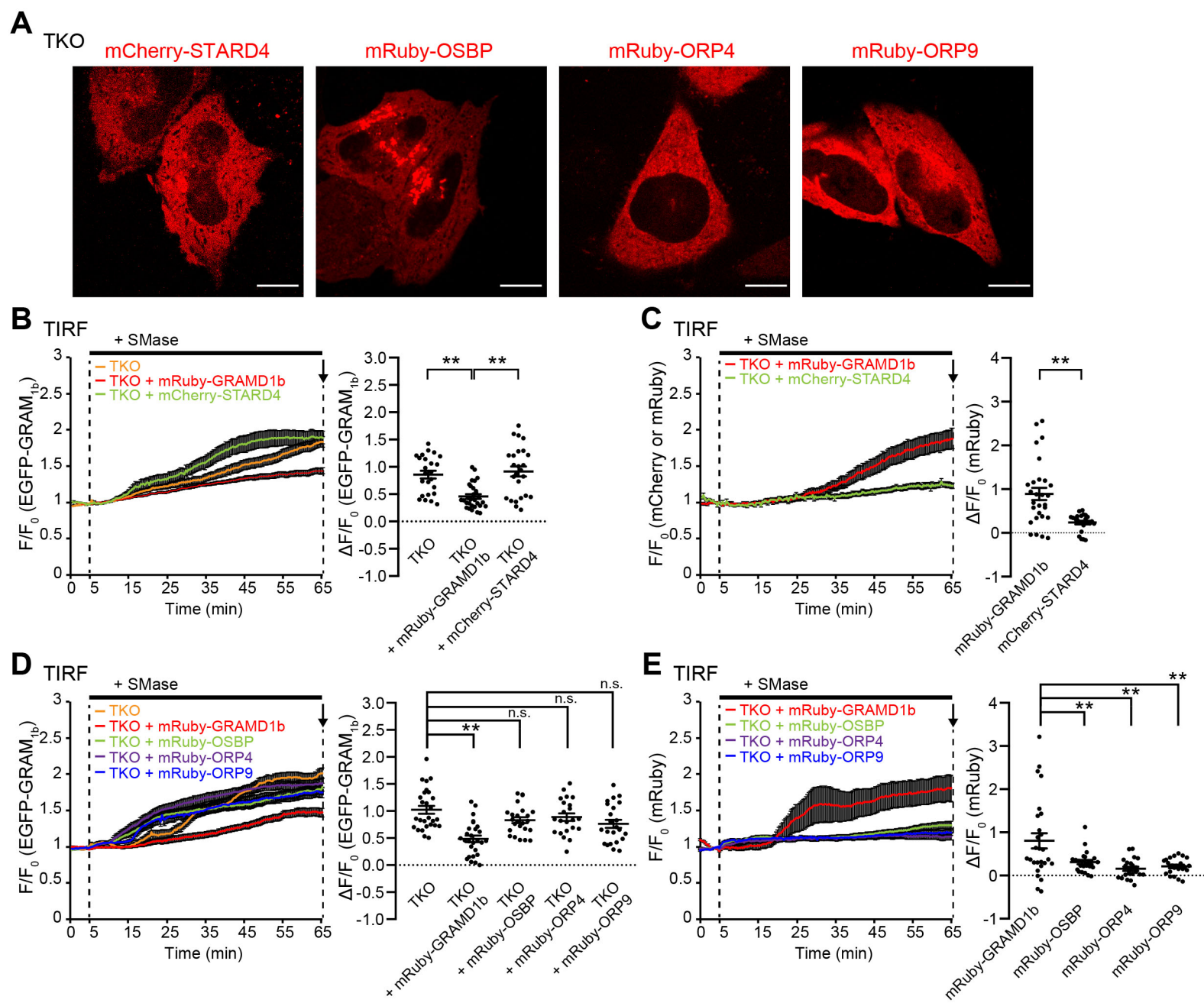


Figure 5-figure supplement 2

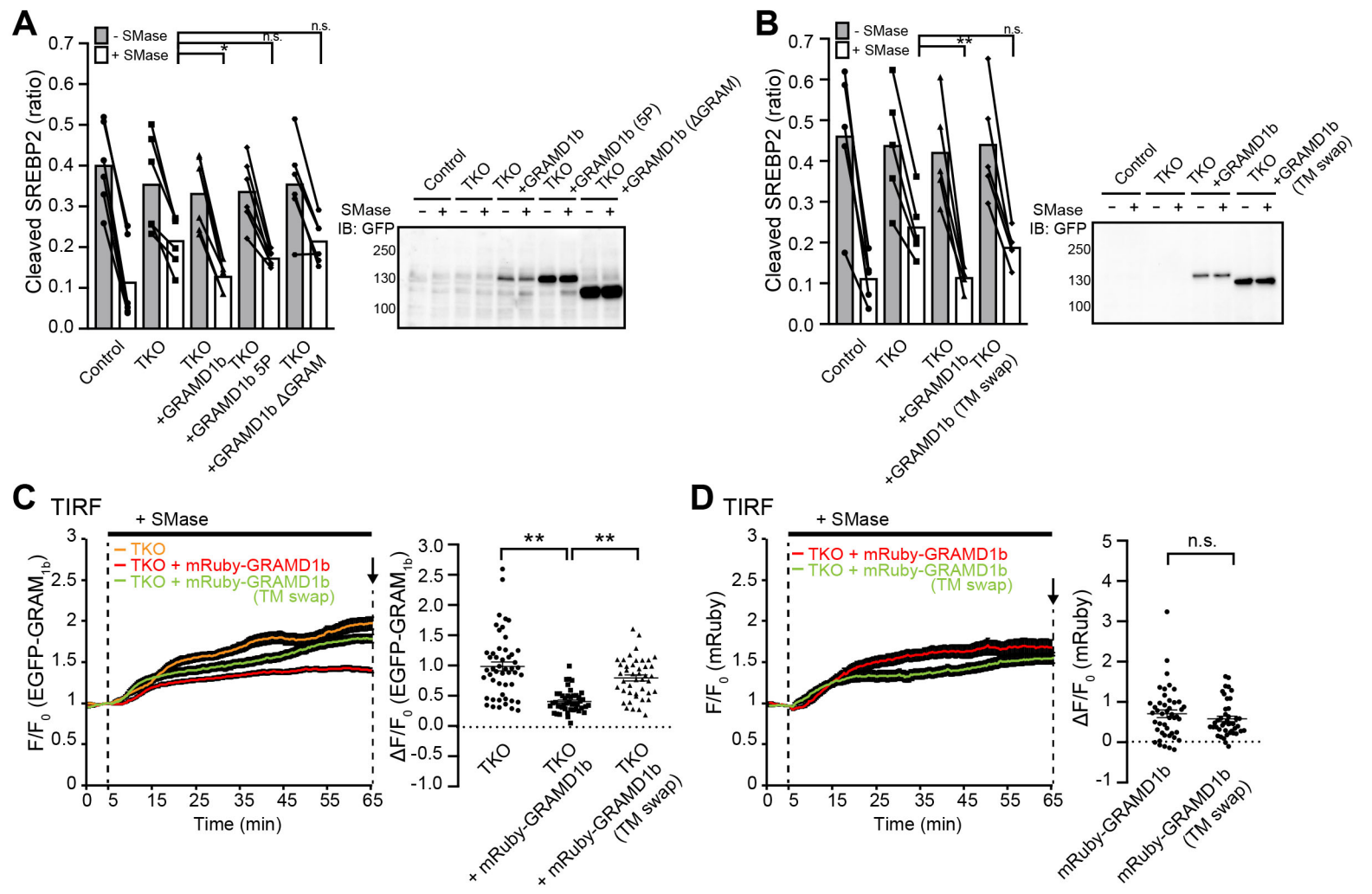


Figure 6-figure supplement 1

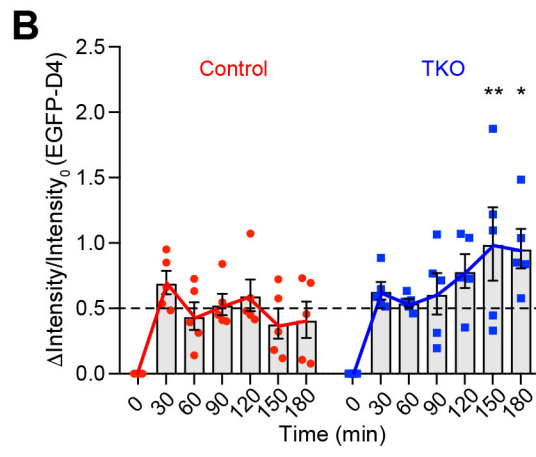
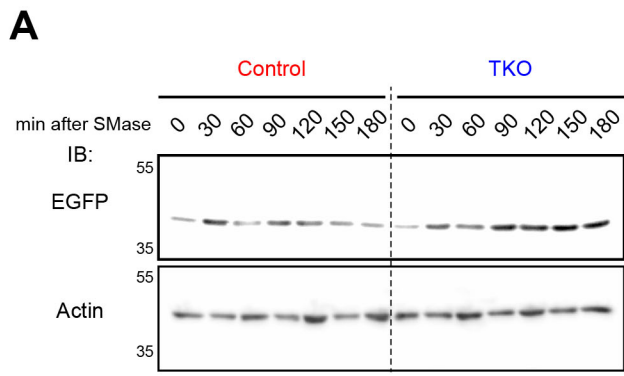


Figure 6-figure supplement 2

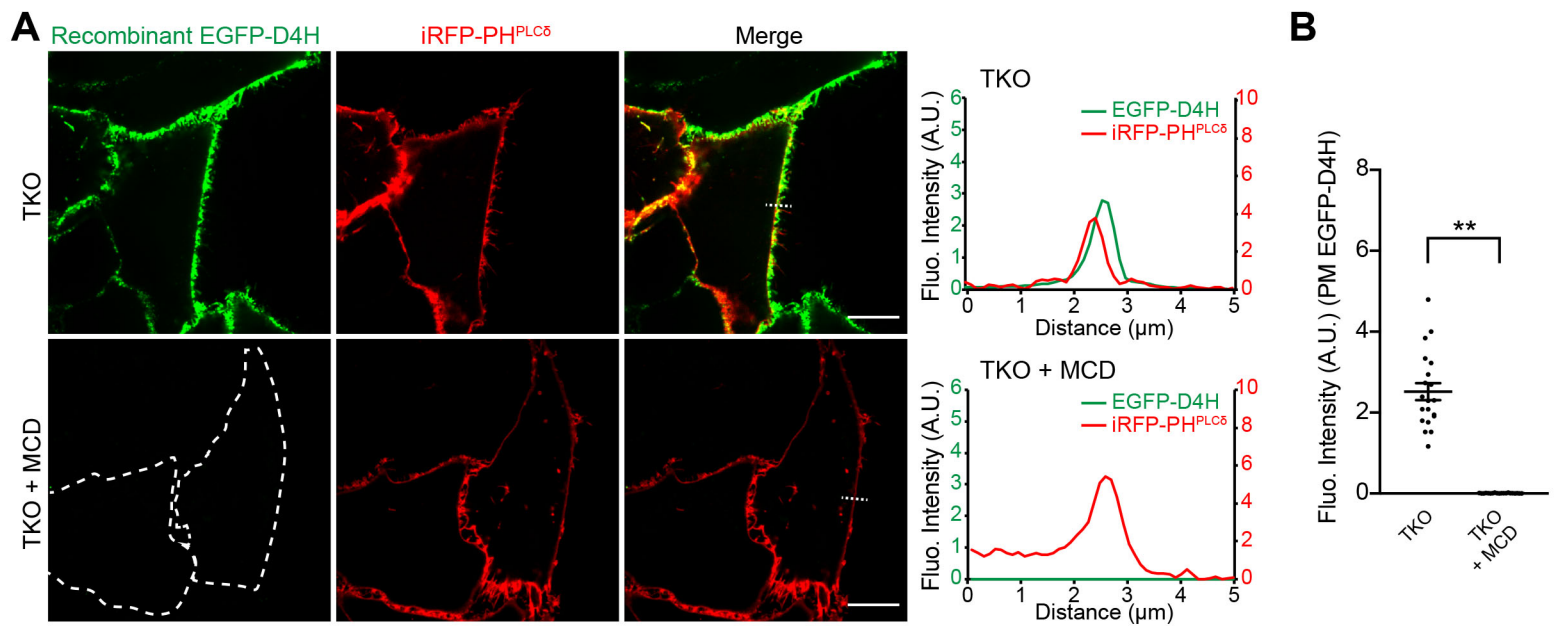
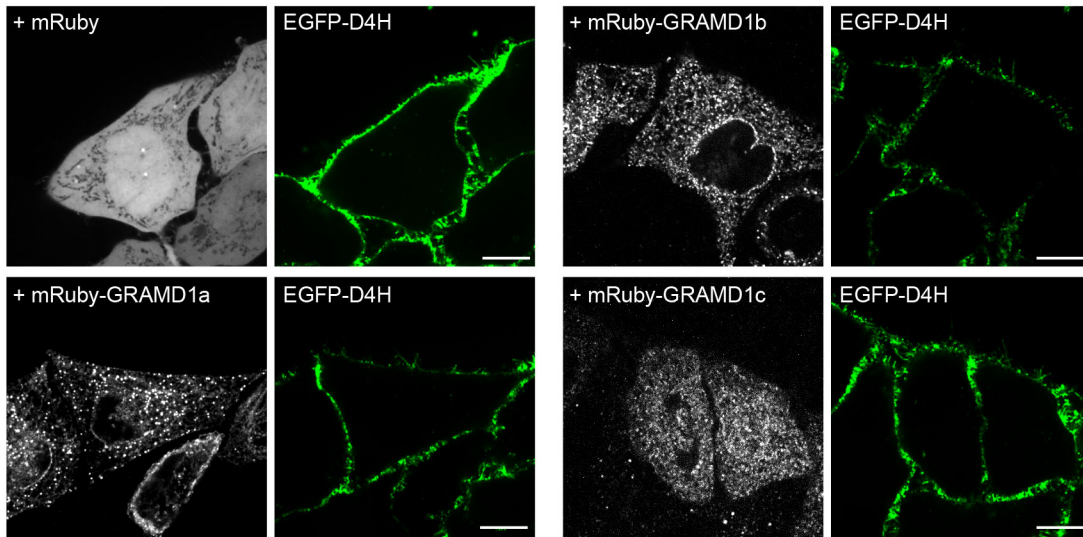
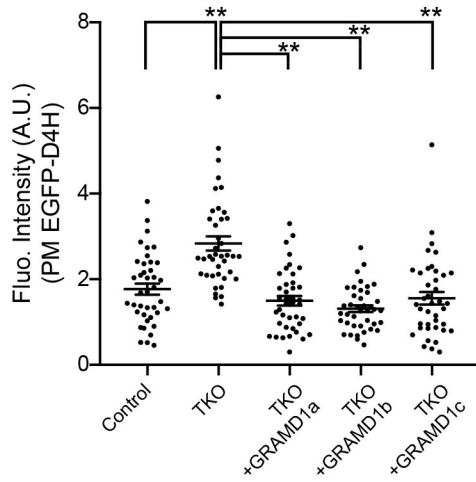
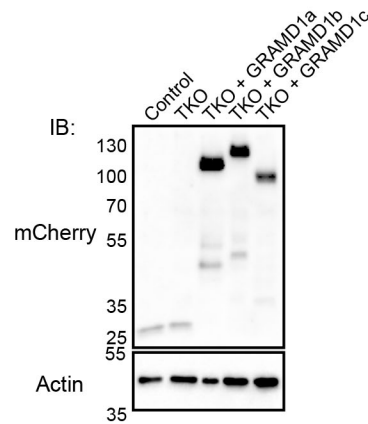
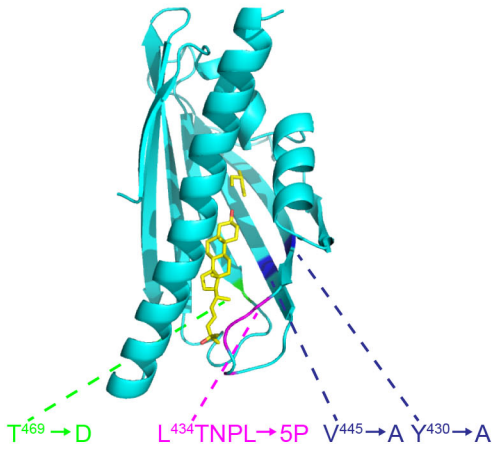
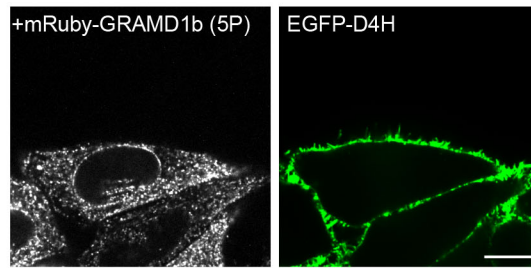
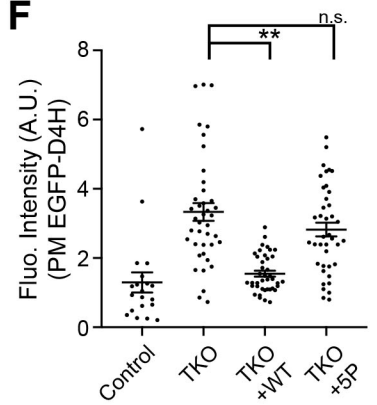
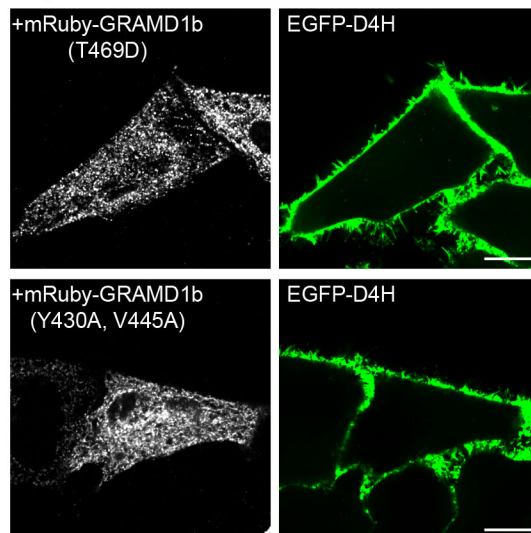
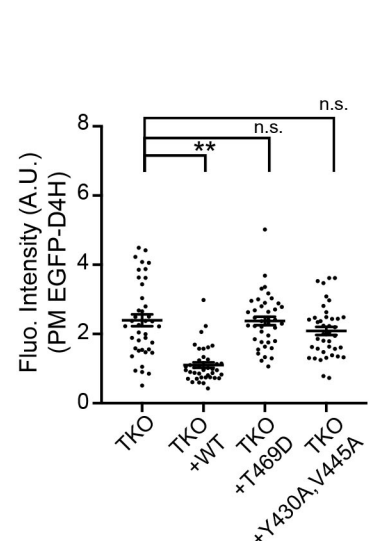
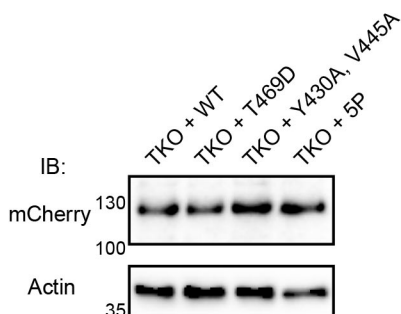


Figure 7-figure supplement 1

A TKO cells**B****C****D****E** TKO cells**F****G** TKO cells**H****I****Figure 7-figure supplement 2**

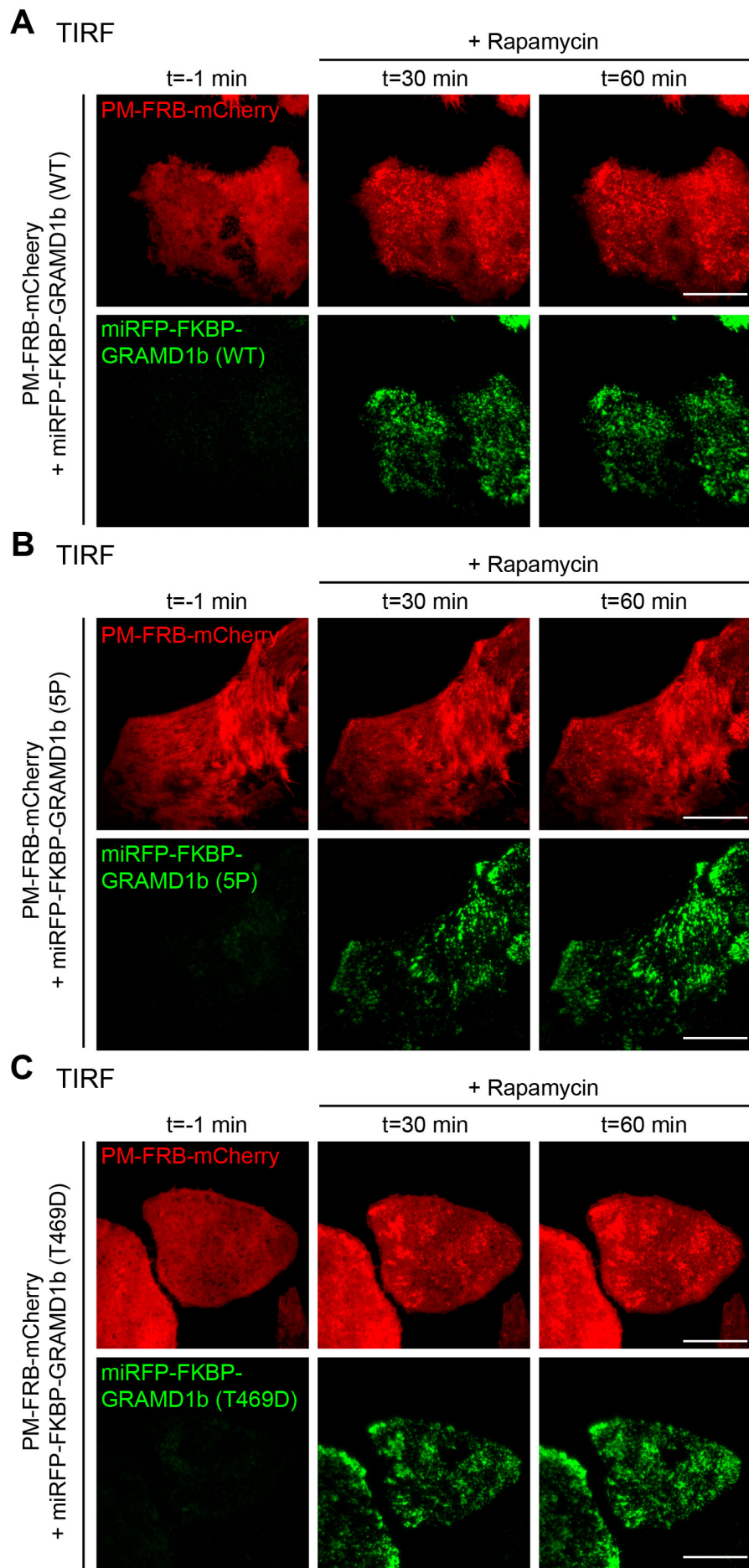


Figure 7-figure supplement 3